IDŐJÁRÁS

QUARTERLY JOURNAL OF THE HUNGAROMET
HUNGARIAN METEOROLOGICAL SERVICE

CONTENTS

VOL. 130 * NO. 1 * JANUARY – MARCH 2026

IDŐJÁRÁS

Quarterly Journal of the HungaroMet Hungarian Meteorological Service

Editor-in-Chief
LÁSZLÓ BOZÓ

Executive Editor
KRISZTINA LABANCZ

EDITORIAL BOARD

BARTHOLY, J. (Budapest, Hungary)
BATCHVAROVA, E. (Sofia, Bulgaria)
FERENCZI, Z. (Budapest, Hungary)
GERESDI, I. (Pécs, Hungary)
HASZPRA, L. (Budapest, Hungary)
HORVÁTH, Á. (Siófok, Hungary)
HORVÁTH, L. (Budapest, Hungary)
HUNKÁR, M. (Keszthely, Hungary)
LASZLO, I. (Camp Springs, MD, U.S.A.)
MAJOR, G. (Budapest, Hungary)
MÉSZÁROS, E. (Veszprém, Hungary)
MÉSZÁROS, R. (Budapest, Hungary)
MIKA, J. (Budapest, Hungary)
MERSICH, I. (Budapest, Hungary)
MÖLLER, D. (Berlin, Germany)
PINTO, J. (Res. Triangle Park, NC, U.S.A.)
PRÁGER, T. (Budapest, Hungary)
PROBÁLD, F. (Budapest, Hungary)
RADNÓTI, G. (Surány, Hungary)
S. BURÁNSZKI, M. (Budapest, Hungary)
SZEIDL, L. (Budapest, Hungary)
SZUNYOGH, I. (College Station, TX, U.S.A.)
TAR, K. (Debrecen, Hungary)
TOTH, Z. (Camp Springs, MD, U.S.A.)
VALI, G. (Laramie, WY, U.S.A.)
WEIDINGER, T. (Budapest, Hungary)
ZEYBEKOGLU, U. (Sinop, Türkiye)

Editorial Office: Kitaibel P.u. 1, H-1024 Budapest, Hungary
P.O. Box 38, H-1525 Budapest, Hungary
E-mail: journal.idojaras@met.hu

Indexed and abstracted in Science Citation Index Expanded™ and Journal Citation Reports/Science Edition
Covered in the abstract and citation database SCOPUS®
Included in EBSCO's database

Subscription by mail:
IDŐJÁRÁS, P.O. Box 38, H-1525 Budapest, Hungary
E-mail: journal.idojaras@met.hu

DOI:10.28974/idojaras.2026.1.1

IDŐJÁRÁS

Quarterly Journal of the HungaroMet Hungarian Meteorological Service
Vol. 130, No. 1, January – March, 2026, pp. 1–28

Air temperature variability during the vegetation period in Central Serbia over the last 70 years

Nikola R. Bačević[1,*], **Milica G. Radaković**[2], **Milena Nikolić**[1,3,4], **Rastko S. Marković**[5], **Nemanja Tomić**[2], **Tijana Tomić**[2], **Dušan Kićović**[6], **Aleksandar Valjarević**[7], **Slobodan B. Marković**[2,8,9], and **Tin Lukić**[2,10]

[1] *University of Priština, Faculty of Sciences and Mathematics, Department of Geography, 38220 Kosovska Mitrovica, Serbia*

[2] *University of Novi Sad, Faculty of Sciences, Department of Geography, Tourism and Hotel Management, Trg Dositeja Obradovića 3, 21000 Novi Sad, Serbia*

[3] *University of Priština in Kosovska Mitrovica, Faculty of Technical Sciences, Department of Architecture, Knjaza Miloša 7, 38220 Kosovska Mitrovica, Serbia*

[4] *Faculty of social sciences, University business academy in Novi Sad*

[5] *Faculty of Natural Sciences and Mathematics, University of Niš, Department of Geography and Tourism, Višegradska 11, 18000 Niš, Serbia*

[6] *Academy for applied studies Belgrade, The College of Tourism, 11000 Belgrade, Serbia*

[7] *University of Belgrade, Faculty of Geography, Department of Geospatial and Environmental Science, Studentski Trg 3/III, 11000 Belgrade, Serbia*

[8] *Serbian Academy of Sciences and Arts, Kneza Mihaila 35, 11000 Belgrade, Serbia*

[9] *University of Montenegro, Cetinjska 2, 81000 Podgorica, Montenegro*

[10] *Rudjer Bošković School, Kneza Višeslava 17, 11030 Belgrade, Serbia*

**Corresponding author E-mail: nikola.bacevic@pr.ac.rs*

(Manuscript received in final form March 31, 2025)

Abstract— This study analyzes trends in three temperature variables (average annual air temperature, maximum air temperature, and minimum air temperature) for 72 time series from 24 meteorological stations in Central Serbia, spanning from 1949 to 2018. Data was sourced from meteorological yearbooks on the website of the Republic Hydrometeorological Institute of Serbia. Three statistical approaches were used: trend equation, trend magnitude, and the non-parametric Mann-Kendall (MK) trend test. GIS was applied to visualize geospatial data distribution. The results indicate a temperature increase in 66 of the 72 time series, with the largest increase of 4.3 °C and the smallest of 0.2 °C. Temperature decreases were recorded in 6 time series, with the largest decrease of -0.5 °C. The MK trend test revealed a statistically significant positive trend in 53 time series. Geospatial analysis showed varying temperatures across the region, with average annual air temperatures ranging from 10.6 °C in Dimitrovgrad to 18.1 °C in Belgrade. These findings offer insights into climate change in Central Serbia, highlighting areas of temperature increase and decrease, and provide a foundation for future climate research and strategy development.

Key-words: climate change, Serbia, average annual temperature trends, vegetation period, Mann-Kendall trend test, GIS

1. Introduction

In this study, for the first time, analyses will be presented for the average annual air temperature (YT-VP), average annual maximum air temperature (YT-VPx), and average annual minimum air temperature (YTn-VP) for the vegetation period on the territory of Central Serbia in the time interval from 1949 to 2018. Numerous works in world literature deal with climate change in a similar or almost the same way, a very popular topic having great importance at the global level. The importance of trend analysis lies in determining changes in a time series of no less than 30 years for a certain variable, which can directly affect changes in the environment (agriculture, flora and fauna, water resources, climatic conditions, ecosystems, etc.), and have an impact also on humans.

Numerous scientific studies deal with the trend analysis of various variables in different parts of our planet (*Hamlet et al*., 2005; *Minetti et al*., 2010; *Li et al*., 2011; *Hua et al*., 2013; *Zeoural et al*., 2013; *Martínez-Austria et al*., 2016; *O'Neil et al*., 2017; *Kabanda,* 2018; *Birara et al*., 2018; *Caloiero,* 2018; *Malik* and *Kumar*, 2020; *Mallick et al*., 2021; *Ahmed et al*., 2022; *Lornezhad et al*., 2023; *Ceyhunlu* and *Ceribasi,* 2024;). Mann's method, which Mann himself presented in his paper "*Nonparametric Tests Against Trend*" in 1945 (*Mann,* 1945), is most often used for such researches. Also, in addition to the abovementioned studies, there are numerous reports from the United Nations (UN) organization known as the "*Intergovernmental Panel on Climate Change*" (IPCC) which is responsible for assessing scientific knowledge about climate change and whose results point to climate change (increasing average temperatures) and give recommendations to governments and international organizations on how to deal with the challenges posed by climate change (IPCC, 2022). The results from the paper by *Hajas* and *Zempléni* (2020), which contains an analysis of network data on daily

temperatures for the time interval from 1950 to 2017 on the European continent, indicate accelerated warming in the last 40 years, especially in the central and southwestern areas of Europe. Moreover, an increase in air temperatures has been recorded in the eastern and central parts of Europe since the 1990s, mostly in the warmer part of the year caused by the greater frequency of arrival of air masses from lower latitudes, which is a consequence of advancing global warming (*Bartoszek* and *Kaszewski*, 2020). An increase in air temperature was also recorded in Northern Europe, as temperature drops were occasionally recorded between 1940 and 1970 and between 1998 and 2013, which can be correlated with the behavior of the Pacific and Atlantic Oscillation and can be considered as climatic fluctuations within climate change (*Gulev et al*., 2013).

Many scientific studies deal with changes in air temperature in the region, namely in Slovenia (*Milošević et al*., 2013; *Tošić et al*., 2016), Croatia (*Radilović et al*., 2020), Bosnia and Herzegovina (*Trbić et al*., 2017; *Popov et al*., 2017, 2018a, 2018b), and Montenegro (*Luković et al*., 2013; 2024; *Burić et al*., 2014, 2015, 2018). Changes in air temperature patterns have already been recorded in the observed area, as indicated by the results obtained by numerous authors. Papers on climate change in Serbia can be classified into two categories: papers that analyze average air temperatures (*Unkašević* and *Tošić*, 2013, 2015; *Gocić* and *Trajković*, 2013; *Malinović-Milićević et al*., 2016; *Putniković et al*., 2018; *Vukoičić et al*., 2018; *Tošić et al*., 2021; *Baumgertel et al*., 2024) and papers that monitor aridity (*Gocić* and *Trajković*, 2014a, 2014b; *Hrnjak et al*., 2014; *Gavrilov et al*., 2019; *Radaković et al*., 2018; *Milentijević et al*., 2018; *Trajković et al*., 2020; *Burić et al*., 2023; *Zivanovic et al*., 2024). In most cases, speaking of the scientific studies mentioned above, air temperatures are generally increasing, which is also in line with this scientific study. A certain number of papers on climate change was carried out at the regional level on the territory of Serbia: Kosovo and Metohija (*Bačević et al*., 2017, 2018; *Gavrilov et al*., 2018; *Radaković et al*., 2018) and Vojvodina (*Hrnjak et al*., 2014; *Gavrilov et al*., 2015, 2016, 2019; *Milentijević et al*., 2020).

As pointed out by *Chervenkov* and *Slavov* (2021), air temperature is a key environmental factor influencing crop growth, development, and yields, particularly the rate of development. On one hand, crops require specific temperatures to complete certain phenophases or their entire life cycle. On the other hand, extremely high and low temperatures can negatively impact crop growth, development, and yield respectively (*Mandić et al*., 2022). This is why variability in average annual air temperature, average annual maximum air temperature, and average annual minimum air temperature should be investigated to conduct regional impact assessments focused on enhancing climate change resilience.

The main goal of this study is the analysis and assessment of long-term trends in average air temperature, average maximum air temperature, and average maximum air temperature for the vegetation period during the time period from

1949 to 2018 in the territory of Central Serbia. The emphasis is placed on the study of the 72 time series for 24 meteorological stations in order to determine variability of various climate parameters, with special reference to the vegetation period from April to October. The analysis includes the application of a non-parametric test (Mann-Kendall test) for detecting trends, assessing the significance of changes, as well as assessing the risk of rejecting or accepting hypotheses about the presence of a trend. Furthermore, one of the goals is to show the geospatial data distribution, whereas the ultimate goal is to provide an overview and understanding of climate change in Central Serbia, to identify areas with an increase or decrease in air temperatures for the analyzed categories, as well as to provide a basis for future research and climate strategies.

2. Material and methods

2.1. Research area

Central Serbia has an exceptional geographical position, because it occupies the central part of the Balkan Peninsula, and thus, represents the most important land connection between the Balkans and this part of Europe. The northern border is represented by the rivers Danube and Sava. The eastern border coincides with the borders of the Republic of Serbia with the Republic of Bulgaria and Romania. The southern border is represented by the border of the Republic of Serbia and the Republic of North Macedonia, as well as the contact between the Autonomous Province of Kosovo and Metohija and Central Serbia. The western border coincides with the borders of Serbia and Montenegro, after which it follows the course of the Drina River. In a regional-geographical sense, Central Serbia includes the following mesoregions: Western Serbia, Eastern Serbia, Southern Serbia, Central Serbia, as well as the microregions of Stari Vlah and Raška and Ibar-Kopaonik region (*Pavlović*, 2019a, 2019b).

The mountain ranges of Dinarides, Rhodopes (Serbian-Macedonian massif) and Carpatho-Balkanides are crossed by river courses, among which the Velika Morava, with its tributaries, dominates. Most of the precipitation comes from the east, that is, from the Atlantic Ocean and the Adriatic Sea. The effect from the Adriatic weakens rashly during crossing of the Dinarides. The amount of precipitation varies from 600 mm, and in some places it exceeds 1100 mm per year. In the southeastern and southwestern parts of Central Serbia, the lowest average annual air temperature is around 2 °C, while the highest average annual temperatures occur in the largest populated places, where the warmest is Belgrade with around 12 °C (*Milovanović et al*., 2022a).

2.2. Materials

The average annual air temperature (YT-VP), average annual maximum air temperature (YTx-VP), and average annual minimum air temperature (YTn-VP) during the vegetation period (P-VG) from 1949 to 2018 were calculated based on publicly available data of the Republic Hydrometeorological Institute of Serbia (https://www.hidmet.gov.rs/). Twenty-four meteorological stations were used, whose data are given in *Table 1* (*Bačević, et al*., 2021), while their position is given in *Fig. 1*. For the purposes of these studies, data on precipitation from 24 meteorological stations were used. Details of station names, geographic coordinates, geographic location and their altitude are shown in *Fig. 1* and *Table 1*.

Fig. 1. Geographical position of Central Serbia in the regional context and in Europe (upper right corner). Meteorological stations used in this study are indicated by black dots.

Table 1. List of meteorological stations located in Central Serbia, their geographic coordinates and altitude, and the name of time series used in this study

No.	Meteorological station	Name of time series	φ (°N)	λ (°E)	*h* (m)
1.	Belgrade	BG-YT-VP; BG-YTx-VP; BG-YTn-VP	44º48′	20º28′	132
2.	Bujanovac	BU-YT-VP; BU-YTx-VP; BU-YTn-VP	42º27′	21º46′	399
3.	Ćuprija	CU-YT-VP; CU-YTx-VP; CU-YTn-VP	43º56′	21º23′	123
4.	Dimitrovgrad	DI-YT-VP; DI-YTx-VP; DI-YTn-VP	43º01′	22º45′	450
5.	Jagodina	JA-YT-VP; JA-YTx-VP; JA-YTn-VP	43º59′	21º23′	115
6.	Knjaževac	KZ-YT-VP; KZ-YTx-VP; KZ-YTn-VP	43º34′	22º15′	263
7.	Kragujevac	KG-YT-VP; KG-YTx-VP; KG-YTn-VP	44º02′	20º56′	181
8.	Kraljevo	KV-YT-VP; KV-YTx-VP; KV-YTn-VP	43º43′	20º42′	215
9.	Kruševac	KS-YT-VP; KS-YTx-VP; KS-YTn-VP	43º37′	21º15′	166
10.	Kuršumlija	KU-YT-VP; KU-YTx-VP; KU-YTn-VP	43º08′	21º16′	384
11.	Leskovac	LE-YT-VP; LE-YTx-VP; LE-YTn-VP	42º59′	21º57′	231
12.	Loznica	LO-YT-VP; LO-YTx-VP; LO-YTn-VP	44º32′	19º14′	121
13.	Negotin	NG-YT-VP; NG-YTx-VP; NG-YTn-VP	44º14′	22º32′	42
14.	Niš	NI-YT-VP; NI-YTx-VP; NI-YTn-VP	43º20′	21º54′	202
15.	Novi Pazar	NP-YT-VP; NP-YTx-VP; NP-YTn-VP	43º08′	20º31′	545
16.	Pirot	PI-YT-VP; PI-YTx-VP; PI-YTn-VP	43º09′	22º35′	373
17.	Požega	PZ-YT-VP; PZ-YTx-VP; PZ-YTn-VP	43º51′	20º02′	311
18.	Sjenica	SJ-YT-VP; SJ-YTx-VP; SJ-YTn-VP	43º16′	20º00′	1038
19.	Smederevska Palanka	SP-YT-VP; SP-YTx-VP; SP-YTn-VP	44º22′	20º57′	121
20.	Valjevo	VA-YT-VP; VA-YTx-VP; VA-YTn-VP	44º17′	19º55′	174
21.	Veliko Gradište	VG-YT-VP; VG-YTx-VP; VG-YTn-VP	44º45′	21º30′	80
22.	Vranje	VR-YT-VP; VR-YTx-VP; VR-YTn-VP	42º33′	21º55′	433
23.	Zaječar	ZA-YT-VP; ZA-YTx-VP; ZA-YTn-VP	43º53′	22º17′	144
24.	Zlatibor	ZL-YT-VP; ZL-YTx-VP; ZL-YTn-VP	43º44′	19º43′	1029

2.3. Methods

For the purposes this scientific study, three different statistical methods were used to analyze trends in average annual air temperature (YT-VP), average annual maximum air temperature (Ytx-VP), and average annual minimum air temperature (Ytn-VP) during the vegetation period. The first method involves calculating of the trend equation for each time series separately (*Bačević et al*., 2022). The second statistical method is the application of the non-parametric

Mann-Kendall trend test to the existing sample (*Papić et al*., 2020). The third method is determining the trend magnitude based on the trend equation (*Bačević et al*., 2020). Trend analysis was calculated using the XLSTAT extension (https://www.xlstat.com/en) within the EXCEL MICROSOFT OFFICE package.

Calculation of the trend equation is based on the application of linear regression to calculate the precipitation trend equation during the vegetation period for each meteorological station, and the equation reads

$$y = ax + b\,. \tag{1}$$

In this equation, y denotes the average annual air temperature (YT-VP), average annual maximum air temperature (YTx-VP), i.e., average annual minimum air temperature (YTn-VP) in the vegetation period expressed in °C, a represents the trend slope that can be positive, negative, or with no trend, x represents the time series, while b represents the value of the air temperature at the beginning of the analyzed period (*Bačević et al*., 2018, 2024; 2025 in press; *Vukoičić et al*., 2018). After this analysis, the determination of the trend magnitude is carried out (*Gavrilov et al*., 2018)

$$\Delta y = y(Pb) - y(Pe)\,, \tag{2}$$

where Δy represents the trend magnitude in °C, $y(Pb)$ is the temperature value (YT-VP, YTx-VP, and YTn-VP) in the first year of the observed period, while $y(Pe)$ is the temperature value (YT-VP, YTx-VP, and YTn-VP) in the last year of the time series. In relation to that, the trend magnitude can be positive (increasing) and negative (decreasing). The trend magnitude can be with no trend, if the specified values are equal.

The third method used in this paper is the Mann-Kendall (MK) trend test for the analysis of air temperature time series (YT-VP, YTx-VP, and YTn-VP) during the vegetation period in Central Serbia (*Mann*, 1945; *Kendall*, 1975). Each value in the time series is assigned a rank. Differences between pairwise ranks are used to calculate the direction and strength of the trend, after which the variance of the MK test is determined to show the randomness of the variability in the data. Low variance indicates low data dispersion, and vice versa. Then follows the calculation of the trend significance, which begins by comparing the calculated test statistic with the data distribution, assuming that there is no trend (H_0 hypothesis). If the test statistics is greater than the critical value from the distribution, it indicates that there is a statistically significant trend (H_a hypothesis). p denotes the value that indicates how much the test statistic exceeds the critical value. In the case when p is less than 0.05 or 5%, the trend results are statistically significant and the H_0 hypothesis is rejected (*Gavrilov et al*., 2018; *Razavi et al*., 2016).

2.3.1. Spatial data analysis

All digital cartographic analyses were conducted using ArcGIS Pro: 3.2.0. Data, which are necessary for mapping, were taken from the Internet and from established databases, obtained during statistical processing. GIS and data modeling are very powerful tools for assessing and calculating meteorological data of an area. In this paper, the kriging method is preferred within the interpolation framework to show the geographical distribution of average precipitation during the vegetation period in the analyzed period. The results of the statistical analysis are spatially represented using the Create Thiessen Polygons analysis. This method was developed by Thiessen, a meteorologist, more than a century ago, and it refers to the creation of a polygon in the center of which a coordinate is entered (*Radaković*, 2018), in this case the coordinate of a meteorological station. Using this method, the entire territory of Central Serbia is divided into areas where the results of linear regression and the Mann-Kendall test are the same: the trend in precipitation during the vegetation period exists as positive, negative, or no trend. All procedures and approaches used for the purpose of this research are presented in the flow chart given in *Fig. 2*.

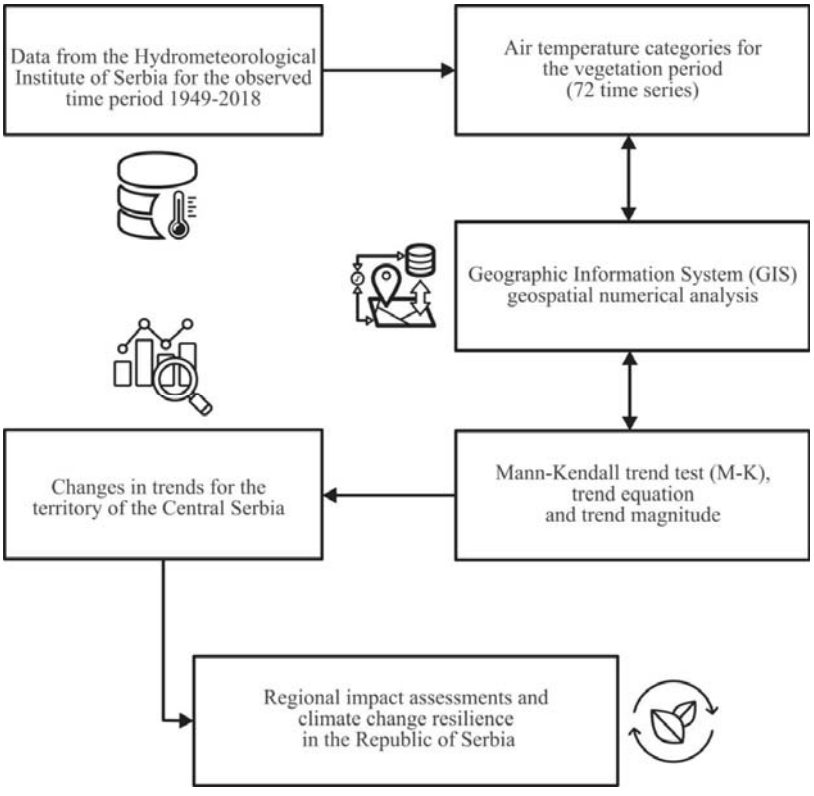

Fig. 2. Flow chart with all the procedures and methods used in this research.

3. Results

3.1. Trend parameters

The results of this scientific study are shown in *Table 2* and *Figs. 3, 4, 5,* and *6*. The analysis for 24 meteorological stations, which are located in the territory of Central Serbia for the time interval from 1949 to 2018, is presented. The processed data and performed analyses refer to the vegetation period (April - October) for the observed area and, based on those variables, the values of the observed equations were calculated. Also, the analysis of 72 time series is presented, which was conducted using a non-parametric trend test (MK). *Table 2* and *Fig. 2* visually show the results obtained for the average annual air temperature, average annual maximum air temperature, average annual minimum air temperature, trend equation, linear trend equation, and trend magnitude. Furthermore, *Fig. 2* visually shows the obtained results for the *p* values, results of trend testing, and evaluation of hypotheses for accepting the trend, that is, rejecting the trend. Spatial distributions for the average annual air temperature, average annual maximum air temperature, and average annual minimum air temperature are shown in *Fig. 7*.

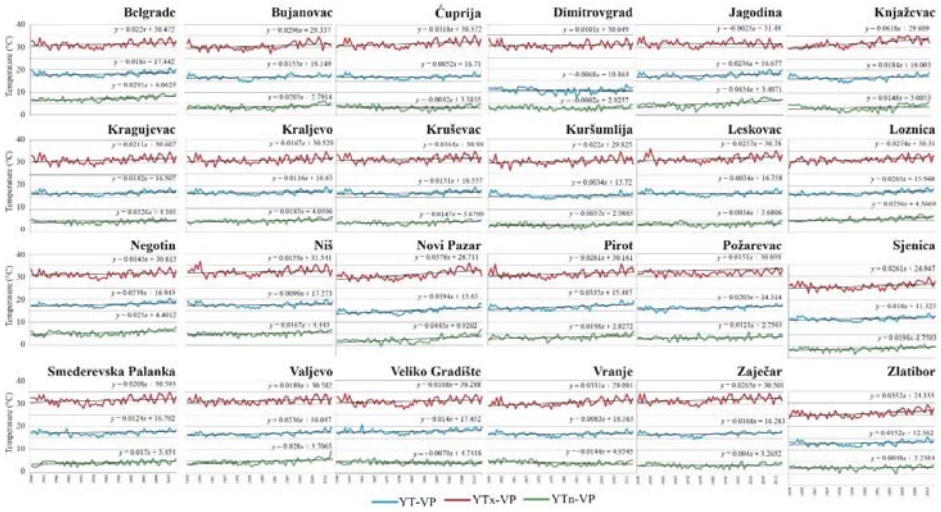

Fig. 3. Results of the average annual surface air temperature YT-VP (blue), average maximum annual surface air temperature YTx-VP (red), and average minimum annual surface air temperature YTn-VP (green) for the vegetation period (April-October, 1949–2018) for 24 meteorological stations in Central Serbia.

Table 2. Names of time series, trend equation y, trend magnitude Dy, average annual air temperature, average annual maximum air temperature and average annual minimum air temperature for the vegetation period for 72 time series, which refer to the territory of Central Serbia

Time series	Trend equation	DyYT-VP (°C)	Average temperature (°C)
BG-YT-VP	y=0.018x+17.442	1.24	18.1
BG-Ytx-VP	y=0.022x+30.472	1.52	31.3
BG-Ytn-VP	y=0.0291x+6.0625	2.0	7.1
BU-YT-VP	y=0.0153x+16.149	1.0	16.7
BU-YTx-VP	y=0.0296x+29.337	2.0	30.4
BU-YTn-VP	y=0.0203x+2.7914	1.4	3.5
CU-YT-VP	y=0.0052x+16.71	0.3	16.9
CU-YTx-VP	y=0.0318x+30.572	2.2	31.7
CU-YTn-VP	y=-0.0042x+3.3835	-0.3	3.2
DI-YT-VP	y=-0.0068x+10.864	-0.5	10.6
DI-YTx-VP	y=0.0101x+ 30.049	0.7	30.4
DI-YTn-VP	y=-0.0002x+2.9237	-0.01	2.9
JA-YT-VP	y=0.0236x+16.677	1.6	17.5
JA-YTx-VP	y=-0.0025x+31.49	-0.2	31.4
JA-YTn-VP	y=0.0454x+3.4071	3.1	5.0
KZ-YT-VP	y=0.0184x+16.003	1.3	16.7
KZ-YTx-VP	y=0.0618x+29.609	4.3	31.8
KZ-YTn-VP	y=0.0148x+3.0053	1.0	3.5
KG-YT-VP	y=0.0142x+16.507	1.0	17.0
KG-YTx-VP	y=0.0211x+30.607	1.4	31.4
KG-YT-nVP	y=0.0126x + 4.101	0.9	4.5
KV-YT-VP	y=0.0116x+16.63	0.8	17.0
KV-YTx-VP	y=0.0167x+30.529	1.1	31.1
KV-YTn-VP	y=0.0183x+4.0596	1.3	4.7
KS-YT-VP	y=0.0131x+16.537	0.9	17.0
KS-YTx-VP	y=0.0164x + 30.99	1.1	31.6
KS-YTn-VP	y=0.0147x+3.6799	1.0	4.2
KU-YT-VP	y=0.0034x+15.72	0.2	15.8
KU-YTx-VP	y=0.022x+29.825	1.5	30.6
KU-YTn-VP	y=0.0057x+2.9885	0.4	3.2
LE-YT-VP	y=0.0034x+16.758	0.2	16.9
LE-YTx-VP	y=0.0237x+30.78	1.6	31.6
LE-YTn-VP	y=0.0034x+3.6806	0.2	3.8
LO-YT-VP	y=0.0263x+15.948	1.8	16.9
LO-YTx-VP	y=0.0274x+30.31	1.9	31.3
LO-YTn-VP	y=0.0256x+4.5669	1.8	5.5
NG-YT-VP	y=0.0239x+16.943	1.6	17.8
NG-YTx-VP	y=0.0145x+30.613	1.0	31.1
NG-YTn-VP	y=0.025x+4.4012	1.7	5.3
NI-YT-VP	y=0.0099x+17.273	0.7	17.6
NI-YTx-VP	y=0.0159x+31.541	1.1	32.1
NI-YTn-VP	y=0.0167x+4.443	1.1	5.0
NP-YT-VP	y=0.0394x+13.65	2.7	15.0

Time series	Trend equation	DyYT-VP (°C)	Average temperature (°C)
NP-YTx-VP	y=0.0578x+28.711	3.9	30.8
NP-YTn-VP	y=0.0443x+0.9202	3.0	2.5
PI-YT-VP	y=0.0335x+15.487	2.3	16.7
PI-YTx-VP	y=0.0261x+30.161	1.8	31.1
PI-YTn-VP	y=0.0198x+2.8272	1.4	3.5
PZ-YT-VP	y=0.0203x+14.514	1.4	15.2
PZ-YTx-VP	y=0.0151x+30.039	1.0	30.6
PZ-YTn-VP	y=0.0121x+2.7561	0.8	3.2
SJ-YT-VP	y=0.016x+11.323	1.1	11.9
SJ-YTx-VP	y=0.0261x+24.947	1.8	25.9
SJ-YTn-VP	y=0.0198x-1.7503	1.4	-1.0
SP-YT-VP	y=0.0124x+16.702	0.8	17.1
SP-YTx-VP	y=0.0208x+30.593	1.4	31.3
SP-YTn-VP	y=0.017x+3.434	1.2	4.0
VA-YT-VP	y=0.0236x+16.047	1.6	16.9
VA-YTx-VP	y=0.0189x+30.582	1.3	31.3
VA-YTn-VP	y=0.028x+3.7065	1.9	4.7
VG-YT-VP	y=0.014x+17.452	0.9	17.9
VG-YTx-VP	y=0.0168x+30.288	1.1	30.9
VG-YTn-VP	y=-0.0079x+4.7418	-0.5	4.5
VR-YT-VP	y=0.0083x+16.565	0.6	16.9
VR-YTx-VP	y=0.0331x+29.091	2.3	30.3
VR-YTn-VP	y=-0.0144x+4.9345	-1.0	4.4
ZA-YT-VP	y=0.0168x+16.283	1.1	16.9
ZA-YTx-VP	y=0.0265x+30.501	1.8	31.4
ZA-YTn-VP	y=0.004x+3.2652	0.3	3.4
ZL-YT-VP	y=0.0152x+12.362	1.0	12.9
ZL-YTx-VP	y=0.0352x+24.335	2.4	25.6
ZL-YTn-VP	y=0.0048x+2.2384	0.3	2.4

The presentation of the obtained results of the above parameters, which are visually shown in *Fig. 3* and *Table 2*, indicates an increase in the average annual air temperature (YT-VP), average annual maximum air temperature (YTx-VP), and average annual minimum air temperature (YTn-VP) for the vegetation period in the observed area. Out of a total of 72 time series, a positive balance (increase in temperature) was recorded in 66 time series, and a negative balance (decrease in temperature) was recorded in 6 time series. The recorded increase in temperature for the variables mentioned above ranges from 0.2 °C (time series KU-YT-VP, LE-YT-VP, and LE-YTn-VP) to 4.3 °C (time series KZ-YTx-VP). Negative balance was recorded for a total of six time series (CU-YTn-VP, DI-YT-VP, DI-YTn-VP, JA-YTx-VP, VG-YTn-VP and VR-YTn-VP), whose values range from -0.01 °C (time series DI-YTn-VP) to -0.5 °C (time series DI-YT-VP and VG-YTn-VP). The average annual air temperature for the vegetation period is 16.2 °C. The average annual maximum air temperature for the vegetation period is 30.7 °C. The average

annual minimum air temperature for the vegetation period is 3.9 °C. More detailed results for other time series are shown in *Table 2*. Moreover, in the same table, the results for the average annual air temperature, average annual maximum air temperature and average annual minimum air temperature, in the vegetation period are shown separately for each meteorological station in the past 70 years in the observed territory.

3.2. Trend assessment

The spatial description of the results obtained by the MK trend test analysis and the evaluation of hypotheses (*p* values, type of hypothesis - the risk of rejecting the hypothesis) are shown in *Figs. 4, 5,* and *6*. Out of a total of 72 time series, most show a statistically significant positive trend. More precisely, H_a hypothesis prevails in 53 time series, where the *p* value is lower than the significance level α, whose value is 0.05. In the remaining 19 time series, there is no trend, where H_0 hypothesis prevails and where the *p* value is higher than the significance level α, whose value is 0.05. Out of 53 time series (*Figs. 3, 4,* and *5*), where a statistically positive trend and H_a hypothesis prevail, a very small percentage of the risk of rejecting this claim, ranging between 0.01% and 1.00%, was recorded in 39 time series. In the remaining 14 time series, the percentage of risk to reject such a claim is insignificantly higher and ranges between 1.00% to 5.00%.

These results for the abovementioned time series indicate that in most cases, the trend is positive and that the temperature has increased in the entire analyzed territory, and that it will continue to be so in the future as well. Also, after the analyses performed in the MK trend test, results were obtained, where there is no trend in 19 time series. The percentage of risk to reject such a claim is significantly higher compared to the recorded risk for time series, where the trend is positive. The risk percentage ranges from 5.14% to 77.17%. In 4 time series (KV-YTx-VP, KS-YTx-VP, PZ-YTx-VP, and VR-YTn-VP) the risk percentage ranges from 5.14% to 6.59%, which indicates that there will certainly be no trend in the future. In 12 time series (CU-YT-VP, CU-YTn-VP, DI-YT-VP, DI-YTx-VP, KZ-YTn-VP, KU-YT-VP, KU-YTn-VP, LE-YT-VP, VG-YTn-VP, VR-YT-VP, ZA-YTn-VP, and ZL-YTn-VP) the percentage of risk to reject this claim ranges from 10.06% to 47.47%, which indicates that a positive trend is possible in the future and that the air temperature may increase. In the remaining 3 time series, the risk percentage of rejecting this claim is above 50.00%. More precisely, the percentage of risk is 57.94% for the time series LE-YTn-VP, 77.17% for the time series DI-YTn-VP, and 77.57% for the time series JA-Ytx-VP, which indicates that it will certainly change to a positive trend in the future and that an increase in air temperature will be recorded.

The obtained results for the trend equation differ from the obtained results of the MK trend test analysis, where a greater number of time series with positive trend was recorded. A total of 59 time series were recorded, where a positive trend

was recorded for 6 more. In 7 time series there is no trend, and in 6 time series the trend is negative, which is also less for 6 time series in relation to the results obtained using MK trend test. These results are shown in more detail in *Figs. 3, 4, 5,* and *6*.

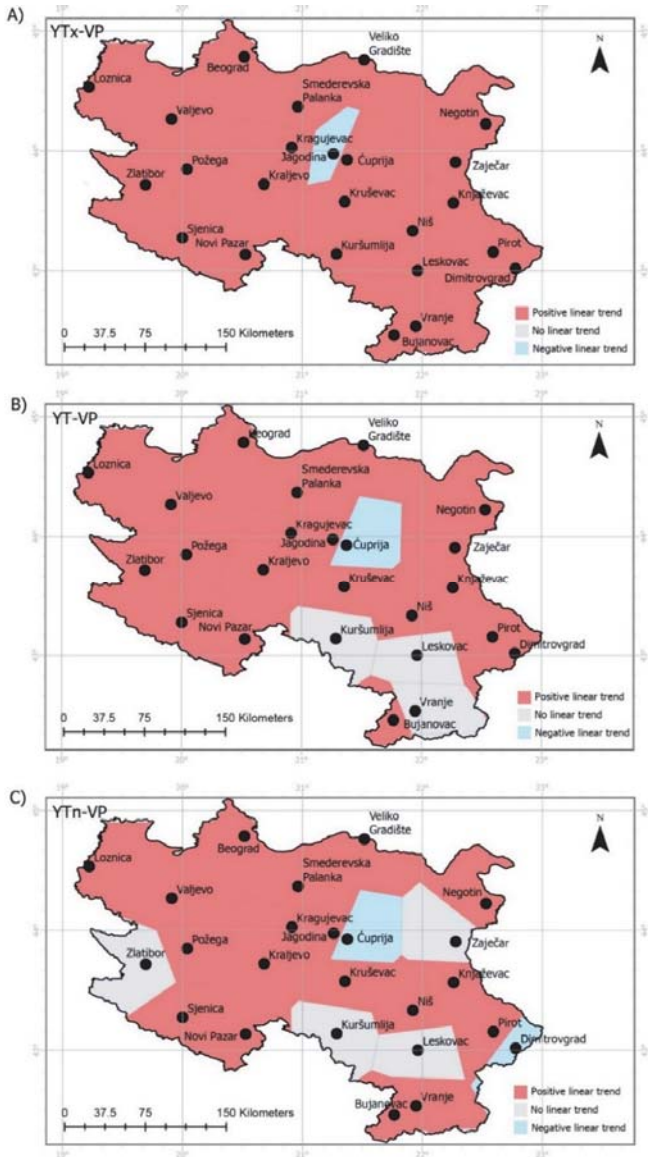

Fig. 4. Cartographic presentation of the obtained results of the linear trend equation movement of A) average annual maximum, B) average annual, and C) average annual minimum air temperatures for the vegetation period in Central Serbia, in the time interval from 1949 to 2018.

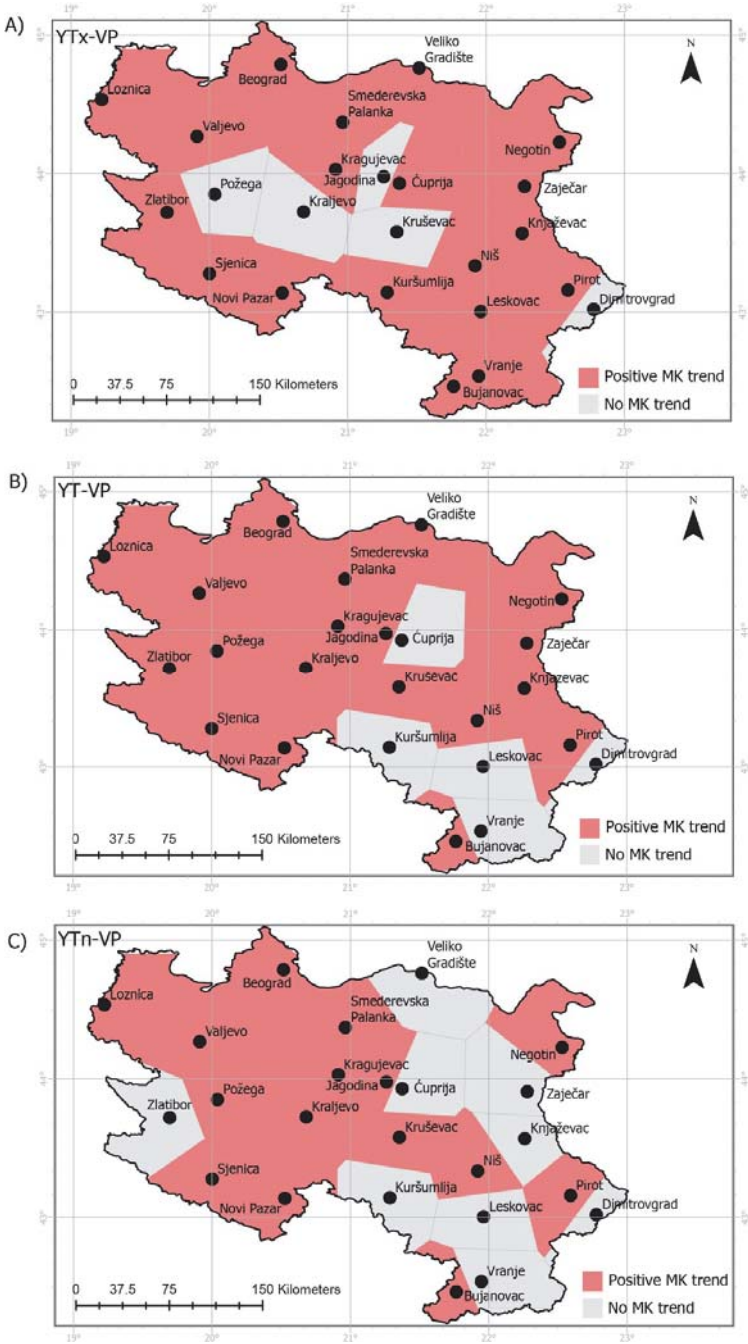

Fig. 5. Cartographic representation of the results obtained from Mann-Kendall trend test of A) average annual maximum, B) average annual, and C) average annual minimum air temperatures for the vegetation period in Central Serbia, in the time interval from 1949 to 2018.

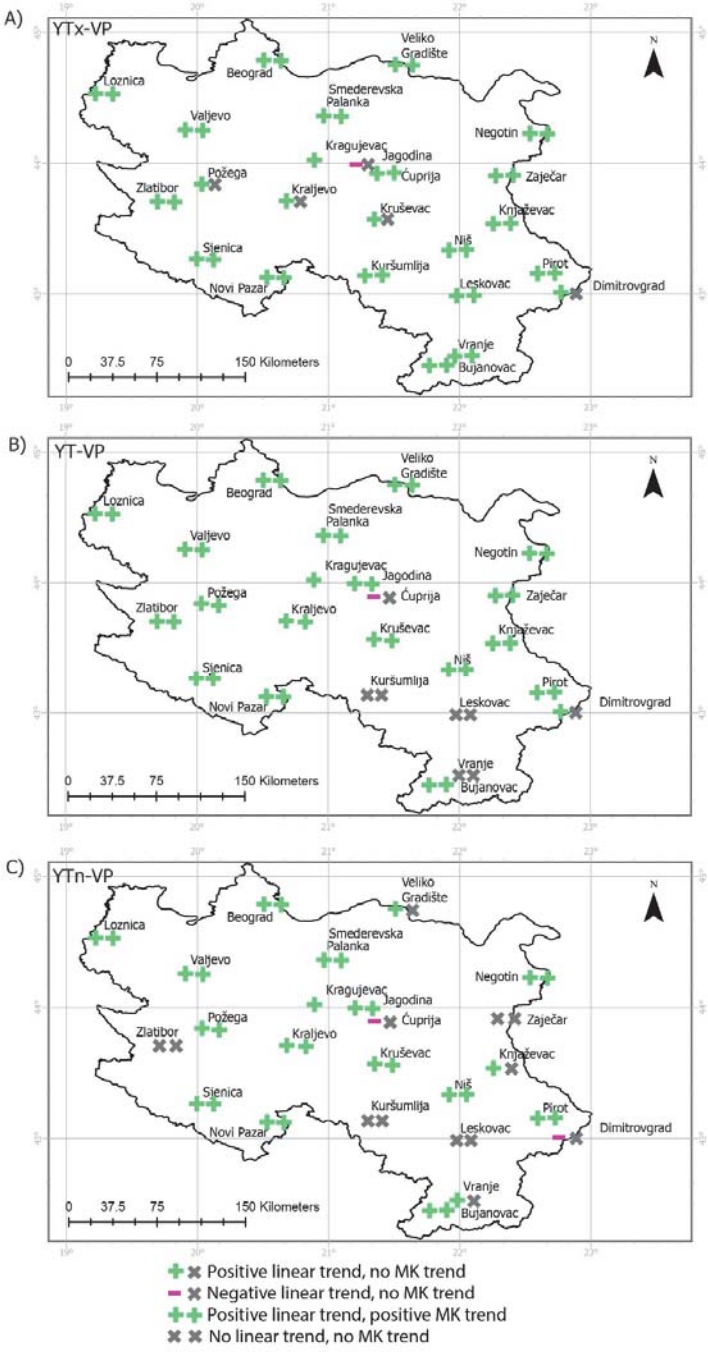

Fig. 6. Comparative presentation of the obtained results of the linear and Mann-Kendall trends of A) average annual maximum, B) average annual, and C) average annual minimum air temperatures for the vegetation period in Central Serbia, in the time interval from 1949 to 2018.

3.3. GIS numerical analysis

Spatial distributions of the average annual air temperature, average annual maximum air temperature, and average annual minimum air temperature for the vegetation period in the time interval from 1949 to 2018 in Central Serbia are shown in more detail in *Fig. 6* (a-c).

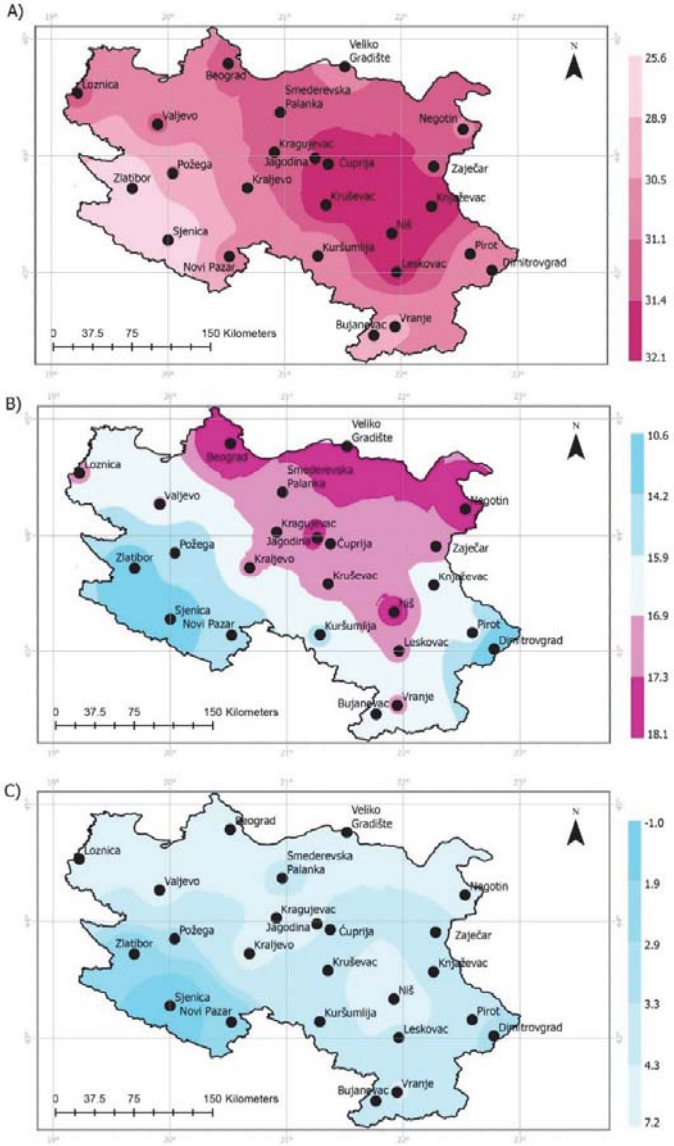

Fig. 7. Spatial distribution of A) average annual maximum, B) average annual, and C) average annual minimum air temperatures for the vegetation period in Central Serbia in °C, in the time interval from 1949 to 2018.

Fig. 6 shows the average annual air temperature (YT-VP), average annual maximum air temperature (YTx-VP), and average annual minimum air temperature (YTn-VP) for the vegetation period in Central Serbia for the time interval from 1949 to 2018. The isotherms follow the temperature values and indicate the influence of the geographical position, orography, altitude, proximity to the Adriatic Sea, and in the last period, the anthropogenic influence should also be mentioned. Average annual air temperatures for the vegetation period in the observed area range from 10.6 °C in Dimitrovgrad to 18.1 °C in Belgrade. Other values of the average annual air temperature for the vegetation period are shown from the lowest to the highest, namely: Sjenica 11.9 °C, Zlatibor 11.9 °C, Novi Pazar 15 °C, Požega 15.2 °C, Kuršumlija 15.8 °C, Bujanovac 16.7 °C, Knjaževac 16.7 °C, Pirot 16.7 °C, Ćuprija 16.9 °C, Loznica 16.9 °C, Leskovac 16.9 °C, Valjevo 16.9 °C, Vranje 16.9 °C, Zaječar 16.7 °C, Kragujevac 17 °C, Kraljevo 17 °C, Kruševac 17 °C, Smederevska Palanka 17.1 °C, Jagodina 17.5 °C, Niš 17.6 °C, Negotin 17.8 °C, Veliko Gradište 17.9 °C.

Average annual maximum air temperatures for the vegetation period in the observed area range from 32.1 °C in Niš to 25.6 °C in Zlatibor. Other values of the average annual air temperature for the vegetation period are shown from the lowest to the highest, namely: Sjenica 25.9 °C, Vranje 30.3 °C, Bujanovac 30.4 °C, Dimitrovgrad 30.4 °C, Kuršumlija 30.6 °C, Požega 30.6 °C, Novi Pazar 30.8 °C, Veliko Gradište 30.9 °C, Kraljevo 31.1 °C, Negotin 31.1 °C, Pirot 31.1 °C, Belgrade 31.3 °C, Loznica 31.3 °C, Smederevska Palanka 31.3 °C, Valjevo 31.3 °C, Jagodina 31.4 °C, Kragujevac 31.4 °C, Zaječar 31.4 °C, Kruševac 31.6 °C, Leskovac 31.6 °C, Ćuprija 31.7 °C, Knjaževac 31.8 °C.

Average annual minimum air temperatures for the vegetation period in the observed area range from -1 °C in Sjenica to 7.1 °C in Belgrade. Other values of the average annual air temperature for the vegetation period are shown from the lowest to the highest, as follows: Zlatibor 2.4 °C, Novi Pazar 2.5 °C, Dimitrovgrad 2.9 °C, Ćuprija 3.2 °C, Kuršumlija 3.2 °C, Požega 3.2 °C, Zaječar 3.4 °C, Bujanovac 3.5 °C, Knjaževac 3.5 °C, Pirot 3.5 °C, Leskovac 3.8 °C, Smederevska Palanka 4 °C, Kruševac 4.2 °C, Vranje 4.4 °C, Kragujevac 4.5 °C, Veliko Gradište 4.5 °C, Kraljevo 4.7 °C, Valjevo 4.7 °C, Jagodina 5 °C, Niš 5 °C, Negotin 5.3 °C, Loznica 5.5 °C.

4. Discussion

Such or similar research, referring to the average annual air temperature, average annual maximum air temperature, and average annual minimum air temperature for the vegetation period in the time interval from 1949 to 2018 has not been done so far in Central Serbia. The obtained results, their differences and similarities were compared with similar results of previous research, whose research subject

is partly the same or similar to the research subject of this scientific study, and they refer to the same observed area, region, European continent, and the world.

With this scientific study, key aspects related to the analyzed climate variables can be highlighted and the followings can be stated. A total of 72 time series were analyzed. Analyses were conducted using trend equations, trend magnitude indicating average increase or decrease in the average annual air temperature, average annual maximum air temperature and average annual minimum air temperature, non-parametric MK test and GIS numerical analysis. The results of the trend equation and trend magnitude indicate an increase in air temperature in most time series. A positive balance was recorded in 66 time series.

Meanwhile, negative balance was recorded in 6 time series. The recorded increase in temperature for the variables mentioned above ranges from 0.2 °C (time series KU-YT-VP, LE-YT-VP, and LE-YTn-VP) to 4.3 °C (time series KZ-YTx-VP). The recorded decrease in air temperature for the variables mentioned above ranges from -0.01 °C (time series DI-YTn-VP) to -0.5 °C (time series DI-YT-VP and VG-YTn-VP) (*Table 2*). The results obtained from the analysis of the MK trend test indicate a positive trend in 53 time series, with a small percentage of risk to reject this claim. No trend was recorded in the remaining 19 time series, with a high percentage of risk to reject this claim (*Figs. 3, 4,* and *5*).

Average annual air temperatures for the vegetation period in the observed area range from 10.6 °C in Dimitrovgrad to 18.1 °C in Belgrade. Average annual maximum air temperatures for the vegetation period in the observed area range from 32.1 °C in Nis to 25.6 °C in Zlatibor. Average annual minimum air temperatures for the vegetation period in the observed area range from -1 °C in Sjenica to 7.1 °C in Belgrade (*Table 2* and *Figs. 5, 6,* and *7*). From the results presented above, it can be concluded that the increase in the average annual air temperature, average annual maximum air temperature, and average annual minimum air temperature for the vegetation period is dominant in Central Serbia.

Similar results were presented in the work of *Bačević et al*. (2021), which refers to the same observed territory. The aforementioned paper uses the same research methodology but deals with a different variable. The differences between these studies lie in the variables: while one analyzed the entire annual period, the other focused on the vegetation period. The results obtained based on the trend equation and trend magnitude indicate an increase in temperature in 70 time series, and a decrease in temperature in the remaining two time series, which is the difference in 4 time series, when it comes to a positive balance. Whereas, in the case where a negative balance occurs, the difference is in 4 time series.

The largest increase in the average air temperature was recorded in the case of the average annual maximum air temperatures for KZ-YTx time series, where the temperature increased by 4.2 °C. This is the same result as in this scientific study, with the exception that the average annual maximum air temperature increased by 4.5 °C. The lowest increase in air temperature was recorded in the case of the average minimum air temperatures (time series ZA-YTn). In this

particular case, an average increase in air temperature of only 0.1 °C was recorded. This differs from the obtained results of this study, where the lowest increase in air temperature of 0.2 °C was recorded in three time series (KU-YT-VP, LE-YT-VP, and LE-YTn-VP).

A decrease in air temperature was recorded in two time series (VR-YTn and VG-YTn), the values of which are -0.6 °C and -0.4 °C, and in this work, this is the case with 6 time series (CU-YTn-VP, DI-YT-VP, DI-YTn-VP, JA-YTx-VP, VG-YTn-VP, and Vr-YTn-VP), whose values range from -0.01 °C to -0.5 °C. (*Tables 2* and *3*). Such differences lie in the number of time series, amounts and range of reduction in the average air temperature. The first case shows a smaller range of values that vary compared to the second case, where the range of obtained values is significantly larger.

Using the MK trend test, the results from the study by *Bačević et al*. (2021) indicate that a positive trend was recorded in 61 time series, while there was no trend in 11 time series. In this paper, the results are somewhat different: a positive trend is observed in 53 time series, while in 19 time series there is no trend. The difference between the results obtained by MK trend test analysis is primarily in the number of time series in which a positive trend is recorded and those in which there is no trend. This means that, in this paper, there is a smaller number of time series (by 8) with a positive trend and a larger number of time series (by 8) with no trend (*Figs. 4* and *8*).

This study can serve as a basis for future research, which would contribute to new additional knowledge about climate changes in the observed territory.

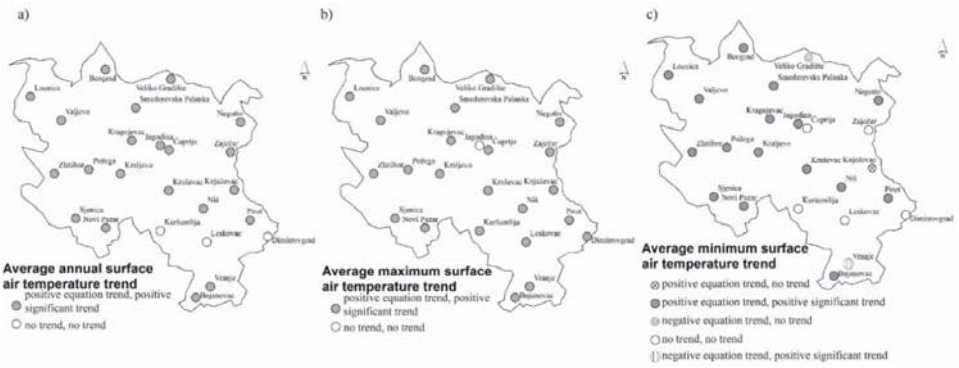

Fig. 8. The results of linear equation trends and MK test: a) average annual surface air temperature; b) average maximum surface air temperature; c) average minimum surface air temperature (*Bačević et al*., 2021).

Table 3. Names of times series, trend equation y, trend magnitude Δy, and probability value p of the confidences for 72 time series (*Bačević et al*., 2021)

Time series	Trend equation	Δy (°C)	Average temperature (°C)
BG-YT	y = 0.0292x + 11.36	2.0	12.1
BG-YT_x	y = 0.0319x + 24.636	2.2	25.8
BG-YT_n	y = 0.0307x + 0.5603	2.1	1.6
BU-YT	y = 0.0157x + 10.481	1.1	11.0
BU-YT_x	y = 0.0363x + 22.988	2.5	24.3
BU-YT_n	y = 0.0237x - 3.1391	1.6	-2.3
CU-YT	y = 0.0131x + 10.747	0.9	11.2
CU-YT_x	y = 0.0358x + 24.629	2.5	25.9
CU-YT_n	y = 0.0065x - 2.5549	0.5	-2.3
DI-YT	y = 0.0085x + 9.7802	0.6	10.1
DI-YT_x	y = 0.0259x + 23.89	1.8	24.8
DI-YT_n	y = 0.0035x - 2.887	0.2	-2.8
JA-YT	y = 0.0204x + 10.954	1.4	11.7
JA-YT_x	y = 0.0027x + 25.412	0.2	25.5
JA-YT_n	y = 0.0438x - 2.3001	3.0	-0.7
KZ-YT	y = 0.0183x + 10.148	1.3	10.8
KZ-Yt_x	y = 0.0611x + 23.941	4.2	26.1
KZ-YT_n	y = 0.0157x - 2.7361	1.1	-2.2
KG-YT	y = 0.0194x + 10.792	1.3	11.5
KG-YT_x	y = 0.0319x + 24.8	2.2	25.9
KG-YT_n	y = 0.0143x - 1.7176	1.0	-1.2
KV-YT	y = 0.0319x + 24.8	1.1	11.4
KV-YT_x	y = 0.0319x + 24.8	1.6	25.6
KV-YT_n	y = 0.0319x + 24.8	1.4	-1.0
KS-YT	y = 0.0178x + 10.666	1.2	11.3
KS-YT_x	y = 0.03x + 24.93	2.1	26.0
KS-YT_n	y = 0.0193x - 2.3684	1.3	-1.7
KU-YT	y = 0.0069x + 10.179	0.5	10.4
KU-YT_x	y = 0.0231x + 24.366	1.6	25.2
KU-YT_n	y = 0.0064x - 2.8218	0.4	-2.6
LE-YT	y = 0.0081x + 10.895	0.6	11.2
LE-YT_x	y = 0.0253x + 25.078	1.7	25.9
LE-YT_n	y = 0.0054x - 2.1455	0.4	-2.0
LO-YT	y = 0.0296x + 10.387	2.0	11.4
LO-YT_x	y = 0.0287x + 25.353	2.0	26.3
LO-YT_n	y = 0.0331x - 1.3454	2.3	-0.2
NG-YT	y = 0.0279x + 10.641	1.9	11.6
NG-YT_x	y = 0.0272x + 24.042	1.9	25.0
NG-YT_n	y = 0.0281x - 1.9027	1.9	-1.0
NI-YT	y = 0.0168x + 11.263	1.2	11.1

Time series	Trend equation	Δy (°C)	Average temperature (°C)
NI-YT_x	y = 0.0235x + 25.561	1.6	26.4
NI-YT_n	y = 0.0185x - 1.0556	1.3	-0.3
NP-YT	y = 0.0405x + 8.1268	2.8	9.5
NP-YT_x	y = 0.0514x + 23.047	3.5	24.9
NP-YT_n	y = 0.0413x - 4.8405	2.8	-3.4
PI-YT	y = 0.0305x + 9.9109	2.1	11.0
PI-YT_x	y = 0.0244x + 24.522	2.1	25.4
PI-YT_n	y = 0.0198x - 2.9205	1.4	-2.2
PZ-YT	y = 0.0207x + 8.8474	1.4	9.6
PZ-YT_x	y = 0.0232x + 24.139	1.6	24.9
PZ-YT_n	y = 0.0239x - 3.7112	1.7	-2.8
SJ-YT	y = 0.0207x + 5.8387	1.4	6.6
SJ-YT_x	y = 0.0371x + 19.309	2.6	20.6
SJ-YT_n	y = 0.0243x - 8.8094	1.7	-8.0
SP-YT	y = 0.0191x + 10.818	1.3	12.0
SP-YT_x	y = 0.0346x + 24.482	2.4	25.7
SP-YT_n	y = 0.0171x - 2.2929	1.2	-1.8
VA-YT	y = 0.0303x + 10.342	2.1	11.4
VA-YT_x	y = 0.0275x + 25.246	2.0	26.2
VA-YT_n	y = 0.041x - 2.4819	2.8	-1.1
VG-YT	y = 0.016x + 10.743	1.1	11.4
VG-YT_x	y = 0.0261x + 23.804	1.8	24.8
VG-YT_n	y = -0.0062x - 0.9246	-0.4	-1.1
VR-YT	y = 0.012x + 10.739	0.8	11.2
VR-YT_x	y = 0.0369x + 23.108	2.6	24.4
VR-YT_n	y = -0.0092x - 0.9409	-0.6	-1.3
ZA-YT	y = 0.0172x + 10.227	1.2	10.8
ZA-YT_x	y = 0.0359x + 24.518	2.5	25.8
ZA-YT_n	y = 0.0011x - 2.6094	0.1	-2.6
ZL-YT	y = 0.0211x + 6.8797	1.5	7.6
ZL-YT_x	y = 0.0437x + 19.045	3.0	20.5
ZL-YT_n	y = 0.0148x - 3.9099	1.0	-3.4

The trends for the average annual air temperature were also analyzed in the papers of *Gavrilov et al*. (2018) and *Milentijević et al*. (2022). The first paper covers the territory of Kosovo and Metohija (southward of the observed area), while the second paper covers the territory of Backa (northward of the observed area). In both papers, trends in the average annual air temperature were analyzed, where a slight increase in air temperature was established, which is confirmed by the trend equation and trend magnitude. The results obtained by the MK trend test

indicate that the H_a hypothesis (positive trend) prevails in most cases. These results match the results of this study, because the distance between the observed meteorological stations is very small.

Similar results were obtained in most of the research conducted in the observed area, showing an increase in the average air temperature and a positive trend. This is consistent with the results of this scientific study (*Bajat et al*., 2015; *Mimić et al*., 2017; *Milentijević et al*., 2021; *Milovanović et al*., 2022b; *Tošić et al*., 2022). Also, the obtained results are in accordance with the research conducted in the region, which coincide with the results of other authors (*Kendrovski* and *Spasenovska*, 2011; *Burić et al*., 2019, 2023; *Milošević et al*., 2017; *Popov et al*., 2019; *Tadić et al*., 2019; *Bačević et al*., 2020, 2022; *Papić et al*., 2020). The results coincide with the findings of other authors who investigated the area of the Balkan Peninsula (*Tsiotas et al*., 2021; *Georgoulias et al*., 2022; *Nikolov* and *Dimitrov*, 2022; *Sakalis*, 2023).

There are also researches that were conducted on the European continent and at the global level, that is, in different parts of the world (*Li et al*., 2013; *Almazroui et al*., 2017; *Fallah-Ghalhari et al*., 2019; *Pasten-Zapata et al*., 2019; *Burić* and *Penjišević*, 2023; *Gentilucci et al*., 2023; *Zareaatkar et al*., 2024). Finally, it is important to mention the official report of the International Panel on Climate Change (IPCC), which also supports these results. These data contribute to the general understanding of climate trends and climate change at local, regional, and global levels.

5. Conclusion

Based on the obtained results of the analyzed variables, as well as the geospatial distribution of the average annual air temperature, average annual maximum air temperature, and average annual minimum air temperature for the vegetation period in the time interval from 1949 to 2018 in the observed area, the following conclusions can be drawn. Necessary data used in this scientific study were taken from meteorological yearbooks of the Republic Hydrometeorological Institute of Serbia, with a total of 24 meteorological stations. Mann-Kendall trend test was used for data processing and trend analysis, for a total of 72 time series. Also, trend equation and trend magnitude were calculated. The geospatial data distribution was done using GIS numerical analysis.

The general conclusion of this scientific study, after the obtained results, is that the average annual air temperature, average annual maximum air temperature, and average annual minimum air temperature for the vegetation period in the territory of Central Serbia are increasing. Based on the trend equation and trend magnitude, an increase in the specified temperatures was recorded in 66 time series, while a decrease in temperature was recorded in 6 time series. The smallest increase of 0.2 °C in the average annual air temperature for the vegetation period

in the observed area was recorded in three time series: KU-YT-VP, LE-YT-VP, and LE-YTn-VP, while the largest increase was recorded in one time series KZ-YTx-VP, and its value is 4.3 °C. The smallest decrease in the average annual air temperature for the vegetation period was recorded in the DI-YTn-VP time series (-0.01 °C), while the largest decrease was recorded in 2 time series, namely: DI-YT-VP and VG-YTn-VP, both with a temperature decrease of -0.5 °C (*Table 2*).

The MK trend test results show that in 53 time series, H_a hypothesis is dominant, where the p value is lower than the significance level α (0.05). On the other hand, there is no trend in the remaining 19 time series, where H_0 hypothesis prevails, with a p value greater than the significance level α (0.05). The geospatial data distribution shows the average air temperature values for each time series individually: a) Average annual air temperatures for the vegetation period in the observed area range from 10.6 °C in Dimitrovgrad to 18.1 °C in Belgrade; b) Average annual maximum air temperatures for the vegetation period in the observed area range from 32.1 °C in Nis to 25.6 °C in Zlatibor; c) Average annual minimum air temperatures for the vegetation period in the observed area range from -1 °C in Sjenica to 7.1 °C in Belgrade (*Fig. 7*). For the entire territory of Central Serbia, the obtained values are as follows. The average annual air temperature for the vegetation period is 16.2 °C. The average annual maximum air temperature for the vegetation period is 30.7 °C. The average annual minimum air temperature for the vegetation period is 3.9 °C.

These results indicate a warming trend in Central Serbia, which may have significant consequences on the local climate and agriculture, as well as on other aspects of the ecosystem (*Mandić et al*., 2022). A decrease in precipitation in some areas, combined with an increase in temperature, may lead to an increased risk of droughts and forest fires (*Bačević et al*., 2024). This indicates the need for adaptation and development of climate change mitigation strategies in this area, as well as in other areas.

Acknowledgement*:* MGR is grateful for L'Oréal-UNESCO For Women in Science award. SBM is grateful for grant F-178 of Serbian Academy of Sciences and Arts. MGR, NT, TT, SBM, and TL gratefully acknowledge the support of the Ministry of Science, Technological Development and Innovation of the Republic of Serbia (Grants No 451-03-137/2025-03/ 200125, 451-03-136/2025-03/200125 & 451-03-65/2024-03/ 200123). Furthermore, SBM and TL emphasize that part of the research was supported by the Program of Cooperation with the Serbian Scientific Diaspora – Joint Research Projects – DIASPORA 2023, from the Science Fund of the Republic of Serbia, under the project LAMINATION (The Loess Plateau Margins: Towards Innovative Sustainable Conservation), Project number: 17807.

References

Ahmed, N., Wang, G., Booij, M.J., Ceribasi, G., Bhat, M.S., Ceyhunlu, A I., and *Ahmed, A.,* 2022: Changes in monthly streamflow in the Hindukush–Karakoram–Himalaya Region of Pakistan using innovative polygon trend analysis. *Stoch Environ Res Risk Assess 36,* 811–830. https://doi.org/10.1007/s00477-021-02067-0.

Almazroui, M., Islam, M.N., Saeed, F., Alkhalaf, A.K., and *Dambul, R.,* 2017: Assessing the robustness and uncertainties of projected changes in temperature and precipitation in AR5 Global Climate Models over the Arabian Peninsula, *Atmosph. Res. 194,* 202–213. https://doi.org/10.1016/j.atmosres.2017.05.005

Bajat, B., Blagojevic, D., Kilibarda, M., Luković, J., and *Tošić, I.,* 2015: Spatial Analysis of the Temperature Trends in Serbia during the Period 1961–2010. *Theor. Appl. Climatol. 121,* 289–301. https://doi.org/10.1007/s00704-014-1243-7

Bačević, R.N., Vukoičić, Z.D., Nikolic, M., Janc, N., Milentijević, N., and *Gavrilov, B.M*., 2017: Arid ityin Kosovo and Metohija, Serbia. *Carpathian J. Earth Environ. Sci. 12*, 563–570.

Bačević, R.N., Pavlović, M., and *Rasljanin, I.,* 2018: Trend Assessing Using Mann-Kendall's Test for Pristina Meteorological Station Temperature and Precipitation Data, Kosovo and Metohija, Serbia. *The University Thought - Publication in Natural Sciences (8)2,* 39-43. https://doi.org/10.5937/univtho8-19513

Bačević, R.N., Valjarević, A., Milentijević, N., Kicovic, D., Ivanovic, M., and *Mujevic, M.,* 2020: Analysis of air temperature trens: City of Podgorica (Montenegro). *Univ. Thought – Publ. Nat.Sci. 10(1),* 31–36. https://doi.org/10.5937/univtho10-24790

Bačević, R.N., Milentijević, M.N., Valjarević, A., Gicic, A., Kicovic, D., Radaković, M., Nikolic, M. and *Pantelic, M*., 2021: Spatio-temporal variability of air temperatures in Central Serbia from 1949 to 2018. *Időjárás 125*, 229–253. https://doi.org/10.28974/idojaras.2021.2.4

Bačević, R.N., Milentijević, M.N., Valjarević, A., Nikolic, M., Stevanovic, V., Kicovic, D., Radaković, G.M., Papić, D. and *Markovic, B.S*., 2022: The analysis of annual and seasonal surface air temperature of southern and southeastern Bosnia and Hercegovina from 1961 to 2017. *Időjárás 126*, 355–374. https://doi.org/10.28974/idojaras.2022.3.5

Bačević, R.N., Valjarević, A., Nikolic, M., Stevanovic, V., Dragojlovic, J., Radaković, G.M., Kicovic, D., Markovic, S.R., Markovic, B.S. and *Lukic, T*., 2024: Determination of changes in the total amount of precipitation using the Mann-Kendall trend test in Central Serbia for the period from 1949 to 2018. *Időjárás 128*, 451–472. https://doi.org/10.28974/idojaras.2024.4.4

Bačević, R.N., Radaković, G.M., Nikolic, M., Valjarević, A., Stevanovic, V., Kicovic, D., Bozovic, R., Markovic, S.R., Markovic, B.S. and *Lukic, T.,* 2025: Precipitation during the vegetation period in Central Serbia during 70 years. *Időjárás 129*, 107–140. https://doi.org/https://doi.org/10.28974/idojaras.2025.2.1

Bartoszek, K. and *Kaszewski, B.M.,* 2022: Changes in the frequency and temperature of air masses over east-central Europe. *Int. J. Climatol. 42(16),* 8214–8231. https://doi.org/10.1002/joc.7704

Baumgertel, A., Lukic, S., Cakovic, M., Lazic, I., Tošić, M., Momirovic, N., Pandey, S., Bezdan, A., Blagojevic, B., and *Djurdjevic, V*., 2024: Spatio-Temporal Analysis of Vegetation Response to Climate Change, Case Study: Republic of Serbia. *Int. J. Environ. Res. 18*(12). https://doi.org/10.1007/s41742-024-00571-z

Birara, H., Pandey, R.P., and *Mishra, S.K.,* 2018: Trend and variability analysis of rainfall and temperature in the Tana basin region, Ethiopia. *J. Water Climate Change 9,* 555–569. https://doi.org/10.2166/wcc.2018.080

Burić, D., Luković, J., Ducic, V., Dragojlovic, J., and *Doderovic, M.,* 2014: Recent trends in daily temperature extremes over southern Montenegro (1951–2010). *Nat. Hazards Earth Syst. Sci.14,* 67–72. https://doi.org/10.5194/nhess-14-67-2014

Burić, D., Ducic, V., Mihajlovic, J., Luković, J. and *Dragojlovic, J.,* 2015: Recent extreme air temperature changes in Montenegro. *Bull. Serbian Geograph. Soc. 95(4),* 53-66. https://doi.org/10.2298/GSGD140626002B

Burić, B.D., Dragojlovic, M.J., Milenkovic, M., Popovic, Z.Lj. and *Doderovic, M.M.,* 2018: Influence of variability of the East Atlantic Oscillation on the air temperature in Montenegro. *Thermal Sci. 22(1B),* 759-766. https://doi.org/10.2298/TSCI170710211B

Burić, D., Dragojlovic, J., Penjisevic-Socanac, I., Luković, J. and *Doderovic, M.,* 2019: Relationship Between Atmospheric Circulation and Temperature Extremes in Montenegro in the Period 1951–2010. In:(eds. *Leal Filho W., Trbić G., Filipovic D*.) Climate Change Adaptation in Eastern Europe. Climate Change Management. Springer, Cham. https://doi.org/10.1007/978-3-030-03383-5_3

Burić, D. and *Penjisevic, I.,* 2023: Southern Hemisphere temperature trend in association with greenhouse gases, El Niño Southern Oscillation, and Antarctic Oscillation. *Időjárás 127,* 23–42. https://doi.org/10.28974/idojaras.2023.1.2

Burić, D., Mihajlovic, J., Ducic, V., Milenkovic, M., and *Andjelkovic, G.* 2023: Contribution to the study of climate change in Serbia using continentality, oceanity, and aridity indices. *Időjárás 127,* 379–399. https://doi.org/10.28974/idojaras.2023.3.6

Caloiero, T., 2018: SPI trend analysis of New Zealand applying the ITA technique. *Geosciences 8(3),* 101. https://doi.org/10.3390/geosciences8030101

Ceyhunlu, A.I. and *Ceribasi, G.,* 2024. Changes in precipitation and air temperature over Turkey using innovative trend pivot analysis method. *J. Water Climate Change 15,* 2446–2463. https://doi.org/10.2166/wcc.2024.041

Chervenkov, H. and *Slavov, K.* 2021: Assessment of agrometeorological indices over Southeast Europe in the context of climate change (1961-2018). *Időjárás, 125,* 255–269. https://doi.org/10.28974/idojaras.2021.2.5

Fallah-Ghalhari, G., Shakeri, F., and *Dadashi-Roudbari, A.,* 2019: Impacts of climate changes on the maximum and minimum temperature in Iran. *Theor. Appl. Climat. 138,* 1539–1562. https://doi.org/10.1007/s00704-019-02906-9

Gavrilov, M.B., Markovic, S.B., Jarad, A. and *Korac, V.M.,* 2015: The analysis of temperature trends in Vojvodina (Serbia) from 1949 to 2006. *Thermal Sci. 19,* 339–350. https://doi.org/10.2298/TSCI150207062G

Gavrilov, M.B., Tošić, I., Markovic, S.B., Unkašević, M., and *Petrovic, P.,* 2016: The analysis of annual and seasonal temperature trends using the Mann-Kendall test in Vojvodina, Serbia. *Időjárás 122,* 203–216.

Gavrilov, M.B., Markovic, S.B., Janc, N., Nikolic, M., Valjarević, A., Komac, B., Zorn, M., Punisic, M., and *Bačević, N*., 2018: Assessing average annual air temperature trends using the Mann– Kendall test in Kosovo. *Acta Geographica Slovenica 58*, 8–25. https://doi.org/10.3986/AGS.1309

Gavrilov, M.B., Lukic, T., Janc, N., Basarin, B., and *Markovic, S.B.,* 2019: Forestry Aridity Index in Vojvodina, North Serbia. *Open Geoscie. 11,* 367–377. https://doi.org/10.1515/geo-2019-0029

Gentilucci, M., Domenicucci, S., Barbieri, M., Hamed, Y., Hadji R., Missaoui, R. and *Pambianchi, G.,* 2023: Spatial Effects of NAO on Temperature and Precipitation Anomalies in Italy. *Water* 15*(21),* 3727. https://doi.org/10.3390/w15213727

Georgoulias, K.A., Akritidis, D., Kalisoras, A., Kapsomenakis, J., Melas, D., Zerefos, S.C. and *Zanis, P.,* 2022: Climate change projections for Greece in the 21st century from high-resolution EURO-CORDEX RCM simulations. *Atmospheric Research 271,* 1–28. https://doi.org/10.1016/j.atmosres.2022.106049

Gocic, M. and *Trajković, S.,* 2013: Analysis of changes in meteorological variables using Mann Kendall and Sen's slope estimator statistical tests in Serbia. *Glob. Planet. Change 100,* 172–182. https://doi.org/10.1016/j.gloplacha.2012.10.014

Gocic, M. and *Trajković, S.,* 2014a: Drought Characterisation Based on Water Surplus Variability Index. *Water Res. Manage. 28,* 3179–3191. https://doi.org/10.1007/s11269-014-0665-4

Gocic, M. and *Trajković, S.,* 2014b: Spatiotemporal characteristics of drought in Serbia. *J. Hydrology 510,* 110–123. https://doi.org/10.1016/j.jhydrol.2013.12.030

Gulev, S.K., Latif, M., Keenlyside, N., Park, W. and *Koltermann, P.,* 2013: North Atlantic Ocean Control on Surface Heat Flux at Multidecadal Timescales. *Nature 499,* 464–467, https://doi.org/10.1038/nature12268

Hajas, C. and *Zempléni, A.,* 2020: Dependent weighted bootstrap for European temperature data: is global warming speeding up? *Időjárás 124,* 349–361. https://doi.org/10.28974/idojaras.2020.3.3

Hamlet, A.F., Mote, P.W., Clark, M.P. and *Lettenmaier, D.P.,* 2005: Effects of temperature and precipitation variability on snowpack trends in the western United States. *J. Climate 18(21),* 4545–4561. https://doi.org/10.1175/JCLI3538.1

Hrnjak, I., Lukic, T., Gavrilov, M.B., Markovic, S.B., Unkašević, M. and *Tošić, I*., 2014: Aridity in Vojvodina, Serbia. *Theor. Appl. Climatol. 115*, 323–332. https://doi.org/10.1007/s00704-013-0893-1

Hua, T., Wang, X., Zhang, C., and *Lang, L.,* 2013: Temporal and spatial variations in the Palmer Drought Severity Index over the past four centuries in arid, semiarid, and semi-humid East Asia. *Chin. Sci. Bull. 58,* 4143–4152. https://doi.org/10.1007/s11434-013-5959-z

http://www.hidmet.gov.rs/ciril/meteorologija/klimatologija_godisnjaci.php (accessed 25 May 2023) http://www.xlstat.com/en/ (accessed 27 October 2023)

IPCC, 2022: Climate Change 2022: Mitigation of Climate Change. Contribution of Working Group III to the Sixth Assessment Report of the Intergovernmental Panel on Climate Change; *Shukla, P.R., Skea, J., Slade, R., al Khourdajie, A., van Diemen, R., McCollum, D., Pathak, M., Some, S., Vyas, P., Fradera, R., Eds.;* Cambridge University Press: Cambridge, UK; New York, NY, USA.

Kabanda, T., 2018: Long-term rainfall trends over the Tanzania coast. *Atmosphere 9,* 155. https://doi.org/10.3390/atmos9040155

Kendall, M.G., 1975: Rank correlation methods. Charles Griffin, London.

Kendrovski, V. and *Spasenovska, M.,* 2011: The Effects on Health of Climate Change in the Republic of Macedonia. [online] pp. 31–76. Ministry of Health: Skopje, the Former Yugoslav Republic of Macedonia. Available from: http://www.un.org.mk/en-publications-full/items/theeffects-on-health-of-climate-change-in-the-republic-of-macedonia.pdf [Accessed on 26 March 2021]

Li, Q., Chen, Y., Shen, Y., Li, X. and *Xu, J.,* 2011: Spatial and temporal trends of climate change in Xinjiang, China. *J. Geograph. Sci. 21,* 1007–1018. https://doi.org/10.1007/s11442-011-0896-8

Li, Z., Wei, Z.G., Lv, S.H., Han, B., Ao, Y.H., and *Chen, H.,* 2013: Verifications of surface air temperature and precipitation from CMIP5 model in Northern Hemisphere and Qinghai-Xizang Plateau. *Plateau Meteorol. 32,* 921.

Lornezhad, E., Ebrahimi, H. and *Rabieifar, H.R.,* 2023: Analysis of precipitation and drought trends by a modified Mann–Kendall method: a case study of Lorestan province, Iran. *Water Supply 23(4),* 1557–1570. https://doi.org/10.2166/ws.2023.068

Luković J., Burić D., Ducic V., Doderovic M. and Milevski I., 2013: Assessment on Temperature Extremes in Montenegro. In: (eds. *Helmis C., Nastos P*.) Advances in Meteorology, Climatology and Atmospheric Physics. Springer Atmospheric Sciences. Springer, Berlin, Heidelberg. https://doi.org/10.1007/978-3-642-29172-2_82

Luković, J., Burić, D., Mihajlovic, J., and *Pejovic, M.* 2024: Spatial and temporal variations of aridity-humidity indices in Montenegro. *Theor. Appl Climatol 155(6)*, 4553–4566. https://doi.org/10.1007/s00704-024-04893-y

Malik, A. and *Kumar, A.* 2020: Spatio-temporal trend analysis of rainfall using parametric and non-parametric tests: Case study in Uttarakhand, India. *Theor. Appl. Climatol. 140,* 183–207. https://doi.org/10.1007/s00704-019-03080-8

Mallick, J., Talukdar, S., Alsubih, M., Salam, R., Ahmed, M., Kahla, N. and *Shamimuzzaman, M.,* 2021: Analysing the trend of rainfall in Asir region of Saudi Arabia using the family of Mann-Kendall tests, innovative trend analysis, and detrended fluctuation analysis. *Theor. Appl. Climatol. 143,* 823–841. https://doi.org/10.1007/s00704-020-03448-1

Malinović-Milicević, S., Radovanovic. M.M., Stanojevic, G. and *Milovanović, B.,* 2016: Recent changes in Serbian climate extreme indices from 1961 to 2010. *Theor. Appl. Climatol. 124,* 1089–1098. https://doi.org/10.1007/s00704-015-1491-1

Mandić, M. V., Vimic, A. V., Rankovic-Vasic, Z., Djurovic, D., Cosic, M., Sotonica, D., Nikolic, D., and Djurdjevic, V. 2022: Observed changes in climate conditions and Weather-Related risks in fruit and grape production in Serbia. Atmosphere, 13(6), 948. https://doi.org/10.3390/atmos13060948

Mann, H.B., 1945: Nonparametric tests against trend. *Econometrica 13,* 245–259.

Martínez-Austria, P.F. Bandala, E.R. and *Patiño-Gómez, C.,* 2016: Temperature and heat wave trends in northwest Mexico. *Physics and Chemistry of the Earth 91,* 20–26. https://doi.org/10.1016/j.pce.2015.07.005

Minetti, J.L., Vargas, W.M., Poblete, A.G., de la Zedra, L.R. and *Acuña , L.R.,* 2010: Regional droughts in southern South America. *Theor. Appl. Climatol. 102(3-4),* 403–415. https://doi.org/10.1007/s00704-010-0271-1

Milentijević, N., Dragojlovic, J., Ristic, D., Cimbaljevic, M., Demirovic, D. and Valjarević, A., 2018: The assessment of aridity in Leskovac Basin, Serbia (1981-2010). *J. Geograph. Inst. "Jovan Cvijic" 68*, 249–264.

Milentijević, N., Bačević, R.N., Ristic, D., Valjarević, A., Pantelic, M. and *Kicovic, D.,* 2020: Application of Mann-Kendal (MK) test in trend analysis of air temperature and precipitation: Case of Macva district (Serbia). *Univ. Thought – Publ. Nat.Sci. 10(1),* 37–43. https://doi.org/10.5937/univtho10-24774

Milentijević, N., Bačević, N., Valjarević, A., Radaković, M., and *Pantelic, M.,* 2021: Assessment of air temperature and precipitation trends: Case study of Macva (Serbia). The 5th Serbian congress of geographers. Novi Sad, Serbia. https://doi.org/10.13140/RG.2.2.35542.16965

Milentijević, N., Valjarević, A., Bačević, R.N., Ristic, D., Kalkan, K., Cimbaljevic, M., Dragojlovic, J., Savic, S. and *Pantelic, M.*, 2022: Assessment of observed and projected climate changes in Backa (Serbia) using trend analysis and climate modeling. *Időjárás 126*, 47–68. https://doi.org/10.28974/idojaras.2022.1.3

Milovanović, B., Stanojevic, G., and *Radovanovic, M.* 2022a: Climate of Serbia. The Geography of Serbia: Nature, People, Economy, 57-68. https://doi.org/10.2298/IJGI2103333J

Milovanović, B., Schubert, S., Radovanovic, M., Vakanjac, V.R. and *Schneider, C.,* 2022b: Projected changes in air temperature, precipitation and aridity in Serbia in the 21st century. *Int. J Climatol. 42,* 1985–2003. https://doi.org/10.1002/joc.7348

Milošević, D., Savic, S. and *Ziberna, I.,* 2013: Analysis of the climate change in Slovenia: Fluctuations of meteorological parameters for the period 1961–2011 (Part I). *Bull. Serbian Geograph. Soc. 93,* 1–14. https://doi.org/10.2298/GSGD1301001M

Milošević, D., Savic, S., Stankov, U., Ziberna, I., Pantelic, M., Dolinaj, D., and *Lescesen, I.,* 2017: Maximum temperatures over Slovenia and their relationship with atmospheric circulation patterns. *Geografie 122,* 1–20. https://doi.org/10.37040/geografie2017122010001

Mimić, G., Mihailovic, D.T. and *Kapor, D.,* 2017: Complexity analysis of the air temperature and the precipitation time series in Serbia. *Theor. Appl. Climatol. 127,* 891–898 https://doi.org/10.1007/s00704-015-1677-6

Nikolov, D. and *Dimitrov, C.,* 2022: Analysis of the variability of the winter precipitations and temperatures in two mountain regions of Bulgaria. International conference: 22nd SGEM International Multidisciplinary Scientific GeoConference 2022, ISSN 1314-2704, 22 (4.1), https://doi.org/10.5593/sgem2022/4.1/s19.35

O'Neil, H.C.L., Prowse, T.D., Bonsal, B.R. and *Dibike, Y.B.,* 2017: Spatial and temporal characteristics in streamflow-related hydroclimatic variables over western Canada. Part 1: 1950–2010. *Hydrology Research 48(4),* 915–931. https://doi.org/10.2166/nh.2016.057

Papić, D., Bačević, R.N., Valjarević, A., Milentijević, N., Gavrilov, B.M., Zivkovic, M., and *Markovic, B.S.,* 2020: Assessment of air temperature trends in South and Southeast Bosnia and Herzegovina (B&H) from 1961 to 2017. *Időjárás 124,* 381–399. https://doi.org/10.28974/idojaras.2020.3.5

Pasten-Zapata, E., Sonnenborg, O.T. and *Refsgaard, J.,* 2019: Climate change: Sources of uncertainty in precipitation and temperature projections for Denmark. *Geological Survey of Denmark and Greenland Bulletin 43,* 1–6. https://doi.org/10.34194/GEUSB-201943-01-02

Pavlović, M. A. 2019a: Geografske Regije Srbije 1 Panonska Makroregija. Univerzitet u Beogradu, Geografski Fakultet, Beograd. (In Serbian)

Pavlović, M. A. 2019b: Geografske Regije Srbije 2 Planinsko-Kotlinsko-Dolinska Makroregija. *Univerzitet u Beogradu, Geografski Fakultet*, Beograd. (In Serbian)

Popov, T., Gnjato, S. and *Trbić, G.,* 2017: Trends in extreme temperatures indices in Bosnia and Herzegovina: A case study of Mostar. *Herald 21,* 107–132. https://doi.org/10.7251/HER2117107P

Popov, T., Gnjato, S. and *Trbić, G.,* 2018a: Changes in temperature extremes in Bosnia and Herzegovina: A fixed treshold-based index analysis. *J. Geograph. Inst. "Jovan Cvijic" SASA 68,* 17–33. https://doi.org/10.2298/IJGI1801017P

Popov, T., Gnjato, S., Trbić, G., and *Ivanisevic, M.,* 2018b: Recent trends in extreme temperature indices in Bosnia and Herzegovina. *Carpathian J. Earth Environ. Sci. 13,* 211–224. https://doi.org/10.26471/cjees/2018/013/019

Popov, T., Gnjato, S. and *Trbić, G.,* 2019: Changes in extreme temperature indices over the Peripannonian region of Bosnia and Herzegovina. *Geografie 124,* 19–40. https://doi.org/10.37040/geografie2019124010019

Putniković, S., Tošić, I., Lazic, L. and *Pejanovic, G.,* 2018: The influence of the large-scale circulation patterns on temperature in Serbia. *Atmosph. Res. 213,* 465–475. https://doi.org/10.1016/j.atmosres.2018.07.003

Radaković, G.M., Tošić, A.I., Bačević ,R.N., Mladjan, D., Markovic S.B., and *Gavrilov M.B*., 2018: The analysis of aridity in Central Serbia from 1949-2015. Theoretical and Applied Climatology 133(3-4), 887-898. https://doi.org/10.1007/s00704-017-2220-8

Radilović, S., Koracin, D., Denamiel, C., Belusic, D., Güttler, I. and *Vilibic, I.,* 2020: Simulated andobserved air temperature trends in the eastern Adriatic. *Atmosph. Sci. Lett. 21,* 951. https://doi.org/10.1002/asl.951

Razavi, T., Switzman, H., Arain, A. and *Coulibaly, P.* 2016: Regional climate change trends and uncertainty analysis using extreme indices: A case study of Hamilton, Canada. *Climate Risk Management, 13,* 43–63.

Sakalis, D.V., 2023: Trend analysis of the annual and seasonal temperature series in the Eastern Coast of Peloponnese (Greece). *Arabian J. Geoscie. 16(11),* 610. https://doi.org/10.1007/s12517-023-11713-6

Tadić, L., Brlekovic, T., Hajdinger, A., and *Spanja, S.,* 2019: Analysis of the Inhomogeneous Effect of Different Meteorological Trends on Drought: An Example from Continental Croatia. *Water 11(12),* 2625. https://doi.org/10.3390/w11122625

Tošić, I., Zorn, M., Ortar, J., Unkašević, M., Gavrilov, M.B. and *Markovic, S.B.,* 2016: Annual and seasonal variability of precipitation and temperatures in Slovenia from 1961 to 2011. *Atmosph.Res. 168,* 220–233. https://doi.org/10.1016/j.atmosres.2015.09.014

Tošić, I., Putniković, S., Tošić, M. and *Lazic, I.,* 2021: Extreme temperature events in Serbia in relation to atmospheric circulation. *Atmosphere 12(12),*1584. https://doi.org/10.3390/atmos12121584

Tošić, I., Tošić, M., Lazic, I., Aleksandrov, N., Putniković, S. and *Djurdjevic, V.,* 2022: Spatio-temporal changes in the mean and extreme temperature indices for Serbia. *Int. J Climatol. 43,* 2391–2410. https://doi.org/10.1002/joc.7981

Trajković, S., Gocic, M., Misic, D. and *Milanovic, M.,* 2020: Spatio-Temporal Distribution of Hydrological and Meteorological Droughts in the South Morava Basin. In: (*eds. Gocic M., Aronica G., Stavroulakis G. & Trajković S.*) Natural Risk Management and Engineering.Springer Tracts in Civil Engineering. *Springer*, Cham. https://doi.org/10.1007/978-3-030-39391-5_11

Trbić, G., Popov, T. and *Gnjato, S.,* 2017: Analysis of air temperature trends in Bosnia and Herzegovina. *Geographica Pannonica 21,* 68–84. https://doi.org/10.5937/GeoPan1702068T

Tsiotas, G., Mamara, A., Argiriou A. and *Tsoukala, K.A.,* 2021: Testing mean air temperature trends in southern Greece: A Bayesian approach. *Int. J. Climatol. 42,* 4989–5015. https://doi.org/10.1002/joc.7516

Unkašević, M. and *Tošić, I.,* 2013: Trends in temperature indices over Serbia: relationships to large-scale circulation patterns. *Int. J. Climatol. 33,* 3152–3161. https://doi.org/10.1002/joc.3652

Unkašević, M. and *Tošić, I.,* 2015: Seasonal analysis of cold and heat waves in Serbia during the period 1949–2012. *Theor. Appl. Climatol 120,* 29–40. https://doi.org/10.1007/s00704-014-1154-7

Vukoičić, Z.D., Milosavljevic, A.S., Penjisevic, T.I., Bačević, R.N., Nikolic, M., Ivanovic, D.R. and *Jandzikovic, M.B.,* 2018: Spatial analysis of temperature and its impact on the sustainable development of mountain in Central and Western Serbia. *Időjárás 122,* 259–283. https://doi.org/10.28974/idojaras.2018.3.3

Zeraatkar, Z., Shahidi, A. and *Memarian, H.,* 2024: Assessment and efficiency of CMIP6 models in simulation and prediction of climatic parameters of precipitation and temperature in the Samalghan basin, Iran. *Időjárás 128,* 59–75. https://doi.org/10.28974/idojaras.2024.1.4

Zeroual, A., Meddi, M. and *Bensaad, S.,* 2013: The impact of climate change on river flow in arid and semi-arid rivers in Algeria. *Hydrology Res. 48(2),* 584–595. https://doi.org/10.2166/nh.2016.244

Zivanovic, S., Gocic, M. and *Tošić, I.,* 2024: Vulnerability of Central Serbian national parks to wildfires. *Időjárás 128,* 99–120. https://doi.org/10.28974/idojaras.2024.1.6

DOI:10.28974/idojaras.2026.1.2

IDŐJÁRÁS

Quarterly Journal of the HungaroMet Hungarian Meteorological Service
Vol. 130, No. 1, January – March, 2026, pp. 29–43

Effects of Southern Oscillation and North Sea-Caspian Pattern on the rainfall intensity series in the Black Sea Region of Türkiye

Aslı Ulke Keskin[1], **Reza Kazembeigi**[1], and **Utku Zeybekoglu**[2, *]

[1]*Faculty of Engineering, Ondokuz May University, 55139, Atakum, Samsun, Türkiye*

[2]*Boyabat Vocational School of Higher Education, Sinop University, 57200 Boyabat, Sinop, Türkiye*

**Corresponding author E-mail: utkuz@sinop.edu.tr*

(Manuscript received in final form June 24, 2024)

Abstract— This study investigates the influence of the Southern Oscillation and North Sea-Caspian Pattern on maximum rainfall intensities in the Black Sea Region of Türkiye. Annual maximum rainfall intensity series from 16 meteorological stations were analyzed, and correlation coefficients were calculated and evaluated at $\alpha = 0.01$, 0.05, and 0.10 significance levels. Results indicate that the Southern Oscillation predominantly affects short- and medium-duration rainfall in Sinop, whereas the North Sea-Caspian Pattern shows significant correlations with medium- and long-duration rainfall in Bartın, Bayburt, and Gümüşhane. These findings highlight the spatially varying influence of atmospheric oscillations on rainfall extremes in the region.

Key-words: Southern Oscillation, North Sea-Caspian Pattern, rainfall intensity; atmospheric oscillation; Türkiye

1. Introduction

Climate refers to the long-term average of atmospheric parameters observed in a specific region. It encompasses not only average conditions but also statistically significant variations, which distinguish climate from weather, defined as instantaneous atmospheric states. To characterize a region's climate, statistical analyses of at least 30-year records of variables such as temperature, precipitation,

wind direction and intensity, relative humidity, and sea level pressure are required. Climate change should be expressed as meaningful long-term variations rather than daily fluctuations, while extreme weather events may reflect or result from such changes (*Sen*, 2019). Recent attention to climate change stems from its wide-ranging effects on human life, socio-economic conditions, and environmental systems.

Hydrometeorology, which bridges hydrology and meteorology, plays a critical role in planning and managing water resources by assessing changes in precipitation, temperature, humidity, evaporation, and river flow, as well as their drivers. With ongoing global climate change, studies utilizing these hydrometeorological parameters have gained increasing importance, as they inform both resource management and disaster mitigation strategies.

The variability of climate parameters is partly influenced by local and global atmospheric circulations. Some circulation patterns exhibit periodic behaviors that can affect regions at large distances simultaneously. Such teleconnections, including the Southern Oscillation (SO) and the North Sea-Caspian Pattern (NCP), represent large-scale atmospheric interactions with significant hydrometeorological impacts (Hurrell et al., 2003). Numerous studies have investigated the influence of atmospheric oscillations on hydrometeorological variables. For example, temperature has been linked to SO and NCP phases (*Türkeş*, 1990; *Kutiel et al.*, 2002; *Türkeş* and *Erlat*, 2008; *Iqbal et al.*, 2016; *Sezen* and *Partal*, 2019; *Hassan* and *Al-Asadi*, 2023), precipitation has shown correlations with SO, North Atlantic Oscillation (NAO), and NCP (*Rodo et al.*, 1997; *Ropelewski* and *Halpert*, 1987; *Kadıoğlu et al.*, 1999; *Chowdhury* and *Beechem*, 2010; *Givati* and *Rosenfeld*, 2013; *West et al.*, 2021; *Hosseini et al.*, 2022), and river flow has also been associated with these indices (*Cullen et al.*, 2002; *Zhang et al.*, 2007; *Karabork* and *Kahya*, 2009; *Tabari et al.*, 2014).

Previous research has revealed that the SO affects precipitation patterns across the Pacific basin (Ropelewski and Halpert, 1987), while NAO and SO modulate seasonal precipitation in Southern Europe, particularly in autumn and winter (*Rodo et al.*, 1997). *Halpert* and *Ropelewski* (1992) reported stronger SO-related temperature effects in tropical regions, excluding the Western Pacific. Petriello (1999) linked sea level pressure, temperature, and precipitation to NAO phases in Europe, America, and Africa, whereas *Hurrell* and *van Loon* (1997) demonstrated that decadal climate variability is influenced by NAO indices. Studies focusing on NCP have also shown region- and season-specific effects on temperature and precipitation (*Ghasemi* and *Khalili*, 2008; *Brunetti* and *Kutiel*, 2011; *del Rio et al.*, 2013; *Nastos et al.*, 2011; *Talaee et al.*, 2014).

Türkiye's climate is influenced by both maritime and continental air masses, as well as low- and high-pressure systems, including Iceland, Siberia, Azores, and Basra lows (*Göktürk* and *Karaca*, 2006). Several atmospheric oscillations, such as NAO, Arctic Oscillation (AO), SO, and NCP, have been shown to significantly affect Türkiye's hydrometeorological variables (*Kahya* and *Karabörk*, 2001;

Türkeş and *Erlat*, 2003; *Kalaycı et al.*, 2004; *Göktürk*, 2005; *Karabörk et al.*, 2005, 2007; *Kutiel* and *Türkeş*, 2005; *Kerimoğlu*, 2008; *Marti et al.*, 2010; *Özturk et al.*, 2011; *Tosunoglu et al.*, 2018; *Partal*, 2018; *Yarbaşı* and *Marti*, 2019; *Akkoyunlu et al.*, 2019; *Yilmaz et al.*, 2020; *Sezen* and *Partal*, 2020; *Demir* and *Koc*, 2021; *Kebapcioglu* and *Partal*, 2022). In particular, ENSO events have been shown to alter precipitation regimes in southern Türkiye (*Kadıoğlu et al.*, 1999), while NAO and SO influence river flows in central and eastern regions (*Cullen* and *deMenocal*, 2000; *Kahya* and *Karabork*, 2001; *Turkes* and *Erlat*, 2003; *Göktürk*, 2005; *Kutiel* and *Türkeş*, 2005; *Karabörk* and *Kahya*, 2009; *Bozyurt* and *Özdemir*, 2017; *Tosunoglu et al.*, 2018; *Sezen* and *Partal*, 2019).

Despite extensive research on atmospheric oscillations and hydrometeorological variables, few studies have examined the relationship between extreme rainfall intensities and oscillation indices (*Lepore et al.*, 2016; *Gehlot et al.*, 2021; *Salameh et al.*, 2022; *An et al.*, 2023; *Ulke Keskin et al.*, 2024). Therefore, this study focuses on evaluating the influence of SO and NCP on annual maximum rainfall intensities across the Black Sea Region of Türkiye. By analyzing these relationships, the study aims to contribute to the understanding of extreme precipitation events, which is critical for flood risk assessment, water resource planning, and regional climate adaptation strategies.

This paper is structured as follows: Section 1 provides the general background and motivation for this study, Section 2 introduces the atmospheric indices, Section 3 presents the data sources, Section 4 details the analysis methods, Section 5 evaluates the results, and Section 6 provides the conclusions.

2. Atmospheric indices

2.1. Southern Oscillation (SO)

The Southern Oscillation (SO) is a large-scale oscillation that expresses the exchange of atmospheric pressure between the western and eastern parts of the Pacific Ocean at tropical latitudes. SO is considered the most notable sign of interannual climatic changes. The extreme phases of this oscillation are known as El Niño and La Niño events. El Niño events correspond to higher-than-normal atmospheric pressure in the southeast Pacific. La Niña events, on the other hand, express the opposite conditions of El Niño events (*Karabork* and *Kahya*, 2009; *Tosunoglu*, 2014; *Tosunoglu et al.*, 2018).

The Southern Oscillation Index (SOI) expresses the pressure difference between the western and eastern Pacific and is defined as the difference between the standardized sea level atmospheric pressure in Tahiti and the sea level atmospheric pressure in Darwin (Australia). SOI refers to the pressure difference between the eastern and western Pacific. When the SOI value, which is positive under normal conditions, drops to negative values, the atmospheric pressure in the eastern Pacific decreases and eastern trades weaken or blow from the west (*Kahya*

and *Dracup*, 1993; *Tosunoglu*, 2014; *Tosunoglu et al.*, 2018). For more details, please refer to *Ropelewski* and *Jones* (1987), *Allan et al.* (1991), and *Können et al.* (1998).

2.2. North Sea-Caspian Pattern (NCP)

The North Sea-Caspian Pattern by *Kutiel* and *Benaroch* (2002), one around the North Sea, the other around the Caspian Sea, is defined as the large-scale atmospheric pressure fluctuation between two regions (*Kutiel* and *Benaroch*, 2002). *Kutiel* and *Benaroch* (2002) revealed the North Sea-Caspian Pattern Index (NCPI). They used this index to indicate the magnitude of the North Sea-Caspian Pattern. When the NCPI is in the positive phase, the negative pressure in the center of the Caspian Sea causes a counterclockwise movement, whereas the pressure in the center of the North Sea causes a clockwise movement. As a result of these two movements, the cold and dry air mass affects the Eastern Mediterranean region from Russia. When the NCPI is in the negative phase, a hot and rainy weather occurs, unlike the situation in the positive phase, and the effect of this air mass is seen in the regions from the South to the Mediterranean. The North Sea-Caspian Pattern generally shows its effect in autumn, winter, and spring, while in summer, its effect is less than the effects of the others (*Tosunoglu*, 2014; *Tosunoglu et al.*, 2018). For more details, please refer to van *Kutiel* and *Benaroch* (2002), *Kutiel et al.* (2002) and *Kutiel* and *Turkes* (2005).

3. Materials

The Black Sea Region of Türkiye, which receives the highest annual precipitation in the country, plays a critical role in human activities and water resources (*Yilmaz et al.*, 2020). The eastern part of the region experiences particularly heavy rainfall (*Gürgen*, 2004). Geographically, the region is located between 40°–42° N latitude and 30°–42.5° E longitude, covering approximately 135000 km², about 18% of Türkiye's total area.

The North Anatolian Mountains, extending parallel to the coast, largely determine the region's topography and climate. Kaçkar Peak, the highest point at 3932 m, is located in the eastern part. Mountain slopes create differences in climate between coastal and inland areas: coastal zones are humid with moderated temperatures due to the sea, whereas inland areas experience lower humidity and greater temperature variation. However, the central part of the Black Sea region allows partial penetration of the sea effect due to relatively lower altitudes (*Turak et al.*, 2011).

Annual maximum rainfall intensity series (mm/min) for 14 standard durations—5', 10', 15', 30', 60', 120', 180', 240', 300', 360', 480', 720', 1080', and 1440'—were recorded at 16 meteorological stations operated by the Turkish State Meteorological Service (TSMS) in the Black Sea Region. For classification

purposes, 5–30-minute rainfalls are considered short-term, 60–360-minute rainfalls medium-term, and 480–1440-minute rainfalls long-term (*Karahan*, 2011, 2019; *Zeybekoglu* and *Karahan*, 2018). *Table 1* lists the stations, their coordinates, altitude, and record periods, while *Figure 1* shows their geographical distribution.

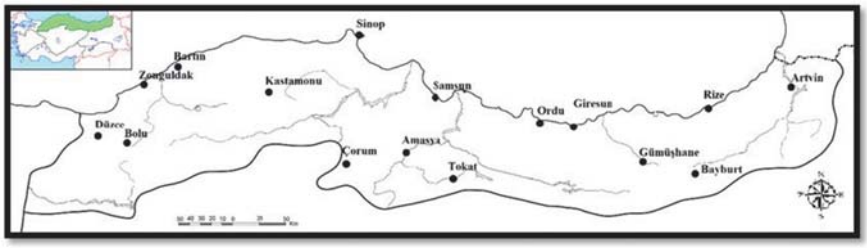

Fig. 1. Spatial distribution of meteorological stations throughout Black Sea Region Türkiye

Table 1. Meteorological observation stations and their records periods in the Black Sea Region

Station Name	Record period	Altidute (m)	Longitude (N)	Latitude (E)
Amasya	1965-2015	40	40.667	35.835
Çorum	1958-2015	776	40.546	34.936
Ordu	1965-2015	5	40.984	37.886
Samsun	1957-2015	4	41.344	36.255
Sinop	1965-2015	32	42.03	35.155
Tokat	1966-2015	611	40.331	36.558
Artvin	1965-2015	613	41.175	41.819
Bolu	1949-2015	743	40.733	31.602
Kastamonu	1948-2015	800	41.371	33.776
Rize	1940-2015	3	41.040	40.501
Düzce	1965-2015	146	40.844	31.149
Giresun	1966-2015	38	40.923	38.388
Bartın	1966-2015	33	41.625	32.357
Bayburt	1966-2015	1584	40.255	40.221
Gümüşhane	1966-2015	1216	40.460	39.465
Zonguldak	1945-2015	135	41.449	31.778

4. Methodology

In this study, the Pearson correlation coefficients were calculated to distinguish between the atmospheric oscillation index and the rainfall intensity (*Bayazıt* and *Oğuz*, 2005):

$$r_{X,Y} = \frac{\sum(x_i - \bar{x})(y_i - \bar{y})}{N S_X S_y} \quad (1)$$

where x_i is the value of the rainfall intensity in the *i*th year of the timeseries, $\bar{x}$ is the average of rainfall intensity, y_i is the *i*th value of the atmospheric oscillation index (AOI), $\bar{y}$ is the average of AOI, N represents the number of data, S_X is the standard deviation value of the rainfall intensity, and S_Y is the standard deviation of the tmospheric oscillation index data.

After obtaining the correlation coefficients the significance levels of $\alpha = 0.01$, $\alpha = 0.05$ and $\alpha = 0.1$ were evaluated by using Student's t-test. The correlation breakpoints were obtained with the distribution (*Bayazıt* and *Oğuz*, 2005):

$$t = \frac{r\sqrt{N-2}}{\sqrt{1-r^2}}, \quad (2)$$

where t represents the test statistic, r represents the correlation value, and N represents the number of data.

5. Results of the relationship between rainfall intensities and atmospheric indices

The correlation coefficients between rainfall intensities and the SO and the NCP indices at the 16 meteorological stations in the Black Sea Region are presented in *Tables 2* and *3*. For each standard duration, correlations were tested for significance at $\alpha = 0.01$, 0.05, and 0.1 using the Student's t-test. Significant correlations are illustrated in Figures 2 and 3, where upward triangles indicate positive correlations and downward triangles indicate negative correlations, with red, blue, and green corresponding to $\alpha = 0.01$, 0.05, and 0.1, respectively. Non-significant correlations are not displayed.

Table 2. Correlation coefficients between SO and rainfall intensities (5'indicates 5-minute rainfall, and so forth)

Station	5'	10'	15'	30'	60'	120'	180'	240'	300'	360'	480'	720'	1080'	1440'
Amasya	-0.11	-0.14	-0.10	-0.05	-0.03	0.00	0.05	0.12	0.15	0.17	0.19	0.22	0.17	0.16
Çorum	-0.13	-0.05	-0.03	0.03	0.06	0.11	0.10	0.08	0.08	0.07	0.06	0.07	0.05	0.06
Ordu	0.09	0.20	0.11	0.15	0.09	0.07	0.11	0.13	0.17	0.21	0.18	0.16	0.18	0.16
Samsun	-0.02	0.03	0.03	0.06	0.01	0.03	0.04	0.03	0.04	0.04	0.06	0.09	0.07	0.05
Sinop	0.35	0.36	0.33	0.30	0.23	0.22	0.22	0.27	0.27	0.27	0.26	0.28	0.22	0.12
Tokat	-0.16	-0.16	-0.15	-0.11	-0.12	-0.09	-0.08	-0.05	-0.04	-0.02	-0.04	-0.04	0.07	0.19
Artvin	0.16	0.23	0.25	0.23	0.21	0.20	0.19	0.19	0.20	0.21	0.19	0.20	0.20	0.28
Bolu	0.03	0.03	0.03	0.06	0.05	0.06	0.06	0.04	0.04	0.03	0.01	0.01	0.02	-0.05
Kastamonu	0.01	-0.03	-0.01	0.00	-0.02	-0.03	-0.03	-0.02	-0.01	0.01	0.01	0.01	0.04	-0.07
Rize	-0.03	-0.06	-0.05	-0.14	-0.20	-0.22	-0.19	-0.15	-0.10	-0.07	-0.08	-0.07	-0.06	-0.08
Düzce	-0.07	-0.03	-0.04	-0.07	-0.07	-0.06	-0.04	-0.03	-0.03	-0.01	-0.01	0.01	0.04	0.09
Giresun	0.06	0.04	0.04	0.01	0.03	0.06	0.05	0.05	0.05	0.06	0.04	0.03	0.00	0.03
Bartın	0.01	0.02	0.04	-0.05	-0.03	-0.04	-0.02	0.03	0.03	0.04	0.10	0.11	0.07	0.09
Bayburt	0.00	-0.02	-0.01	-0.02	-0.04	-0.11	-0.16	-0.19	-0.20	-0.21	-0.24	-0.25	-0.22	-0.22
Gümüşhane	-0.08	-0.09	-0.07	-0.06	-0.07	-0.09	-0.10	-0.10	-0.09	-0.09	-0.11	-0.11	-0.12	-0.03
Zonguldak	0.11	0.10	0.10	0.09	0.06	0.05	0.04	0.05	0.06	0.07	0.06	0.06	0.06	0.07

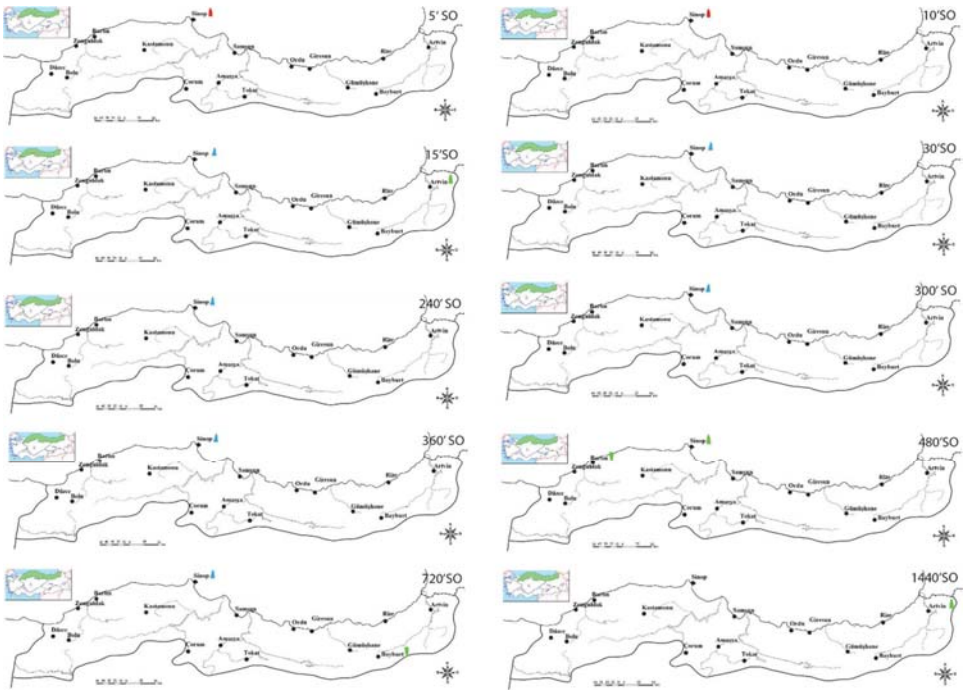

Fig. 2. Spatial distribution of correlation between SO and rainfall intestiy series of 14 standard durations in the Black Sea Region Türkiye.

According to *Table 2* and *Fig. 2*, significant correlations between rainfall intensities and SO were predominantly observed at Sinop, indicating that higher SO index values generally lead to increased rainfall. Short-term rainfalls (5–30 minutes) displayed positive correlations at $\alpha = 0.01$ for 5' and 10', and at $\alpha = 0.05$ for 15' and 30'. For medium-term rainfalls (60–360 minutes), significant positive correlations were found at $\alpha = 0.05$ for 240', 300', and 360', and at $\alpha = 0.1$ for 60' and 480'. Long-term rainfalls (480–1440 minutes) showed significant correlations at $\alpha = 0.05$ for 720', and at $\alpha = 0.1$ for 360', 480', and 1440'.

Other stations also showed occasional significant correlations. Artvin had positive correlations at $\alpha = 0.1$ for 15' and 1440' durations, while Bayburt showed a negative correlation at $\alpha = 0.1$ for 720'. No significant correlations were observed for 120' and 180' rainfalls across most stations. These results suggest that the influence of SO is highly localized, with Sinop showing the most consistent response across multiple rainfall durations. Short-duration rainfalls tend to be more consistently affected, whereas medium- and long-duration rainfalls show sporadic correlations in other stations, likely due to local topography and regional climatic conditions.

Table 3. Correlation coefficients between NCP and rainfall intensities (5'indicates 5-minute rainfall, and so forth)

Station	5'	10'	15'	30'	60'	120'	180'	240'	300'	360'	480'	720'	1080'	1440'
Amasya	0.00	-0.02	-0.01	0.06	0.10	0.09	0.08	0.07	0.08	0.10	0.12	0.08	0.03	-0.03
Çorum	-0.11	-0.07	-0.08	-0.02	0.00	0.02	0.06	0.07	0.08	0.08	0.09	0.06	0.04	-0.05
Ordu	0.05	0.09	0.14	0.10	0.16	0.09	0.09	0.07	0.08	0.09	0.08	0.08	0.12	0.19
Samsun	0.14	0.14	0.03	0.02	0.01	-0.02	-0.04	-0.04	-0.03	-0.06	-0.02	0.00	-0.01	0.00
Sinop	0.00	-0.01	-0.02	-0.01	0.01	-0.06	-0.09	-0.10	-0.11	-0.12	-0.16	-0.20	-0.16	-0.13
Tokat	0.06	0.14	0.11	0.10	0.13	0.11	0.13	0.12	0.11	0.06	0.10	0.10	-0.08	-0.28
Artvin	0.15	0.24	0.19	0.08	-0.01	-0.09	-0.12	-0.10	-0.05	0.04	0.12	0.15	0.17	0.33
Bolu	0.00	0.03	0.06	0.10	0.07	0.07	0.11	0.12	0.14	0.18	0.19	0.27	0.20	0.12
Kastamonu	0.06	0.12	0.16	0.14	0.10	0.06	0.05	0.04	0.07	0.08	0.07	0.01	-0.01	0.04
Rize	-0.10	-0.16	-0.12	-0.13	-0.23	-0.20	-0.17	-0.13	-0.11	-0.14	-0.15	-0.18	-0.18	-0.21
Düzce	0.02	0.12	0.13	0.09	0.10	0.07	0.06	0.04	-0.04	-0.07	-0.09	-0.08	-0.01	0.02
Giresun	-0.20	-0.20	-0.20	-0.14	-0.07	-0.02	-0.06	-0.09	-0.11	-0.11	-0.15	-0.16	-0.11	-0.09
Bartın	0.03	0.06	0.10	-0.14	-0.08	-0.10	-0.05	0.08	0.08	0.12	0.28	0.30	0.20	0.26
Bayburt	0.00	-0.05	-0.04	-0.04	-0.11	-0.31	-0.45	-0.51	-0.55	-0.57	-0.65	-0.68	-0.60	-0.60
Gümüşhane	-0.21	-0.25	-0.20	-0.15	-0.18	-0.24	-0.28	-0.28	-0.25	-0.25	-0.29	-0.29	-0.33	-0.08
Zonguldak	0.21	0.20	0.21	0.18	0.12	0.10	0.08	0.10	0.13	0.14	0.12	0.12	0.11	0.15

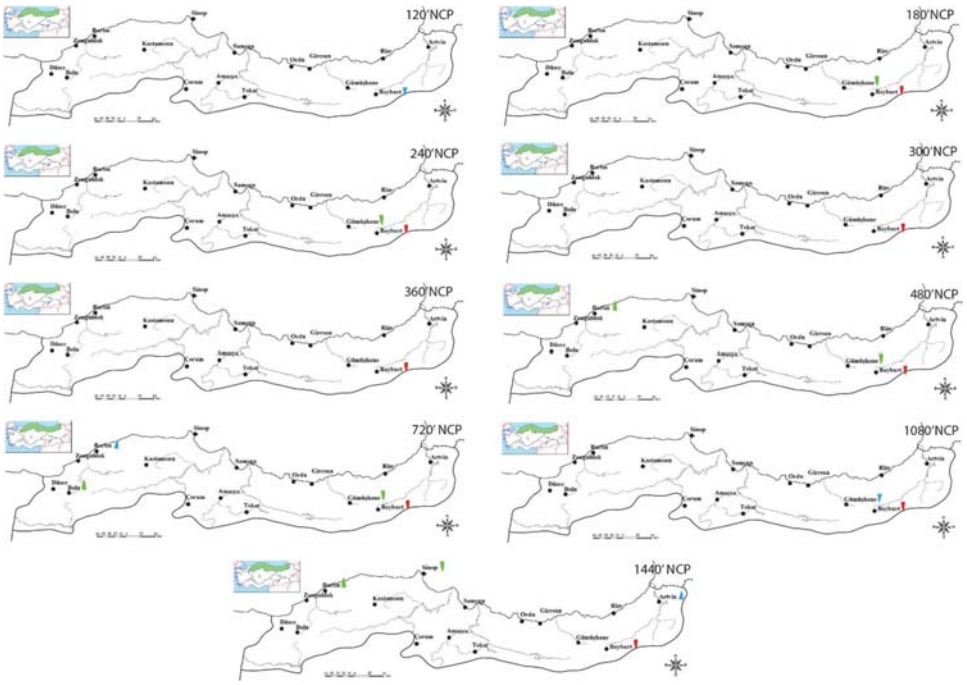

Fig. 3. Spatial distribution of correlation between NCP and rainfall intestiy series of 14 standard durations in the Black Sea Region ofTürkiye.

According to *Table 3* and *Fig. 3*, Significant correlations with NCP were mainly observed at Bartın, Gümüşhane, and Bayburt, predominantly affecting medium- and long-term rainfall durations. Short-duration rainfalls (5–60 minutes) did not show significant correlations. For medium-term rainfalls: 120' rainfall showed negative correlation in Bayburt ($\alpha = 0.05$); 180' rainfalls had negative correlations in Gümüşhane ($\alpha = 0.1$) and Bayburt ($\alpha = 0.01$); 240' rainfalls were negatively correlated in Gümüşhane ($\alpha = 0.1$) and Bayburt ($\alpha = 0.01$); 300' and 360' rainfalls were negatively correlated in Bayburt at $\alpha = 0.01$.

Long-term rainfalls also displayed station-specific correlations. At 480', positive correlation was observed in Bartın ($\alpha = 0.1$), negative in Gümüşhane ($\alpha = 0.1$) and Bayburt ($\alpha = 0.01$). For 720' rainfalls, Bartın showed positive correlation ($\alpha = 0.05$), Bayburt negative ($\alpha = 0.01$), and Gümüşhane positive at $\alpha = 0.1$. At 1080', a negative correlation was found in Gümüşhane ($\alpha = 0.05$). For 1440', negative correlations were observed in Bayburt ($\alpha = 0.01$) and Artvin ($\alpha = 0.05$), while Tokat and Bartın showed negative and positive correlations, respectively, at $\alpha = 0.1$.

These patterns indicate that NCP predominantly influences medium- and long-duration rainfalls, with positive correlations in Bartın and negative

correlations in Bayburt and Gümüşhane. The differences in sign and significance across stations highlight the spatial variability of NCP effects, likely modulated by elevation, topography, and distance from the coast.

6. Discussion and conclusion

This study examined the effects of atmospheric oscillations on rainfall intensities in the Black Sea Region of Türkiye, focusing on the SO and the NCP indices. The analysis of 16 meteorological stations revealed that SO primarily affects Sinop, while NCP shows significant correlations in Bartın, Bayburt, and Gümüşhane. These findings are consistent with previous studies demonstrating that Türkiye's hydrometeorological parameters are sensitive to large-scale atmospheric oscillations (*Turkes* and *Erlat*, 2003; *Karabork* and *Kahya*, 2003, 2009; *Kutiel* and *Turkes*, 2005; *Tosunoglu et al.*, 2018; *Sezen* and *Partal*, 2019, 2020).

The results indicate that SO generally intensifies rainfall in Sinop across short-, medium-, and some long-term durations, whereas its effect on other stations is limited or absent. This aligns with previous findings suggesting that the impact of SO on precipitation is often highly localized and influenced by local topography and coastal effects (*Kahya* and *Karabork*, 2001; *Karabork* and *Kahya*, 2009; Ç*akıroglu et al.*, 2017). On the other hand, NCP predominantly affects medium- and long-duration rainfall in the eastern and northern parts of the region, with positive correlations in Bartın and negative correlations in Bayburt and Gümüşhane, reflecting the spatial heterogeneity of NCP influence. This is consistent with earlier studies showing that NCP impacts temperature and precipitation patterns differently across regions due to elevation, proximity to the coast, and local climatological conditions (*Kutiel* and *Turkes*, 2005; *Göktürk*, 2005; *Çakıroglu et al.*, 2017; *Tosunoglu et al.*, 2018).

These findings have important implications for hydrometeorology and water resource management in the Black Sea Region. Understanding the relationships between atmospheric oscillations and rainfall intensities can contribute to better planning for flood risk, water supply, and disaster management. For instance, stations showing consistent positive correlations with SO or NCP may experience intensified precipitation under certain atmospheric conditions, which could increase the risk of floods or landslides. Incorporating these indices into predictive models could improve the forecasting of extreme rainfall events and support proactive measures in local disaster preparedness strategies (*Celik et al.*, 2020; *Gunduz*, 2022; *Usta*, 2023).

This study also highlights the need for further regional analyses across Türkiye. By extending similar investigations to other geographic regions, researchers can better understand the spatial variability of atmospheric oscillation effects and their contributions to climate change and extreme weather events.

Moreover, evaluating rainfall intensity along with other hydrometeorological variables, such as temperature, humidity, and flow, may provide a more comprehensive understanding of regional climate dynamics.

In conclusion, the study demonstrates that atmospheric oscillations play a significant and duration-dependent role in shaping rainfall intensities in the Black Sea Region. SO primarily affects short- and medium-duration rainfalls in Sinop, while NCP influences medium- and long-duration rainfalls in Bartın, Bayburt, and Gümüşhane, with both positive and negative correlations depending on the station. These insights are valuable for climate-related risk assessment, water resource management, and disaster mitigation strategies, and contribute to the national and international literature by focusing on rainfall intensity, which is a critical parameter for understanding extreme hydrological events.

Data availability: Rainfall data provided by the Turkish State Meteorological Service (TSMS) can be purchased from https://mevbis.mgm.gov.tr/mevbis/ui/index.html#/Workspace, (Purchase number: 20171010D771).

Author contributions: AUK: investigation, methodology, supervision, validation and writing (original draft, review and editing). RK: investigation, methodology, formal analysis and writing (original draft, review and editing). UZ: data curation, investigation, methodology, formal analysis, validation, visualization, supervision and writing (original draft, review and editing).

Competing interests: The authors declare that none of the authors has any competing interests.

Acknowledgements: The authors thank the Turkish State Meteorological Service for providing the meteorological data. The authors also thank the reviewers for their constructive criticisms which have considerably improved this manuscript.

References

Akkoyunlu, B.O., Baltaci, H., and *Tayanc, M.,* 2019: Atmospheric conditions of extreme precipitation events in western Turkey for the period 2006–2015. *Nat. Hazards Earth Syst. Sci. 19,* 107–119. https://doi.org/10.5194/nhess-19-107-2019

Allan, R. J., Nicholls, N., Jones, P., and *Butterworth, I.J.,* 1991: A Further Extension of the Tahiti-Darwin SOI, Early ENSO Events and Darwin Pressure. *J. Climate 4(7)*, 743–749. https://doi.org/10.1175/1520-0442(1991)004<0743:afeott>2.0.co;2

An, D., Eggeling, J., Zhang, L., He, H., Sapkota, A., Wang, Y.C., and *Gao, C.,* 2023: Extreme precipitation patterns in the Asia–Pacific region and its correlation with El Ni˜ no- Southern Oscillation (ENSO). *Sci. Rep. 13(1)*, 12. https://doi.org/10.1038/s41598- 023-38317-0

Bayazıt, M., and *Yeğen Oğuz, E.B.*, 2005: Mühendisler İçin İstatistik (Üçüncü Baskı), Birsen Yayınevi, İstanbul, Çağlayan (in Turkish).

Bozyurt O., and *Özdemir, M.A.*, 2017: Arctic Oscillation's Many Years Trends and the Effects of Arctic Oscillation Over Minimum Mean Temperature Values in Turkey. *Afyon Kocatepe University Journal of Social Sciences 19(1),* 123–135 (in Turkish). https://doi.org/10.5578/jss.54124

Brunetti, M., and *Kutiel, H.*, 2011: The relevance of the North-Sea Caspian Pattern (NCP) in explaining temperature variability in Europe and the Mediterranean. *Nat. Haz. Earth Syst. Sci. 11(10),* 2881–2888. https://doi.org/10.5194/nhess-11-2881-2011

Chowdhury, R., and *Beecham, S.,* 2010: Australian rainfall trends and their relation to the southern oscillation index. *Hydrological Proc. 24(4),* 504–514. https://doi.org/10.1002/hyp.7504

Cullen, H.M., and *Demenocal, P.B.,* 2000: North Atlantic influence on Tigris–Euphrates streamflow. *Int. J. Climatol. 20(8),* 853–863. https://doi.org/10.1002/1097-0088(20000630)20:8<853::AID-JOC497>3.0.CO;2-M

Cullen, H.M., Kaplan, A., and *Arkin, P.A.,* 2002: Impact of the North Atlantic Oscillation on Middle Eastern climate and streamflow. *Climatic Change 55(3),* 315–338. https://doi.org/10.1023/A:1020518305517

Çakıroglu, E.M., Cevher, N.K., and *Ağırbaş, E.,* 2017: The Meteorological Investigation of Turkish Coasts of the Black Sea. *Journal of Anatolian Environ. Animal Sci. 2(3),* 53–58 (in Turkish). https://doi.org/10.35229/jaes.358566

Çelik, İ.H., Usta, G., Yılmaz, G., and *Yakupoğlu, M.,* 2020: An Assessment on the Technological Disasters Experienced in Turkey (Between the Years of 2000-2020). *ACU International Journal of Social Sciences 6(2),* 49–57 (in Turkish). https://doi.org/10.22466/acusbd.776580

del Rio, S., Iqbal, M.A., Cano-Ortiz, A., Herrero, L., Hassan, A., and *Penas, A.,* 2013: Recent mean temperature trends in Pakistan and links with teleconnection patterns. *Int. J. Climatol. 33(2),* 277–290. https://doi.org/10.1002/joc.3423

Demir, U.S., and *Koc, A.C.,* 2021: Investigation of the North Atlantic Oscillation and Indian Ocean Dipole Influence on Precipitation in Turkey with Cross-Spectral Analysis. *Atmosphere 12*, 99. https://doi.org/10.3390/atmos12010099

Fendeková, M., Pekárová, P., Fendek, M., Pekár, J., and *Škoda, P.,* 2014: Global drivers effect in multi-annual variability of runoff. *J. Hydrol. Hydrometeorol. 62,* 169–176. https://doi.org/10.2478/johh-2014-0027

Gehlot, L.K., Jibhakate, S.M., Sharma, P.J., Patel, P.L., and *Timbadiya, P.V.,* 2021: Spatio-temporal variability of rainfall indices and their teleconnections with El Ni˜ no- Southern Oscillation for Tapi Basin, India. *Asia-Pac. J. Atmos. Sci. 57*, 99–118. https://doi.org/10.1007/s13143-020-00179-1

Ghasemi, A., and *Khalili, D.,* 2008: The effect of the North Sea-Caspian pattern (NCP) on winter temperatures in Iran. *Theor. Appl Climatol. 92(1),* 59–74. https://doi.org/10.1007/s00704-007-0309-1

Givati, A., and *Rosenfeld, D.,* 2013: The Arctic Oscillation, climate change and the effects on precipitation in Israel. *Atmospheric Research 132,* 114–124. http://dx.doi.org/10.1016/j.atmosres.2013.05.001

Gundüz, F., 2022: Lessons Learned from the Perspective of Women and Gender in Disasters, The Case of Haiti, and Japan Earthquake. *IBAD Journal of Social Sciences 12,* 440-460 (in Turkish). https://doi.org.tr/10.21733/ibad.1039215

Gürgen, G., 2004: The Maximum Rainfalls in the Eastern Black Sea Region and their Importance in terms of Floods. *Gazi University Journal of Gazi Educational Faculty 24(2)*, 79-92 (in Turkish).

Göktürk, O.M., and *Karaca, M.,* 2006: *North Sea–Caspıan Pattern And Its Influence On Thehydrometeorologıcal Parameters Over Basıns Of The Gap Regıon*. Proceedings of the Fifth GAP Engineering Congress, 26–28 April, Şanlıurfa, Türkiye (in Turkish).

Göktürk, O.M., 2005: *North Sea-Caspian pattern and its influence on the hydrometeorological parameters over Turkey*. Master Thesis, Istanbul Technical University, Eurasia Institute of Earth Sciences, 53, İstanbul.

Halpert, M.S., and *Ropelewski C.F.,* 1992: Surface temperature patterns associated with the Southern Oscillation. *Journal of Climate 5(6),* 577–593. https://doi.org/10.1175/1520-0442(1992)005<0577:STPAWT>2.0.CO;2

Hassan, M.W., and *Al-Asadi, K.A.W.H.,* (2023): Analysis of large-scale correlations on temperatures over Iraq. *Arab Gulf Journal of Scientific Research 41(1),* 2-17. https://doi.org/10.1108/AGJSR-05-2022-0046

Hosseini, S.M., Kashki, A., and *Karami, M.,* 2022: Analysis of the North Atlantic Oscillation Index and rainfall in Iran. *Model. Earth. Syst. Environ. 8*, 3647–3656. https://doi.org/10.1007/s40808-021-01309-y

Hurrell, J.W., Kushnir, Y., Ottersen, G., and *Visbeck, M.,* 2003: An Overview Of The North Atlantic Oscillation: Climatic Significance And Environmental Impact. *Geophysical Monograph 134,* 1–35. https://doi.org/10.1029/134GM01

Hurrell, J.W., and *van Loon, H.,* 1997: Decedal Variations In Climate Associated With The North Atlantic Oscillation. *Climatic Change 36,* 301-326. https://doi.org/10.1023/A:1005314315270

Iqbal, M.A., Penas, A., Cano-Ortiz, A., Kersebaum, K., Herrero, L., and *del Rio S.,* 2016: Analysis of recent changes in maximum and minimum temperatures in Pakistan. *Atmospheric Research 168,* 234–249. https://doi.org/10.1016/j.atmosres.2015.09.016

Kadioglu, M., Tulunay, Y., and *Borhan, Y.,* 1999: Variability of Turkish precipitation compared to El Nino events. *Geophys. Res. Lett. 26(11),* 1597–1600. https://doi.org/10.1029/1999GL900305

Kahya, E., and *Dracup, J.A.,* 1994: The influences of type I ENSO and La Niña events on streamflows in the southwestern United States. *Journal of Climate 7(6),* 965–976. http://dx.doi.org/10.1175/1520-0442(1994)007%3C0965:TIOTEN%3E2.0.CO;2

Kahya, E., and *Karabork, M.C.,* 2001: The analysis of El Nino and La Nina signals in streamflows of Turkey. *Int. J. Climatol. 21(10),* 1231–1250. https://doi.org/10.1002/joc.663

Kalaycı, S., Karabörk, M.Ç., and *Kahya, E.,* 2004: Analysis of el nino signals on turkish streamflow and precipitation patterns using spectral analysis. *Fresenius Environ. Bull. 13(8),* 719–725.

Karabork, M.C., and *Kahya, E.,* 2009: The links between the categorised Southern Oscillation indicators and climate and hydrologic variables in Turkey. *Hydrol. Process. 23(13),* 1927–1936. https://doi.org/10.1002/hyp.7331

Karabork, M.C., and *Kahya, E.,* 2003: The teleconnections between the extreme phases of the southern oscillation and precipitation patterns over Turkey. *Int. J. Climatol. 23(13),* 1607–1625. https://doi.org/10.1002/joc.958

Karabörk, M.Ç., Kahya, E., and *Karaca, M.,* 2005: The influences of the Southern and North Atlantic Oscillations on climatic surface variables in Turkey. *Hydrol. Process. 19,* 1185–1211. https://doi.org/10.1002/hyp.5560

Karabörk, M.Ç., Kahya, E., and *Kömüşcü, İ.A.,* 2007: Analysis of Turkish precipitation data: homogeneity and the Southern Oscillation forcings on frequency distributions. *Hydrol. Process. 21,* 3203–3210. https://doi.org/10.1002/hyp.6524

Karahan, H., 2011: Determination of Rainfall Intensity-Duration-Frequency Relationships Using Differential Evolution Algorithm. 108Y299, Research Project, The Scientific and Technological Research Council of Turkey (TUBITAK), Final Report, Ankara, Türkiye (in Turkish).

Karahan, H., 2019: Determination of homogeneous sub-regions by using intensity-duration-frequency relationships and cluster analysis: an application for the Aegean Region. *Pamukkale University J. Eng. Sci. 25(8),* 998–1013 (in Turkish). https://doi.org/10.5505/pajes.2019.09365

Kebapcioglu, E. and *Partal, T.,* 2022: The Impacts of Global Atmospheric Oscillations on Büyük Menderes and Gediz Streamflows. *J. Nat. Haz. Environ. 8(1)*, 1–13 (in Turkish). https://doi.org/10.21324/dacd.910666

Kerimoğlu, O., 2008: Influence of large scale atmospheric systems on Hydrology and ecology of Turkish lakes. Master Thesis, Middle East Technıcal Unıversity, Ankara.

Können, G.P., Jones, P.D., Kaltofen, M.H. and *Allan, R.J.,* 1998: Pre-1866 extensions of the Southern Oscillation Index using early Indonesian and Tahitian meteorological readings. *J. Climate 11(9)*, 2325–2339. https://doi.org/10.1175/1520-0442(1998)011%3C2325:PEOTSO%3E2.0.CO;2

Kutiel, H., and *Benaroch, Y.,* 2002: North Sea–Caspian Pattern (NCP)—an upper level atmospheric teleconnection affecting the eastern Mediterranean: identification and definition. *Theor. Appl Climatol. 71(1–2),* 17–28. https://doi.org/10.1007/s704-002-8205-x

Kutiel, H., Maheras, P., Turkes, M., and *Paz, S.,* 2002: North Sea–Caspian Pattern (NCP)—an upper level atmospheric teleconnection affecting the eastern Mediterranean: implications on the regional climate. *Theor. Appl Climatol. 72(3-–4),* 173–192. https://doi.org/10.1007/s00704-002-0674-8 .

Kutiel, H., and *Turkes, M.,* 2005: New evidence for the role of the North Sea—Caspian Pattern on the temperature and precipitation regimes in continental central Turkey. *Geografiska Annaler: Series A, Physical Geography 87(4),* 501–513. https://doi.org/10.1111/j.0435-3676.2005.00274.x

Marti, A.I., Yerdelen, C., and *Kahya, E.,* 2010: Enso modulatıons on streamflow characterıstıcs. *Earth Scı. Res. J. 14(1)*, 31–43.

Lepore, C., Allen, J.T., and *Tippett, M.K.,* 2016: Relationships between hourly rainfall intensity and atmospheric variables over the contiguous United States. *J. Clim. 29 (9)*, 3181–3197. https://doi.org/10.1175/JCLI-D-15-0331.1

Nastos, P., Philandras, C., Founda, D., and *Zerefos, C.,* 2011: Air temperature trends related to changes in atmospheric circulation in the wider area of Greece. *Int. J. Remote Sens. 32(3),* 737–750. https://doi.org/10.1080/01431161.2010.517796

Öztürk, T., Türkeş, M., and *Kurnaz, M.L.,* 2011: Analysing Projected Changes in Future Air Temperature and Precipitation Climatology of Turkey by Using RegCM4.3.5 Climate Simulations. *Aegean Geographical J. 20(1),* 17–27.

Partal, T., 2018: Wavelet based periodical analysis of the precipitation data of the Mediterranean Region and its relation to atmospheric indices. *Model. Earth. Syst. Environ. 4,* 1309–1318. https://doi.org/10.1007/s40808-018-0505-2

Petriello, P., 1999: *The North Atlantic Oscillation 1959-1998: A Data Study*. Master Thesis, Faculty of Graduate Studies and Research in partial fiilfilment of the requirements, Montreal, Kanada.

Rodo, X., Baert, E., and *Comin, F.,* 1997: Variations in seasonal rainfall in Southern Europe during the present century: relationships with the North Atlantic Oscillation and the El Niño-Southern Oscillation. *Climate Dynamics 13(4),* 275–284. https://doi.org/10.1007/s003820050165

Ropelewski, C.F., and *Halpert, M.S.,* 1987: Global and regional scale precipitation patterns associated with the El Niño/Southern Oscillation. *Month. Weather Rev. 115(8),* 1606–1626. https://doi.org/10.1175/1520-0493(1987)115<1606:GARSPP>2.0.CO;2

Salameh, A.A.M., Ojeda, M.G.V., Esteban-Parra, M.J., Castro-Díez, Y., and *G´amiz-Fortis, S.R.,* 2022: Extreme rainfall indices in southern levant and related large-scale atmospheric circulation patterns: a spatial and temporal analysis. *Water 14*, 3799. https://doi.org/10.3390/w14233799

Sen, Z., 2009: *İklim Değişikliği Tatlı Su Kaynakları ve Türkiye*. Su Vakfı Yayınları, 1–12, İstanbul, Türkiye (in Turkish).

Sezen, C., and *Partal, T.,* 2020: The effects of Mediterranean oscillation on temperature and precipitation data in Turkey. *J. Water Climate Change 11(3),* 722–743. https://doi.org/10.2166/wcc.2019.192

Sezen, C., and *Partal, T.,* 2019: The impacts of Arctic oscillation and the North Sea Caspian pattern on the temperature and precipitation regime in Turkey. *Meteorol. Atmospheric Phys. 131,* 1677–1696. https://doi.org/10.1007/s00703-019-00665-w

Tabari, H., Abghari, H., and *Talaee, P.H.,* 2014: Impact of the North Atlantic Oscillation on streamflow in western Iran. *Hydrol. Proces. 28(15),* 4411–4418. https://doi.org/10.1002/hyp.9960

Talaee, P.H., Tabari, H., and *Ardakani, S.S.,* 2014: Hydrological drought in the west of Iran and possible association with large-scale atmospheric circulation patterns. *Hydrol. Proces. 28(3),* 764–773. https://doi.org/10.1002/hyp.9586

Tosunoglu, F., 2014: Investıgatıng the relatıonshıp between atmospherıc oscıllatıons and meteorologıcal and hydrologıcal droughts. PhD thesis, Atatürk University, Erzurum, Turkey.

Tosunoğlu, F., Can, İ., and *Kahya, E.,* 2018: Evaluation of spatial and temporal relationships between large-scale atmospheric oscillations and meteorological drought indexes in Turkey. *Int. J. Climatol. 38(12),* 4579–4596. https://doi.org/10.1002/joc.5698

Turak, A., Balkız, Ö., Ambarlı, D., Durmuş, M., Özkil, A., Yalçın, S., Özüt, D., Kınıkoğlu, Y., Meydan Kocaman, T., Cengiz, S., Albayrak, F., Kurt, B., Zeydanlı, U., and *Bilgin, C.,* 2011: Doğa Koruma Merkezi (DKM) Karadeniz Bölgesi Sistematik Koruma Planlaması, Ankara (in Turkish).

Turkes, M., and *Erlat, E.,* 2003: Precipitation changes and variability in Turkey linked to the North Atlantic Oscillation during the period 1930–2000. *Int. J. Climatol. 23(14),* 1771–1796. https://doi.org/10.1002/joc.962

Turkes, M., and *Erlat, E.,* 2008: Influence of the Arctic Oscillation on the variability of winter mean temperatures in Turkey. *Theor. Appl. Climatol. 92(1),* 75–85. https://doi.org/10.1007/s00704-007-0310-8

Türkeş, M., 1990: Türkiye'de Kurak Bölgeler ve Önemli Kurak Yıllar. PhD Thesis, Istanbul University, 195, İstanbul.

Ulke Keskin, A., Kazembeigi, R., and *Zeybekoglu, U.,* 2024: Evaluation of the relationships between atmospheric indices and rainfall intensities: Black Sea region Türkiye. *Regional Studies in Marine Science 77*, 103627. https://doi.org/10.1016/j.rsma.2024.103627

Usta, G., 2023: Statistical Analysis of Disasters in the World (1900-2022). *Gümüşhane University Journal of Social Sciences Institute 14(1),* 172–186 (in Turkish).

Ward, P.J., Kummu, M., and *Lall, U.,* 2016: Flood frequencies and durations and their response to El Niño Southern Oscillation: Global analysis. *J. Hydrol. 539*, 358–378. https://doi.org/10.1016/j.jhydrol.2016.05.045

West, H., Quinn, N., and *Horswell, M.,* 2021: Monthly Rainfall Signatures of the North Atlantic Oscillation and East Atlantic Pattern in Great Britain. *Atmosphere 12*, 1533. https://doi.org/10.3390/atmos12111533

Yarbaşı, G.E., and *Martı, A.İ.,* 2019: The Effect of The Southern Oscillation on Yeşilirmak Basin. *Ulusal Çevre Bilimleri Araştırma Dergisi 2(3),* 112–121 (in Turkish).

Yılmaz, C.B., Demir V., and *Sevimli M.F.,* 2020: Relationship of Black Sea Precipitation with North Atlantic Oscillation. *Gazi Journal of Engineering Sci. 6(3),* 248–254 (in Turkish). https://dx.doi.org/10.30855/gmbd.2020.03.08

Zeybekoğlu U., and *Karahan H.,* 2018: Investigation of Rainfall Intensity Series of Standart Duration with Trend Analysis Methods. *Pamukkale University J. Eng. Sci*. 24(6), 974–1004 (in Turkish). https://doi.org/10.5505/pajes.2017.54265

Zhang, Q., Xu, C-y., Jiang, T., and *Wu, Y.,* 2007: Possible influence of ENSO on annual maximum streamflow of the Yangtze River, China. *J. Hydrol. 333(2),* 265–274. https://doi.org/10.1016/j.jhydrol.2006.08.010

DOI:10.28974/idojaras.2026.1.3

IDŐJÁRÁS

Quarterly Journal of the HungaroMet Hungarian Meteorological Service
Vol. 130, No. 1, January – March, 2026, pp. 45–68

Statistical structure of the homogenized precipitation time series of Hungary

Part 2: Statistics of days and areas with precipitation in Hungary

Károly Tar[1,*], **Sándor Szegedi**[1], **István Hadnagy**[2], **Tamás Tóth**[1], and **István Lázár**[1]

[1]*University of Debrecen,Department of Meteorology,*
H-4032 Egyetem tér 1, Debrecen, Hungary

[2]*Ferenc Rákóczi II Transcarpathian Hungarian College of Higher Education,*
Department of Biology and Chemistry,
UA-90200 Kossuth Square, 6, Beherove, Ukraine

**Corresponding author E-mail: tarko47@gmail.com*

(Manuscript received in final form June 10, 2025)

Abstract— The database of the present examination is the homogenized and interpolated precipitation time series of Hungary, which is diurnal amounts of precipitation for the 1233 grid cells, covering the area of the country for 1971–2022, in the state of the database in 2023. Firstly, the diurnal amount of precipitation over the area of the country, which is the sum of precipitation that falls in each grid cell over the area of the country has been chosen as a variable to be analyzed. Its annual and monthly characteristics have been analyzed for different independent variables. Secondly, spatial characteristics of the diurnal amount of precipitation, that is its distribution among the grid cells have been examined as well. Based on the above time series, nationwide dry, nationwide rainy, and locally rainy/dry days can be distinguished. In this article, we examine the frequency and precipitation yield of both nationwide, and locally rainy days. Precipitation tendency of an area is measured by the frequency of rainy days on the area and their precipitation yield based on the statistics of rainy days per grid. Our basic goal is to explore the temporal and spatial distribution of rainy days nationwide and locally.

Key-words: nationwide rainy days, rainy days and areas

1. Introduction

The database of our study comprises the homogenized and interpolated precipitation time series of Hungary, specifically the daily precipitation totals for 1233 grids covering the country from 1971 to 2022, as of 2023 (*HungaroMet*, 2023). As a variable to be analyzed, we chose the daily precipitation falling on the territory of the country, i.e., the sum of the daily precipitation of all grids. We analyze the annual and monthly properties of this precipitation sum in the case of various independent variables. On the other hand, we also examine the properties of the spatial, i.e., grid-by-grid distribution of daily precipitation.

To analyze the temporal structure of different precipitation characteristics, we used the national daily precipitation time series, which consist of the daily precipitation amounts in all grids. Based on this time series, nationwide dry, nationwide rainy, and locally rainy/dry days can be distinguished. On a nationwide dry day, no measurable precipitation falls in any grid, and on a nationwide rainy day, there is precipitation in all of them. On a rainy/dry day, there is at least one grid, but fewer than all, in which measurable precipitation falls. The spatial structure of precipitation characteristics was explored by analyzing the rainy days per grid.

The frequency of 0 mm precipitation per day or grid is a measure of drought. In our previous article (*Tar et al.,* 2025) we analyzed the temporal and spatial statistical structure of nationwide dry and locally dry days.

In this article, we examine the frequency and precipitation yield of nationwide rainy days and rainy (nationwide or locally) days. The precipitation tendency of an area is measured by the frequency of rainy days on the area and their precipitation yield based on the statistics of rainy days per grid. That is, the area unit is 1 grid.

Our basic goal is to explore the temporal and spatial distribution of rainy days nationwide and locally.

2. Spatial and temporal statistics of rainy days

A rainy day/grid is defined as a day when/where the amount of precipitation exceeds 0.1 mm per day/grid. Statistical features of rainy grids per day and rainy days per grid have been analyzed in this chapter.

2.1. Nationwide rainy days

The days when there is precipitation in each grid that is the number of dry grids is 0 are the *nationwide rainy days*. Their number is 847, namely about half (51.2%) of the number of *nationwide dry days* and 4.5% of the total 18628 days of the studied period. It means that every 22nd day is a nationwide rainy day on average.

Nationwide rainy days are separated by locally rainy days and nationwide dry days. The length of the periods containing such days is between 0 and 171, it is 21 days on average during the studied period in good accordance with the previous estimation. The length of the above-mentioned period is 0 if a nationwide rainy day is followed by a similar day. The length of the intervals is between 0 and10 days in 45% of the cases. Most of them have a length of 0 days, which is 12% of the total nationwide rainy days. It means that a nationwide rainy day is followed by a locally rainy day or a nationwide dry day with a higher (88%) probability in the time series.

Nationwide rainy days (RDC) provide more than a quarter (26.1%, 9,795,494 mm) of the total amount of precipitation (37,580,312 mm).

Most important statistics of the number of nationwide rainy days per year can be seen in *Table 1.*

Table 1. The most important statistics of the number of nationwide rainy days per year

average, days	**[1]stand.dev., days**	**[2]coeff. of var.**	**median, days**	**[3]maximum, days**	**[4]minimum, days**	**mode, days**
16.6	5.04	*0.30*	16	36	9	18

Legends: [1]: standard deviation; [2]: coefficient of variation; [3]: 2010; [4]: 1973, 1983;

There have been 16.6 nationwide rainy days on average per year during the studied period. Their annual number are between 36 (2010) and 9 (1973, 1983) days, respectively. All of them are between 26 and 9 days, except for the maximum. There is a weak linear trend in their temporal change with about a 1-day increase per 10 years.

Based on the values of the average, the median and the mode, the empirical distribution can be approximated with a normal distribution. It has been confirmed via a classification using 5-day-wide classes (*Fig. 1*). However, this way, there have been only 7 classes. Due to this, the degree of freedom of the χ^2-test is 1 (because of contractions), which makes the 0.05 level of acceptance uncertain. It is visible that in 74.5% (38 years) of the studied period, the number of nationwide rainy days has been between 10 and 20 annually (*Fig. 1*).

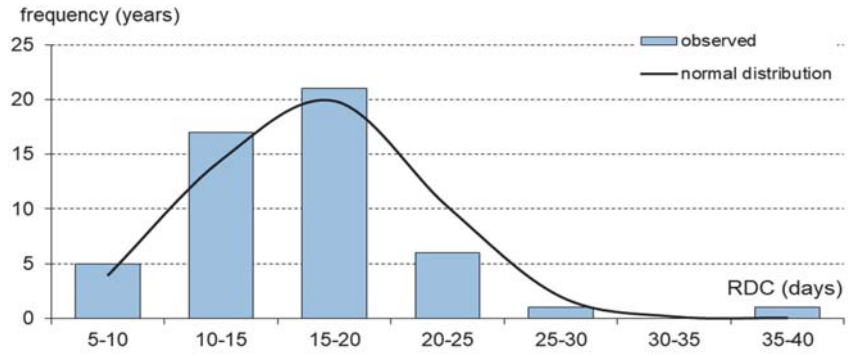

Fig. 1. Distribution of the annual number of nationwide rainy (RDC) days.

Annual precipitation yield of the nationwide rainy days has been examined, as well. The most important statistical characteristics of the precipitation on the *847 nationwide rainy days* are presented in *Table 2.*

Table 2. The most important characteristics of precipitation on nationwide rainy days

[1]average, mm	[2]stand. dev. mm	[3]coeff. of var.	[4]minimum, mm	[5]maximum, mm	median, mm
11,564.9	6,077.5	*0.53*	1,754.0	38,613.9	10,310.8

Legends: [1]: precipitation per nationwide rainy day; [2]: standard deviation; [3]: coefficient of variation; [4]: December 13, 1998; [5]: May 15, 2010;

According to the table, the average precipitation on the nationwide rainy days (11,564.9 mm) is 5.73 times higher than the average precipitation per day during the total studied period (2,017.4 mm).

The mode can be determined from the frequency distribution of the precipitation (between 1,754 and 38,614 mm) of the nationwide rainy days unequivocally.

The maximum of the distribution (140 days, 16.5% of the total nationwide rainy days) is in the 6,000–8,000 mm interval. Therefore, the mode is about 7,000 mm *(Fig. 2)*.

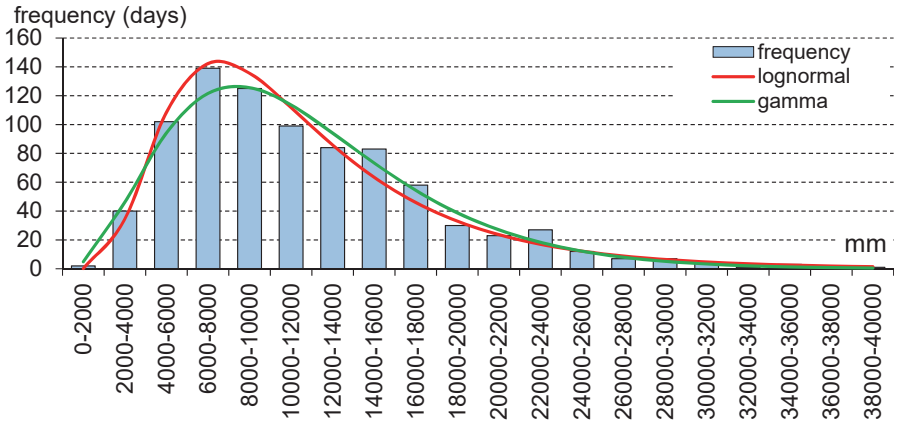

Fig. 2. Frequency distribution and approximation of rainfall on nationwide rainy days with the lognormal and gamma distributions.

The observed frequencies have been approximated with lognormal and gamma distributions. The lognormal distribution fits the empirical frequencies at a 0.05 significance level. Since the gamma distribution is frequently applied in climate statistics, especially in modeling parameters related to precipitation (*Dobosi* and *Felméry*, 1971; *Dévényi* and *Gulyás*, 1988; *Matyasovszki*, 2002), an approximation has been made with this distribution, as well. According to the χ^2-test, it has provided a better fit than the previous one, but the significance level has not improved.

The relationship between the annual number and annual amount of precipitation of nationwide rainy days has also been studied. *Fig. 3* shows a strong linear relationship between these parameters, according to the *Miller-test* (*Miller,* 1997; *Hadnagy*, 2020; 2023) at a significance level of 0.01, with a correlation coefficient of $r = 0.8932$. According to the regression coefficient, a change of 1 day in the number of nationwide rainy days results in a change of 12,036 mm in the precipitation of these days, on average. Based on the determination coefficient, the *number* of nationwide rainy days determines the *amount of rainfall* of these days in 80%.

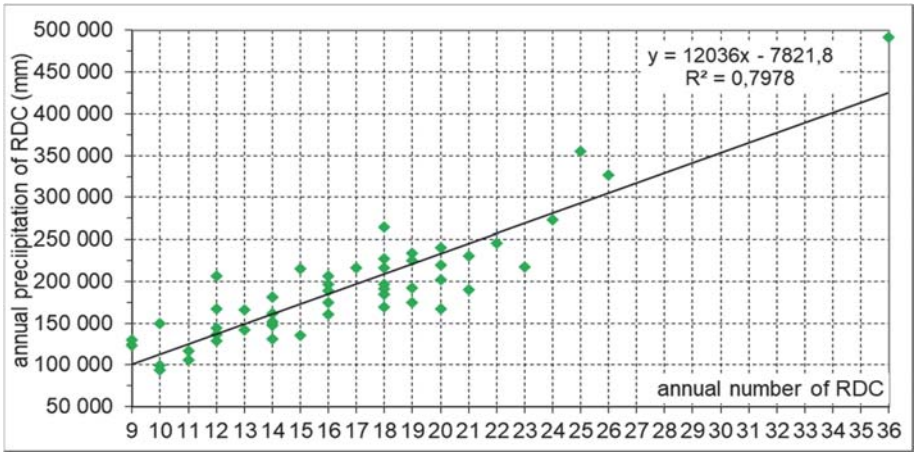

Fig. 3. Linear regression between the annual precipitation of nationwide rainy days and the annual number of such days

The relationships between the annual sums of the precipitation that fell nationwide and the precipitation that fell on rainy days nationwide have been examined also.

According to *Fig. 4*, the highest amount of precipitation fell in 2010 with 1,205,816 mm *over the area of the country* which is 3.2% of the total precipitation of the 51 years of the studied period. However, the absolute minimum of annual precipitation occurred in the next year with 515,299 mm (1.4%). Close to this, the precipitation in 2000 was 519,498 mm which can be considered as 1.4% as well. The maximum and minimum of the *precipitation of the nationwide rainy days* occured in 2010 and 2011 also. Annual precipitation of the nationwide rainy days in 1981 and 2002 are close to the minimum. The ratio of the precipitation of nationwide rainy days compared to the annual precipitation is the second and third lowest as well in those years with 14.1% and 15.5%, respectively. The highest percentage occurred in 2010 too with 40.8%, but there are values close to it in the 2000's with 38.1% in 2016, 39.0% in 2000, and 39.5% in 2005. 26% of the annual precipitation fell on the nationwide rainy days on average during the studied period.

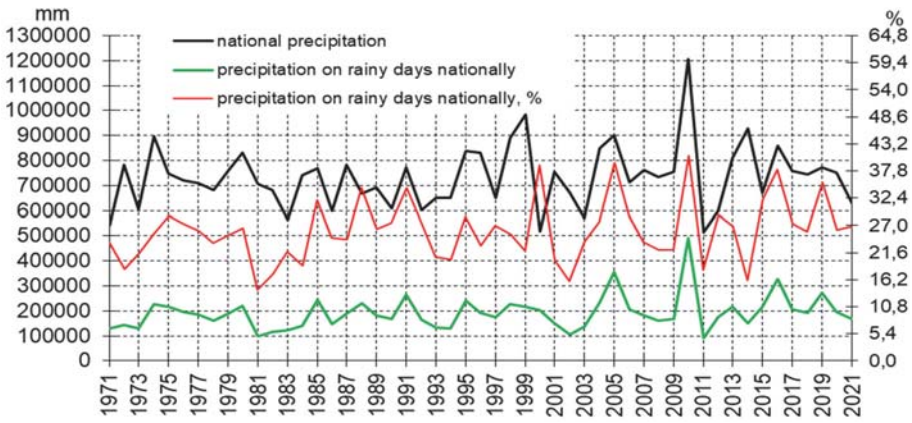

Fig. 4. The annual sums of the precipitation that fell nationwide and the precipitation that fell on rainy days nationwide, as well as the % values of the latter.

It has been examined also, whether the amount of precipitation or the number of nationwide rainy days has a stronger impact on the annual amount of precipitation. According to the linear regression between the annual amount of precipitation and the number and precipitation of nationwide rainy days, the correlation coefficients are $r = 0.7231$ for the precipitation and $r = 0.5880$ for the days. According to the *Miller-test* cited, both correlation coefficients are significantly different from 0. Their determination coefficients are 52% and 35%, respectively. Because of the strong relationship between the two variables (see *Fig. 4*), it cannot be stated that they determine the annual national amount of precipitation together in 87% anyway.

The "days" curve in *Fig. 5* shows the monthly distribution of the number (847) of rainy days nationwide. It is visible, that nationwide precipitation has the highest probability in November followed by October, May, September, and December. Nationwide precipitation has the lowest probability in July. Seasonally, the ratio of nationwide rainy days is the following: *autumn, 31.3%, winter*, 26.2%, *spring*, 22.6%, *summer, 19.8%.* The second curve (*precipitation*) shows the annual trend of the amount of precipitation in % of all such daily precipitation amounts (9,795,494 mm). The similarity between the two curves proves the strong relationship that the monthly amount of precipitation of nationwide rainy days is determined by both the intensity of the precipitation and the number of such days. The determination coefficient is 65%.

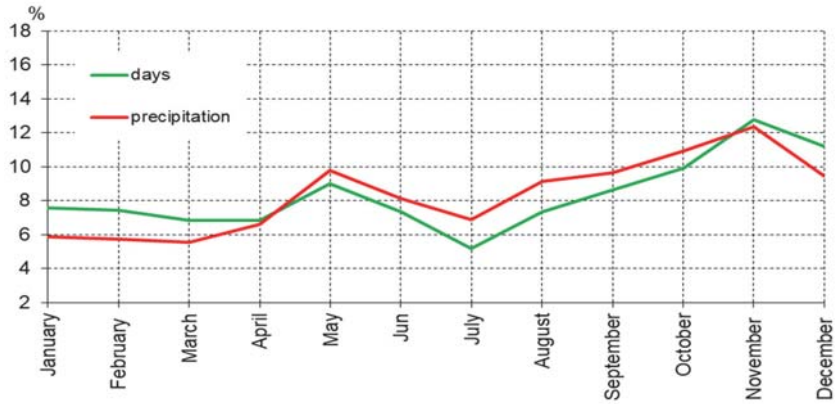

Fig. 5. The monthly distribution of rainy days nationwide (*days*) and the annual trend of the amount of precipitation in % of all such daily precipitation amounts (*precipitation*).

Fig. 6 shows the annual trend of the monthly number of nationwide rainy days (*%1*) as a percentage of the total number of months of the studied period (51*31, 51*30, …). The absolute minimum is in July, when the relative frequency of nationwide rainy days is 3%. There are two local maxima in May with 5% and in November with 7%. The latter is the absolute maximum: the most nationwide rainy days occur in that month in Hungary**.**

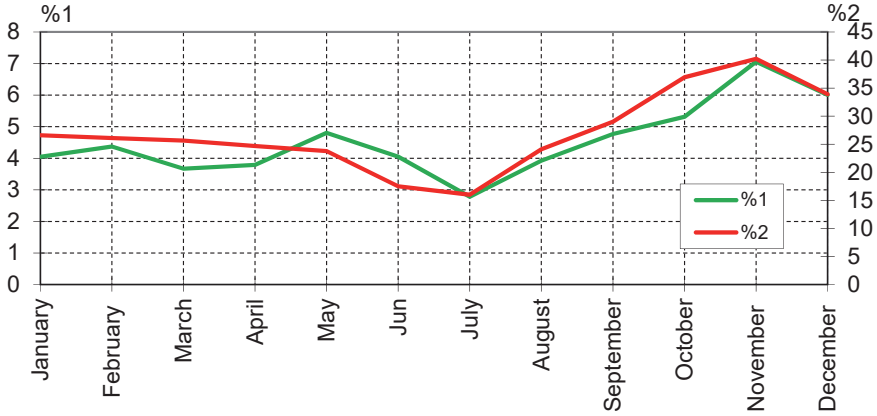

Fig. 6. Annual trend of the monthly number of nationwide rainy days (*%1*) and monthly precipitation (*%2*) nationwide.

The second curve in the figure (%2) shows the annual trend of the monthly precipitation nationwide as a percentage of the monthly precipitation amounts,

namely, it shows how the precipitation of the nationwide rainy days is related to the total monthly amount of precipitation. There are only two extremities of the curve now in harmony with the maximum and minimum of the first curve. According to this, the precipitation of the nationwide rainy days provides 16% and 40% of the total monthly precipitation in June and November, respectively.

2.2. Rainy days

The days when the national daily precipitation is not 0, namely it is more than 0.1 mm in one grid cell at least, are *rainy days*. The number of these days is 16,983 (all days are nationwide dry days numbers), 5% (847 days) of them are the nationwide rainy days. Rainy days (including nationwide rainy days), according to this definition, involve 91.2% of all days. Therefore, it is the probability of precipitation anywhere over the country during a day with a good approximation.

Most important statistical characteristics of the national daily precipitation (in all grids) of rainy days during the studied period are presented in *Table 3*. The average precipitation amount on rainy days is 2,203.5 mm/day, which is approximately 190 mm higher than the national average for the period, including nationwide dry days, too (*Tar et al.,* 2025).

Table 3. Characteristics of the nationwide daily precipitation (in all grids) in the sample of rainy days

average, mm	**[1]stand. dev., mm**	**[2]coeff. of var.**	**minimum, mm**	**maximum, mm**	**median, mm**	**mode, mm**
2,203.5	3,820.2	*1.73*	0.1	3,8 613	524.7	0.28

Legends: [1]: standard deviation; [2]: coefficient of variation;

There is no significant difference between the variation coefficients, supposedly; while there is a significant difference between the values of the median and the mode, probably.

Based on the distribution of the sample, 92.4% of the precipitation amounts of rainy days are between 0.1 and 8,000 mm. Almost 50% of them fall in the 0.1–500 mm interval. In this interval, the highest frequency is between 0.1 and 100 mm (33.5%), and 14.5% is between 0.1 and 10 mm. In the latest interval, the maximum is in the 0.1-1 mm class, that is, the mode is in that interval.

The *annual number of rainy days* is alternating between 355 (1999, 2014) and 305 (1992). It is 333 days, on average. The standard deviation is 10.9 days, so the variation coefficient is 0.03, which is the lowest value among the parameters examined so far. It means that this characteristic is highly stable. The median is 332 days, while the mode is 330 days. It means that it is reasonable to approximate the distribution of the sample with the normal distribution.

Fig. 7 shows the observed and approximated frequencies. The approximation is very good according to the χ^2-test; although it is uncertain because of the unification of classes, which was necessary to make the test executable.

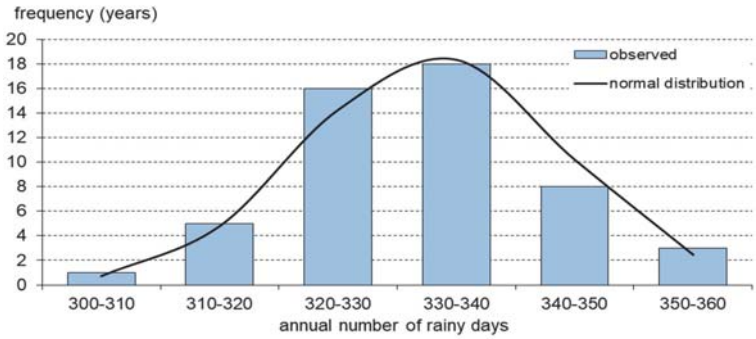

Fig. 7. Empirical distribution of annual rainy days and approximation to the normal distribution

Fig. 8 shows the linear stochastic relationship between the annual national precipitation sum (APA) and the *number* of rainy days (RDC), per year. As both variables have normal distribution, the significant difference of the correlation coefficient from 0 can be determined using the *t*-test (*Vincze*, 1975). According to the test, the $r = 0.4118$ correlation coefficient differs from 0 at a significance level of 0.01. This way, the two variables are considered as weakly correlated. Based on the determination coefficient (r^2), the annual number of rainy days determines the annual national precipitation sum in about 17% only. It is determined by other factors, mainly the intensity of the precipitation in 83%. Based on the regression coefficient, a 1-day change in the number of rainy days.

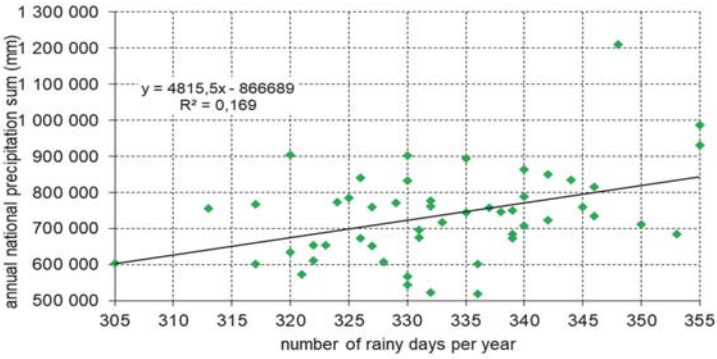

Fig. 8. Linear regression of the annual national precipitation sum (APA) and the number of rainy days (RDC) per year.

The annual precipitation intensities (APA/RDC), namely, the amount of precipitation of a rainy day (mm/day) have been calculated as well. It is between 1,541.9 (2011) and 3,475.9 (2010) mm/day. It is 2,210.2 mm/day on average and its standard deviation is 354,3 mm/day. Therefore, the variation coefficient is 0.16. The median is 2,200.9 mm/day, and the value of the mode is 2,300 estimated from the distribution. The conditions required for approximation using the normal distribution are given this way. Since both original variables have a normal distribution, the parameter derived from them can be considered as having a normal distribution as well without testing.

The times of the extreme values of the annual intensities are in coincidence with the minimum and maximum of the annual precipitation sums. The temporal pattern of APA/RDC is in harmony with the trend of APA; the trend lines are parallel, as it can be seen in *Fig. 9*.

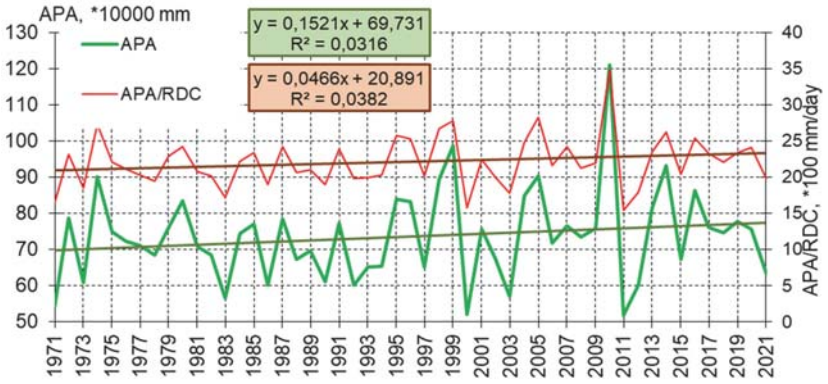

Fig. 9. Time change of the annual precipitation amount (APA) and the annual precipitation intensity (APA/RDC)

The annual trend of rainy days, namely the distribution of their number per month, is presented in *Fig. 10*.

The first curve (*%1*) shows the annual trend of the number of rainy days per month compared to the total number of rainy days (16,983). This data, with a standard deviation of 1.7%, gives the probability of having precipitation anywhere over the country (in any grid cells) on any days of a given month. This probability is around 9% in January and December, followed by May, June, and July with 8.5%. This probability is the lowest in September with 7.4% and February with 7.8%. Seasonal data are: winter: 25.8%, summer: 25.0%, spring: 24.8%, and autumn: 24.3%, respectively.

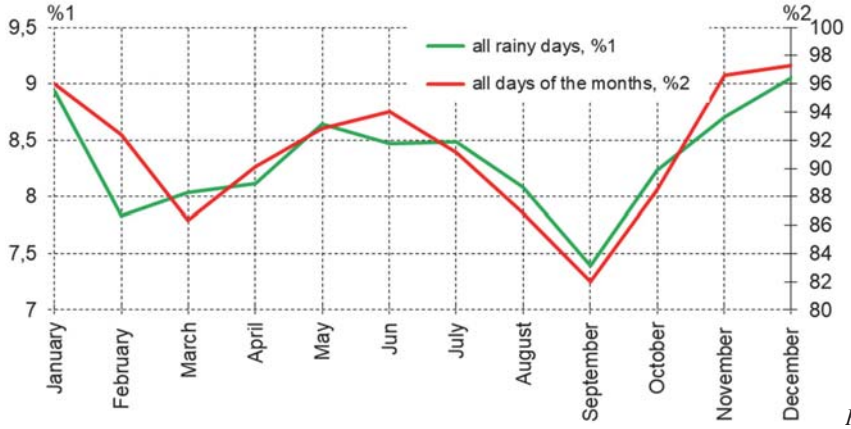

Fig. 10.
Annual trend of the number of rainy days per month as a percentage of all rainy days (*%1*) and of all days of the months included in the processing (*%2*)

There is no constant base of reference in the case of the second curve (%2) in *Fig. 10,* since the number of rainy days per month is given as a percentage of all days of the months included in the processing (51*31, 51*30,…). Therefore, the numbers show the percentage of rainy days somewhere/anywhere in the country within a month. These ratios are over 90% in November, December, January, and February (namely, in the late autumn and winter), and in April, May, June, and July, respectively. Consequently, there is a high probability of precipitation anywhere in the country on almost all days of these months. The occurrence of the studied phenomenon has a probability of less than 90% in the early spring, late summer, and early autumn, with a minimum of 82% in September.

2.3. The most important statistical characteristics of rainy days per grid cell

The spatial pattern of precipitation can be analyzed by studying the sum of rainy days per grid cell. The sum of rainy days per grid cell (the number of rainy grids) is 10,916,603, which is 47.5% of the total number of cases (22,968,324). 9.6% of the rainy grid cells are the grid cells of the nationwide rainy grids (847*1,233= 1,044,351). The most important statistical characteristics of the sum of rainy days per grid (DWP_g) and their average number per year (DWP_g/year) are given in *Table 4.*

There are 8,854 rainy days per grid cell on average, which is 0.08% of the number of all rainy grid cells (the number of rainy days in all grid cells is 10,916,603). The variation coefficient supports the relative stability of this

variable around the average. The number of values over and under the average are 640 (51.9%) and 592 (48.1%), respectively.

Table 4. The most important statistical characteristics of the sum of rainy days per grid (DWP_g) and their average number per year (DWP_g/year)

statistical characteristics	DWP_g	DWP_g/year
average, days	8,854	174
[1]stand. dev., days	531	10
[2]coeff. of var.	*0.06*	*0.06*
[3]minimum, days	5,473	107
[4]maximum, days	10,142	199
median, days	8,878	174
mode, days	8,891	174

Legends: [1]: standard deviation; [2]: coefficient of variation;
[3]($\varphi = 47.5$; $\lambda = 16.8$); [4]($\varphi = 47.8$; $\lambda = 21.8$), ($\varphi = 47.8$; $\lambda = 21.9$);

The spatial distribution of *rainy days* per grid cell is between 10,142 and 5,473 during the studied period. The increasing order of DWP_g values shows that the higher values are concentrated between the 20.8°E and 22.1°E longitudes and the 47.8°N and 48.4°N latitudes. This is more or less the same area that has been identified in our previous paper (*Tar et al.,* 2025), since dry (DNP_g) and rainy (DWP_g) days per grid are complementary to each other. There is no such geographical concentration identified in the case of the lower values at the beginning of the line. The minimum with 29.4% occurs in the western part of the country, which is followed by a grid in the east with 29.7%.

The dry (DNP_g) and rainy (DWP_g) days per grid are complementary to each other, so their sum is the total number of days of the studied period (18,628). In the case of annual averages, it is DNP_g/year + DWPg/year = 365 or 366, that is the number of days in a year. From this, according to the comments made in connection with *Fig. 8*, it follows that was described in the distribution analysis of the number of dry days per year (DNP_g/year, *Tar et al.,* 2025), which also applies to the DWP_g/year characteristics. Therefore, the empirical frequencies cannot be acceptably approximated by the possible theoretical distributions.

The relationship between the annual average of rainy days per grid (DWP_g/year) and the geographical coordinates of the grid cells (φ, λ) has also been examined using linear regression. Because of the above-mentioned relationships between the DNP_g/year and DWP_g/year characteristics and the statements in *Tar et al.* (2025), correlation coefficients differ significantly from 0, again. Therefore, the statements regarding *dry days* are also true for this case, considering the change in the sign of the correlation and regression coefficients. Based on the realistic stochastic relationship, we prepared the complement of

DNP_g/year (*Tar et al*., 2025), a map showing the distribution of the annual average of rainy days per grid (DWP_g/year) during the examined period (see *Fig. 11*).

The map of the spatial distribution of the annual average of rainy days per grid is the inverse of the map of the annual average of dry days per grid. According to this, the annual averages of rainy days per grid are the highest in the northeastern part of the country in the Nyírség, and the Hajdúság regions. Minima occur sporadically within the Hungarian Small Plain over the Hanság and the Rábaköz regions.

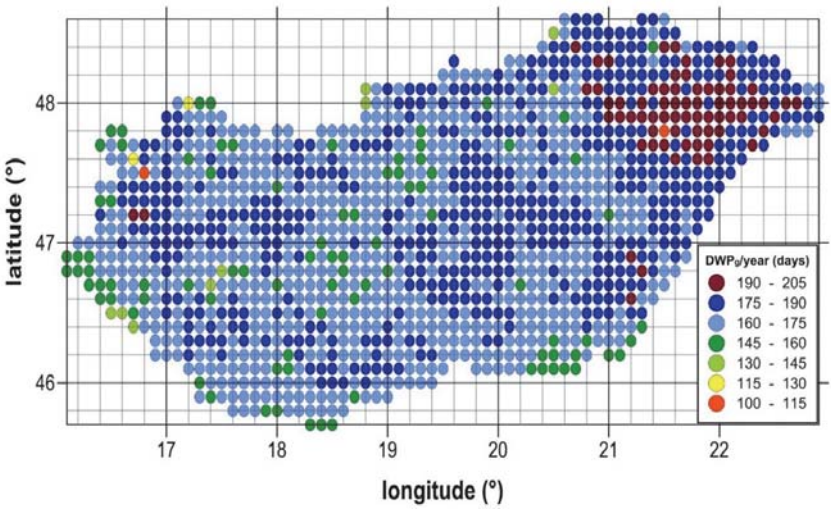

Fig. 11. Distribution of the annual average of rainy days per grid (DWP_g/year) in the examined period.

2.4. Statistics of the amount of precipitation per grid

The most important characteristics of the amount of precipitation per grid (APR_g) and its annual average (APR_g/year) during the studied period are shown in *Table 5*. The two coefficients of variation are equal trivially, which proves the relatively high stability of the measure of standard deviation around the average. Supposedly, there are some concentration points in the distribution of both datasets around some values. Values of the mode have been estimated from the distributions.

Table 5. The most important characteristics of the amount of precipitation per grid (APR_g) and its annual average (APR_g/year)

statistical characteristics	APR_g	APR_g/year
average, mm	30,478.8	597.6
[1]stand. dev., mm	3,292.6	64.6
[2]coeff. of var.	0.11	0.11
[3]minimum, mm	26,127.1	512,3
[4]maximum, mm	42,352.5	830,4
median, mm	29,456.4	577,6
[5]mode, mm	28,500.0	570.0

Legends: [1]: standard deviation; [2]: coefficient of variation;
[3]: ($\varphi = 47.1$; $\lambda = 20.3$); [4]: ($\varphi = 48.1$; $\lambda = 20.5$); [5]: from distribution

Frequency distribution of both data sets has been determined. Applying 1,000 mm classes for APRg, 46.7% of the values have been between 27,000 and 30,000 mm. The maximal frequency is 212 grid cells, and 17.2% of which falls into the 28,000-29,000 mm class; this way the mode is 28,500 mm. 20 mm classes have been applied in the case of the annual average of the precipitation amount per grid (*Fig. 12*). APR_g/year values fall into the 520 and 600 mm class in 60.3% of the grid cells. The maximal frequency is 213 grid cells, and 17.3% of which is in the 560-580 mm class; so the mode is 570 mm. The coincidence of the latter with the previous results is due to the application of appropriate classes. Attempts have been made to approximate both distributions with the theoretical distributions used previously. Unfortunately, all these attempts have failed.

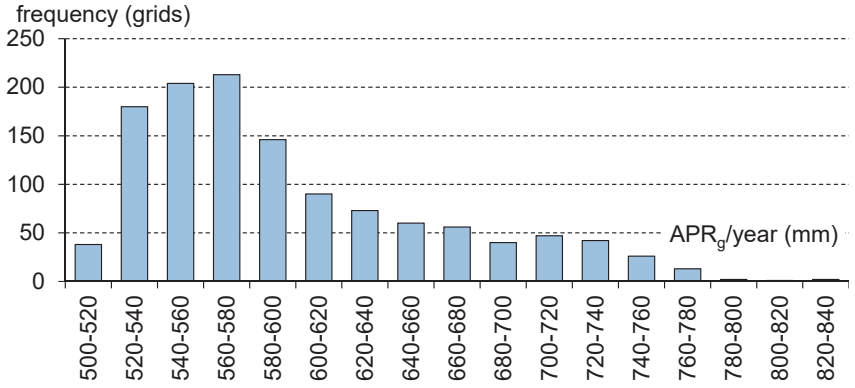

Fig. 12. Distribution of the annual average of precipitation per grid (APR_g/year).

A detailed analysis of the distribution of the annual average precipitation per grid cell has been presented, as follows.

Adding the 500–520 mm class to the former four classes of between 520–600 mm and modifying the upper limit of the fourth to 597.6 mm, the number of grid cells, which have an average *annual precipitation amount, that is lower* than the nationwide average, can be determined. Their number is 765, which is 62% of all grids (namely, 62% of the total area of Hungary). 28,335.8 mm per grid on average, that is 57.7% of the total precipitation of the studied period has fallen in these five categories, which involves nearly the two-thirds of all grid cells. The annual mean precipitation (the average of APR_g/year) is 555.6 mm in these grid cells. The geographic coordinates of these grid cells are λ=16.6°E – 22.5°E and φ=45.9°N – 48.6°N, that is, they are dispersed over almost the total area of the country. The distribution of the grid cells according to λ is wider, since the grids involved are spaced over 60 from the possible 69 lines of longitude, while, according to φ, they are spaced over 27 lines from the possible 30.

The *average annual precipitation amount is higher* than the nationwide average in the remaining 468 grid cells, which is 38% of the country's area. 3,3981.7 mm per grid on average, that is 42.3% of the total precipitation of the studied period has fallen into these grid cells. The average of APR_g/year is 666.3 mm in this case. The geographic coordinates of these grid cells are spaced in a wider line of longitude interval than the former ones: they are spaced λ=16.1°-22.9° and φ=45.7°- 48.6°. The distribution of the grid cells according to λ covers an even wider interval, as they are spaced over 63 lines of longitude, while their distribution according to φ is spaced over 27 of the possible 30 again.

The following examination has been carried out to study the spatial pattern of the above-defined 765 and 468 grid cells.

Considering the *distribution according to* λ in the case of the APR_g/year ≤ 597.6 mm, there are 765 grid cells spaced over 60 lines of longitude, namely 12.85 grid cells per line of longitude on average. This value is presented in *Fig. 13 part a,* beside the values given for the lines of longitude. Values higher or equal to this, occur between 18.6°E and 21.9°E, namely, between the meridians that cross the northeastern corner of the Lake Velence and the town of Nagykálló. The 468 grid cells, where the average annual precipitation amount is higher than the nationwide average, are spaced over 63 lines of longitude, which means 7.4 grid cells per line (6 lines where there are no such grids are not involved in the average). According to *Fig. 13 a,* the grid cells with high precipitation amounts are concentrated along the lines of longitude that cross the Kőszegi Mountains, the towns of Szekszárd and Dunaújváros between the lines of 16.4°E and 18.6°E longitudes, respectively.

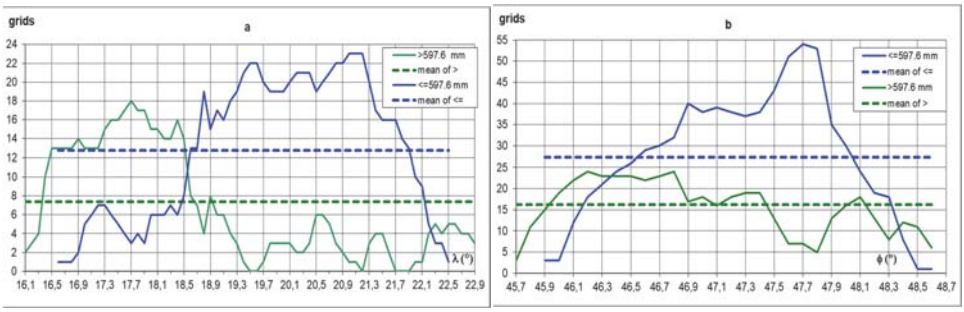

Fig. 13. Distribution of grids having an average annual precipitation amount that is lower or higher than the national average (597.6 mm), according to longitude (a: λ) and latitude (b: φ),.

In the case of the *distribution according to φ,* the 765 grid cells where the annual mean precipitation is under the nationwide average, are spaced over 28 lines of latitude, and the average is 27.3 grid cells per line. Values equal or higher than this are spaced between the 46.6°N and 48°N latitudes that is about between the lines of Lenti – Paks – Békéscsaba and Pétervására – Tiszalök – Baktalórántháza, according to *Fig. 13 b*. In the case of CSMg/year > 597.6 mm, 468 grid cells are spaced over 30 lines of latitude; namely, 15.6 grid cells per line of latitude. Based on *Fig.13 b,* values higher than this are spaced between 45.9°N and 47.4°N, and 48°N and 48.1°N, which is between the lines that of Mohács - Kőszeg, and Budapest - Debrecen, respectively.

The results of the analyses above have been summarized in *Fig. 14,* which shows the spatial pattern of annual mean precipitation. The annual average of the rainfall per grid has a basically meridional-zonal distribution due to the strengthening continental effect from the west to the east on one hand, and the orographic effect on the other. The rainiest areas in southwest Transdanubia, the Central Transdanubian Mountains, Alpokalja, Mecsek, and the Bakony Mountains – where the Mediterranean effect is significant – get nearly twice as much precipitation than the Central Great Hungarian Plain, such as the regions of Jászság, Hortobágy, Nagykunság, and the plain between the Maros and Körös Rivers, and partly the Kiskunság. Due to the orographic effect, the amount of precipitation is over the nationwide average in the Transdanubian low mountains, the highest parts of the North Hungarian Mountains: Börzsöny, Mátra, Bükk, and Zemplén, and the Szatmár–Bereg Plain (due to the orographic effect of the northeastern Carpathians in the case of this latter one).

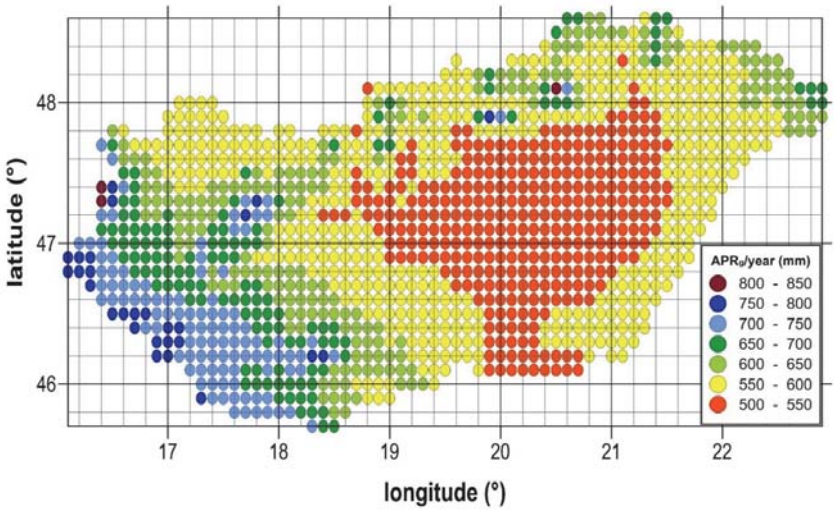

Fig. 14. Distribution of the annual average of the rainfall per grid (APR_g/year, mm) in the examined period

Values of the precipitation intensity per grid (IPR_g=APR_g/DWP_g given in mm/day) have been determined as well. Its most important statistical characteristics have been presented in *Table 6*.

Table 6. The most important statistical characteristics of the precipitation intensity per grid (APR_g/DWP_g)

average mm/day	**[1]stand. dev., mm/day**	**[2]coeff. of var.**	**[3]minimum, mm/day**	**[4]maximum, mm/day**	**median, mm/day**	**[5]mode, mm/day**
3.46	0.48	*0.14*	2.72	5.92	3.34	3.2

Legends: [1]: standard deviation; [2]: coefficient of variation; [3]: ($\varphi = 47.1$; $\lambda = 20.3$); [4]: ($\varphi = 48.1$; $\lambda = 20.5$); [5]: from distribution

The location of the minimum and maximum of precipitation intensity per grid is in coincidence with the coordinates of the extreme values of rainy days per grid (DWP_g), namely, this parameter has a stronger impact on it. The minimum is where the maximum DWP_g is, while the maximum is located where this parameter reaches its minimum. The spatial pattern is like that of dry days per grid (DNP_g). These values have no direct relationship to the spatial pattern of DWP_g.

Linear correlation coefficients between the precipitation intensities per grid and the geographic coordinates (φ,λ) of the grid cells can be considered

significant, since it is valid for both components (APR_g and DWP_g). Now the correlation coefficients are $r_\lambda = -0.6374$, and $r_\varphi = -0.3468$. For DNP_g, the correlation coefficients are $r_\lambda = -0.4308$, and $r_\varphi = -0.3357$. Dependence on the longitude is stronger in both cases and stronger in the case of APR_g/DWP_g than for DNP_g. However, according to the regression coefficients of the precipitation intensity per grid (-0.1862 and -0.2452), changes in the latitude cause larger differences in the precipitation intensity per grid than changes in the longitude.

On the basis of the latter results, the map of spatial distribution of precipitation intensity per grid (IPR_g, mm/day) during the studied period has been compiled. The map is shown in *Fig. 15*.

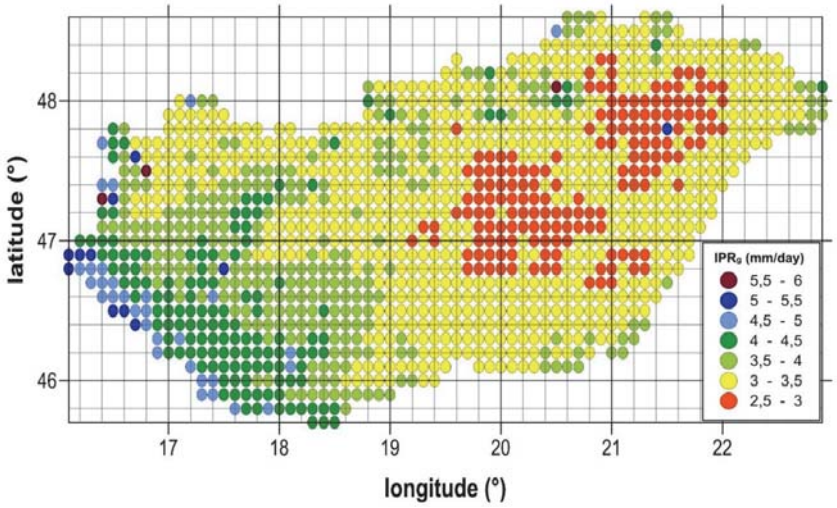

Fig. 15. Spatial distribution of precipitation intensity per grids (IPR_g, mm/day) during the examined period.

Similarly to annual precipitation amounts, higher values can be found along the Dráva River and over the regions of the Central Transdanubian Mountains, the Alpokalja, and the highest areas of the Northern Central Mountains. Lowest values are concentrated in the central part of the Great Hungarian Plain over the regions of Jászság, Nagykunság, Hortobágy, Hajdúság, and Nyírség.

3. Discussion and conclusions

The database of the present study is the homogenized and interpolated precipitation time series of Hungary, namely diurnal precipitation data from the 1233 grid cells that cover the area of Hungary for the 1971–2022 period. The diurnal amount of nationwide precipitation, namely the sum of diurnal precipitation in all grid cells, has

been chosen as the studied variable. Firstly, the annual and monthly characteristics of this variable have been analyzed in the case of different independent variables. Secondly, spatial patterns of precipitation, or otherwise their distribution per grid cell has been analyzed as well. In our previous article (*Tar et al*., 2025), we analyzed the statistical structure of dry days and areas. We considered a day as dry when there was no measurable precipitation (greater than 0.1 mm). The dryness of an area was measured by the frequency of dry days there.

In this article, we explored the statistical structure of rainy days in four levels.

The days, when there is precipitation in each grid, namely the number of dry grids is 0, are the *nationwide rainy days*. Their number is 847, namely about half of the *nationwide dry days* and 4.5% of the total days of the studied period. It means that every 22nd day is a nationwide rainy day on average.

Nationwide rainy days are separated by locally rainy days and nationwide dry days. The length of the periods containing such days is between 0 and 171; it is 21 days on average during the studied period, in good accordance with the previous estimation. The length of the period is 0 if a nationwide rainy day is followed by a similar day. The length of the intervals is between 0 and 10 days in 45% of the cases. Most of them have a length of 0 day, which is 12% of the total nationwide rainy days. It means that a nationwide rainy day is followed by a locally rainy day or a nationwide dry day with a higher (88%) probability in the time series.

There have been 16.6 nationwide rainy days on annual average during the studied period. Their annual number are between 36 (2010) and 9 (1973, 1983), all of them are between 26 and 9, except for the maximum. There is a weak linear trend in their temporal change with about a 1-day increase per 10 years.

The average precipitation on the nationwide rainy days is 5.73 times higher than the average precipitation per day during the total studied period. The observed frequencies have been approximated with lognormal and gamma distributions. The lognormal distribution fits the empirical frequencies at a significance level of 0.05. Since the gamma distribution is frequently applied in climate statistics, especially in modeling parameters related to precipitation, an approximation has been made with this distribution, as well. According to the χ^2 test, it has provided a better fit than the previous one, but the significance level has not improved.

The relationship between the annual number and annual amount of precipitation of nationwide rainy days has also been studied. A strong linear relationship has been found according to the test applied at a significance level of 0.01 with a correlation coefficient of $r = 0.8932$. According to the regression coefficient, a change of 1 day in the number of nationwide rainy days results in a change of 12,036 mm in the precipitation of these days on average. Based on the determination coefficient, the *number* of nationwide rainy days determines the *amount of rainfall* on these days in 80%.

The annual sums of the precipitation that fell nationwide and the precipitation that fell on rainy days nationwide has also been compared. The highest amount of precipitation fell in 2010 with 1,205,816 mm *over the area of*

the country, which is 3.2% of the total precipitation of the 51 years of the studied period. However, the absolute minimum of annual precipitation occurred in the next year with 515,299 mm (1.4%). The precipitation in 2000 is close to this with 519,498 mm, which can be considered as 1.4% as well. The maximum and minimum *precipitation of the nationwide rainy days* occurred both in 2010 and 2011. Annual precipitation of the nationwide rainy days in 1981 and 2002 is close to the minimum. The ratio of the precipitation of nationwide rainy days compared to the annual precipitation is the second and third lowest in these years with 14.1% and 15.5%, respectively. The highest percentage occurred in 2010, with 40.8%, but there are values close to it in the 2000's with 38.1% in 2016, 39.0% in 2000, and 39.5% in 2005. 26% of the annual precipitation fell on the nationwide rainy days on average, during the studied period.

The monthly distribution of the number (847) of rainy days nationwide has been studied as well. Nationwide precipitation has the highest probability in November followed by October, May, September, and December. Nationwide precipitation has the lowest probability in July. Seasonally, the decreasing order of the proportion of the ratio of nationwide rainy days is autumn, winter, spring, and summer. The annual course of the number of nationwide rainy days and the amount of precipitation per month is very similar. This shows the clear relationship that the amount of precipitation of monthly nationwide rainy days strongly depends on the number of such days in addition to the intensity of precipitation. However, the coefficient of determination in this case is 65%.

The days when the national daily precipitation is not 0, namely it is more than 0.1 mm in one grid cell at least, are *rainy days*. The number of these days is 16,983 (all days are nationwide dry days), 5% of them are the nationwide rainy days. Rainy days, according to this definition, involve 91.2% of all days. Therefore, it is the probability of precipitation anywhere over the country during a day with a good approximation.

Average precipitation of rainy days is 2,203.5 mm/day, which is approximately 190 mm higher than the average for the whole studied period comprising the nationwide dry days. Based on the distribution of the sample, 92.4% of the precipitation amounts of rainy days are between 0.1 and 8,000 mm. Almost 50% of them fall in the 0.1-500 mm interval. In this interval, the highest frequency is between 0.1 and 100 mm (33.5%), and 14.5% is between 0.1 and 10 mm. In the latest interval, the maximum is in the 0.1-1 mm class, that is, the mode is in that interval.

The annual number of rainy days is alternating between 355 (1999, 2014) and 305 (1992). It is 333 on average. According to the variation coefficient, this characteristic is highly stable. Due to the small differences between the average, the median, and the mode, the approximation with the normal distribution has been successful.

The relationship between the annual national precipitation sum and the *number* of rainy days per year has been proved to be linear according to the *t*-test. According

to the test, the r = 0.4118 correlation coefficient differs from 0 at a significance level of 0.01. This way, the two variables are considered as weakly correlated. Based on the determination coefficient (r^2), the annual number of rainy days determines the annual national precipitation sum in about 17% only. This parameter is determined by other factors, mainly the intensity of the precipitation, in 83%. Based on the regression coefficient, a 1-day change in the number of rainy days results in a 4,811 mm change in the annual mean nationwide precipitation amount.

Annual precipitation intensity, namely the amount of precipitation of a rainy day (mm/day), has also been calculated. Its value is between 1,541.9 (2011) and 3,475.9 (2010) mm/day. It is 2,210.2 mm/day, on average. Since both original variables have a normal distribution, the parameter derived from them can be considered normally distributed without testing.

The times of the extreme values of the annual intensities are in coincidence with the minimum and maximum of the annual precipitation sums. The temporal pattern of APA/RDC is in harmony with the trend of APA, the trend lines are parallel as in *Fig. 9*.

The ratio of the number of rainy days per month and all rainy days (16,983) gives the probability of having precipitation anywhere over the country (in any grid cells) on any days of a given month. This probability is around 9% in January and December, followed by May, June, and July with ~8.5%. This probability is the lowest in September with 7.4% and February with 7.8%. Seasonal data are as follows: winter: 25.8%, summer: 25.0%, spring: 24.8%, and autumn: 24.3%.

The number of rainy days per month, given as a percentage of all days included in the processing, shows the percentage of rainy days somewhere/anywhere in the country within a month. These ratios are over 90% in November, December, January, and February (namely, in the late autumn and winter), and April, May, June and July, respectively. Consequently, there is a quite high probability of precipitation anywhere in the country on almost all days of these months. The occurrence of the studied phenomenon has a probability of less than 90% in the early spring, late summer, and early autumn, while its minimum is 82% in September.

The spatial pattern of precipitation can be analyzed by studying the sum of rainy days per grid cell. The sum of rainy days per grid cell (the number of rainy grids) is 47.5% of the total number of cases. 9.6% of the rainy grid cells are the cells of the nationwide rainy grids.

The distribution of *rainy days* per grid cells is between 10,142 and 5,473 days, with an average of 8,854 days. Their annual minimum and maximum are 107 and 174 days, respectively.

The linear relationship between the annual average of rainy days per grid and the geographical coordinates of the grid cells has also been examined. Because dry and rainy days per grid cell are complementary to each other, the statements regarding *dry days* are true for this case, also considering the change in the sign of the correlation and regression coefficients. Based on the realistic stochastic

relationship, the map of the distribution of the annual average of rainy days per grid in the examined period has been compiled. The map of the spatial distribution of the annual average of rainy days per grid is the inverse of the map of the annual average of dry days per grid. According to this, the annual averages of rainy days per grid are the highest in the northeastern part of the country. Minima occur sporadically within the Small Hungarian Plain.

The amount of precipitation per grid, the extremities, its annual average, and the variation coefficient during the studied period prove the relatively high stability of this characteristic. Supposedly, the distribution of both datasets contains some concentration points around some values. The value of the mode has been estimated from the distributions.

Details of the distribution of the annual average precipitation per grid have been studied. In 60.3% of the grid cells, its values fall into the 520–600 mm class. The maximal frequency is 213 grid cells, which is 17.3% of the 560-580 mm class, so the mode is 570 mm. The amount of annual average precipitation in Hungary during the studied period was 597.6 mm.

The average annual precipitation amount is higher than the national average in 765 cells, which is 62% of all grids (that is 62% of the total area of Hungary), where 57.7% of the total precipitation of the studied period has fallen. The annual mean precipitation is 555.6 mm in these grid cells. The average annual precipitation amount is higher than the nationwide average in the remaining 468 grid cells, which is 38% of the area of the country. The annual mean precipitation is 666.3 mm in these grid cells. The geographic coordinates of these grids are spaced almost over the total area of Hungary.

Spatial distribution of these grid cells according to longitude and latitude has been examined to trace the concentration of precipitation along certain coordinates, that is, over some regions of Hungary.

We found that those grid cells, where the average annual precipitation amount is lower than the nationwide average, are spaced between the 18.6°E and 21.9°E longitudes. The 468 grid cells, where the average annual precipitation amount is higher than the nationwide average, are spaced west of these grids, between the 16.4°E and 18.6°E longitudes. Regarding the latitude-related distribution, the same intervals are spaced between the 46.6°N and 48°N, and 45.9°N and 47.4°N latitudes, with a much stronger overlap.

The spatial distribution of the annual average of the rainfall per grid cell is governed by the strengthening continental effect from the west to the east on one hand, and the orographic effect on the other. The rainiest areas in southwest Transdanubia get nearly twice as much precipitation as the Central Great Hungarian Plain. Due to the orographic effect, the precipitation amount is over the nationwide average in the highest parts of the Central Transdanubian Mountains and Northern Central Mountains, as well as the Szatmár–Bereg Plain (due to the orographic effect of the northeastern Carpathians, in this latter case).

Precipitation intensity per grid cell have also been determined. Their most important statistical characteristics are as follows: the average is 3.46, the minimum is 2.72, and the maximum is 5.92 mm/day, respectively.

The location of the minimum and maximum is now aligned with the extrema of the number of rainy days per grid. The minimum of the intensity is in the grid where the latter parameter has its maximum, and the maximum is where the latter parameter has its minimum. In other words, the intensity depends more strongly on the number of rainy days. The spatial distribution of intensity, therefore, approaches the spatial distribution of dry days per grid.

Linear correlation coefficients between the precipitation intensity per grid and the geographic coordinates of the grid cells differ from 0, since they are valid for both components. Zonal dependence is stronger than meridional again and stronger than in the case of dry days. However, according to the regression coefficients of the precipitation intensity per grid, changes in the latitude cause larger differences in the precipitation intensity per grid than changes in the longitude. Based on the latter results, the map of the spatial distribution of precipitation intensity per grid during the studied period has been compiled.

Similarly, to the annual precipitation amounts, higher values can be found along the Dráva River and over the regions of the Central Transdanubian Mountains, Alpokalja, and the highest areas of the Northern Central Mountains. At the same time, lowest values are concentrated into the central part of the Great Hungarian Plain, over the regions of Jászság, Nagykunság, Hortobágy, Hajdúság, and Nyírség.

References

Dévényi D. and *Gulyás O.*, 1988: Matematikai statisztikai módszerek a meteorológiában. Tankönyvkiadó, Budapest. (in Hungarian)

Dobosi Z. and *Felméry L.,* 1971: Klimatológia. Egyetemi jegyzet, Tankönyvkiadó, Budapest. (in Hungarian)

Hadnagy I., 2020: A felszín közeli szélmező energetikai jellemzése Kárpátalján. Egyetemi doktori (PhD) értekezés. Debreceni Egyetem, Természettudományi és Informatikai Doktori Tanács, Földtudományok Doktori Iskola. (in Hungarian)

Hadnagy I., 2023: A felszín közeli szélmező energetikai jellemzése Kárpátalján. Monográfia. II. RF KMF-„RIK-U" Kft, Bergszász-Ungvár. (in Hungarian)

HungaroMet, 2023. Meteorológiai Adattár. (in Hungarian) https://odp.met.hu/climate/homogenized_data/gridded_data_series/daily_data_series/from_1971/precipitation_sum/

Matyasovszky I., 2002: Statisztikus klimatológia. Idősorok elemzése. *ELTE Eötvös Kiadó*, Budapest. (in Hungarian)

Miller, R.G., 1997: Beyond ANOVA: Basics of Applied Statistics. Chapman & Hall/CRC, University of Stanford, California, USA, 336 p.

Tar, K., Szegedi, S., Hadnagy, I., Lázár, I. and *Tóth, T*. 2025. Statistical Structure of the Homogenized Precipitation Time series of Hungary. Part 1: Statistics of dry days and areas in Hungary. *Időjárás 129*, 395–417. https://doi.org/10.28974/idojaras.2025.4.2

Vincze I. 1975. Matematikai statisztika ipari alkalmazásokkal. Műszaki Könyvkiadó, Budapest. (in Hungarian)

DOI:10.28974/idojaras.2026.1.4

IDŐJÁRÁS

Quarterly Journal of the HungaroMet Hungarian Meteorological Service
Vol. 130, No. 1, January – March, 2026, pp. 69–85

Investigation of wind effect at Samsun, Zonguldak, and Trabzon airports in Turkiye

Ömer Faruk Uzun[1,*] and **Ramazan Gürsel Hoşbaş**[2]

[1] *Sinop University, Boyabat Vocational School, Department of Architecture And Urban Planning, Sinop, Türkiye*

[2] *Yıldız Technical University, Faculty of Civil Engineering, Department of Surveying Engineering, İstanbul, Türkiye*

**Corresponding author E-mail: ofuzun@sinop.edu.tr*

(Manuscript received in final form January 30, 2025)

Abstract—Accurate management of weather conditions plays a critical role in ensuring safe and efficient flight operations in the aviation industry. In this context, the wind factor has a direct impact on aircraft performance and pilot decision-making mechanisms, especially during landing and takeoff processes. Within the scope of the study, 16 years of wind data recorded between 2008 and 2023 at Samsun Çarşamba, Zonguldak, and Trabzon airports located in the Black Sea Region are analyzed. Innovative Trend Analysis (ITA) and Innovative Polygon Trend Analysis (IPTA) methods are used to analyze the trends of wind direction, speed, and sudden changes. According to the results obtained, the dominant wind direction at Samsun Çarşamba and Zonguldak airports was determined as east (E), while a dominant wind effect was determined in the south-southwest (SSW) direction at Trabzon Airport. The study reveals the effects of wind factor on flight safety and operational efficiency and provides recommendations for the measures to be taken in the aviation sector and future practices.

Key-words: wind factor, flight safety, airport operations, crosswind and tailwind, trend analysis

1. Introduction

One of the key components of safe and efficient flight operations in the aviation industry is the correct management of weather conditions. In this context, the wind plays an important role in all phases of flight, but especially in the landing and takeoff processes. Based ont he aviation accident database of the National TransportationSafety Board, *Fig. 1* shows the percentage of the different phases of flight in the total number of flight accidents (*NTSB*, 2019)

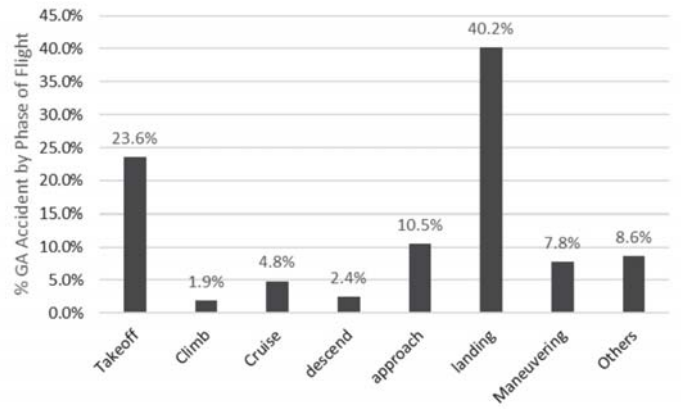

Fig.1. Aircraft accidents by positions in 2019.

2022 data of the Flight Safety Foundation also provides up-to-date support for this information (*FSF*, 2022; *Fig.2*).

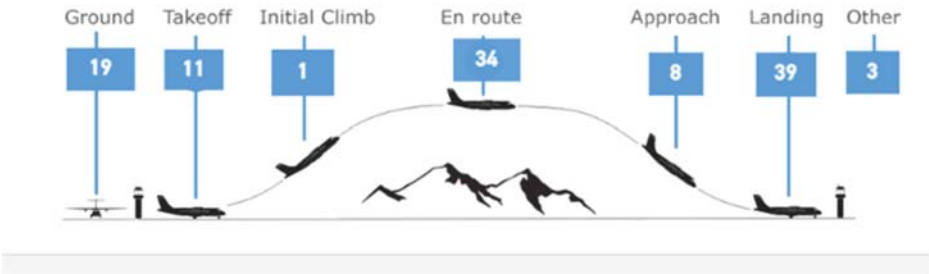

Fig.2. Aircraft accidents according to positions in 2022.

Wind direction, speed, and sudden changes directly affect both aircraft performance and pilots decision-making processes. While headwind shortens the takeoff distance and enables the aircraft to take off quickly, tailwind lengthens

this distance and can make takeoff more complicated. Similarly, crosswind makes it difficult for the aircraft to move stably on the runway and increases the risk of deviation from the runway during landing (*Hahn*, 1989; *Robins* and *Delisi*, 1993; *Slihta et al*., 2015; *Stival et al.,* 2017; *Castilho et al.* 2018; *Nechaj et al*., 2019; *Onwuadiochi et al*., 2019; *Maslovara* and *Mirković,* 2021; *Nae,* 2021; *Jiang et al.,* 2023; *Ghozali et al.,* 2024*; Khattak et al.,* 2024; *Li et al.,* 2024; *Lu,* 2024; *Scherllin-Pirscher et al*., 2025; *Yan* and *Song*, 2024).

Wind shear, which refers to sudden changes in wind direction and speed, is considered one of the most dangerous weather events in aviation. These events, especially during takeoff and landing, cause sudden speed and direction changes at low altitudes, making it difficult to control the aircraft. The FAA (Federal Aviation Administration) has been promoting advanced radar technologies and simulation systems to reduce the rate of wind shear-related accidents since the 1980s (*Kurdyukov et al*., 2004; *FAA,* 2021; *Zhang et al*., 2019; *Chen et al*., 2025; *Huang et al*., 2024; *Salahudden*, 2024). However, it has been proven by many studies that pilot training plays a key role in dealing with such situations (*Van Zante* and *Bond*, 2003; *Yang et al*., 2021; *Dolzhenko et al*., 2024; *Korecki et al*., 2024).

When evaluated from an aerodynamic perspective, the effect of wind on the aircraft is related to basic parameters such as lift, drag, and thrust. For example, a strong headwind reduces the aircraft's speed relative to the ground, significantly shortening the takeoff distance. In addition to reducing fuel consumption, this also increases operational efficiency (*FSF*, 1999). However, in the case of a tail wind, this advantage is lost and take-off distance increases significantly (*Aviation NZ*, 2023; *Liu et al*., 2022). Especially on short runways or high-density altitudes, tail wind can make the negative effects on aircraft performance more obvious (*Fahlgren*, 2007).

The effects of crosswind present a different aerodynamic challenge. Crosswind makes it difficult for the aircraft to remain in line with the runway during landing and is highly dependent on the pilot's control ability (*Ebbatson et al*., 2007). Aircraft manufacturers such as Airbus and Boeing have differentiated crosswind limits according to aircraft models, and these limits vary depending on the aircraft type and pilot experience (*Van Es et al*., 2001; *Airbus*, 2020; *Boeing*, 2019*; Wu* and *Liu*, 2021). Simulation-based studies have been conducted to better understand crosswind effects, and it has been emphasized that pilots' decision-making mechanisms in such conditions depend on the quality of training (*Castilho et al*., 2018; *Sumaja et al*,. 2019).

The impact of wind on flight operations is not limited to the landing and takeoff phases. On long-haul flights, jet streams can significantly affect aircraft fuel consumption and flight times. Flight routes that are correctly aligned with jet streams provide great advantages both economically and environmentally.

The effect of wind on landing and takeoff is related not only to weather conditions, but also to the location of the airport and the runway arrangements.

Geographically, airports in areas subject to frequent wind shear present a higher risk during landing and takeoff. For example, the old Kai Tak Airport in Hong Kong witnessed great difficulties in landing aircraft due to frequent crosswind conditions, and this has inspired many analysis studies in aviation history (*Grace et al*., 1957).

In addition, other factors such as atmospheric density, temperature, and humidity can increase the impact of wind. In hot and humid weather conditions, air density decreases, which negatively affects the ability of aircraft to generate lift. Especially at airports located at high altitudes, these effects become more pronounced. It is of great importance for pilots to correctly manage aircraft performance in such conditions (*Aviation NZ*, 2023).

Carefully monitoring the wind factor around airports is vital to ensure flight safety and operational efficiency. The use of weather radar systems and wind measuring devices enables accurate assessment of wind conditions. Predicting wind patterns by analyzing long-term weather conditions is also important for infrastructure planning of airports. In this context, international authorities recommend using at least 10 years of data in wind and wind trend studies. Both the NOAA Climate Prediction Center (*NOAA*, 2020) and the Federal Aviation Administration (*FAA*, 2020) support using 10 years or more of data in such operational and analysis studies. In this study, Samsun, Zonguldak, and Trabzon airports, which are three provinces from the Black Sea Region where wind has intense influence, were examined. 16 years of data between 2008 and 2023, which could provide maximum data for three cities, were used within the scope of the study.

Mismanagement of the wind factor can lead to adverse effects not only on aircraft performance but also on operational costs. Accurate analysis of atmospheric phenomena such as jet streams can reduce fuel consumption in long-haul flights and contribute to environmental sustainability. However, at airports in regions with frequent wind shear, the implementation of advanced simulation and training programs can strengthen safety by increasing pilots ability to cope with such situations.

As a result, constantly monitoring the wind factor around airports and taking appropriate measures not only increases flight safety, but also increases sectoral efficiency by shortening flight times and saving fuel. Maintaining such monitoring and management processes in an integrated manner will provide both technical and economic benefits in the aviation sector.

Also wind speed and direction play a critical role in airport design, because taking off and landing from the wind increases safety. Therefore, runways are positioned according to the long-term wind direction and speed in the region. Using wind rose analysis, prevailing wind directions are determined and the layout of the runways is planned accordingly. Since crosswinds can make flight operations difficult, this situation is also taken into account; if necessary, runways are designed in different directions. Since excessive wind speeds can increase the

risk of turbulence, this factor is evaluated during airport site selection. In addition, environmental factors and terrain structure can affect the behavior of the wind. All these analyses are necessary for airport operations to be safe and efficient.

The present study has been conducted for the purpose of investigating the temporal changes in wind speed values at Samsun, Trabzon, and Zonguldak airports in the Black Sea Region of Türkiye. To this end, monthly average wind speeds and directions from the Turkish State Meteorological Service for the period 2008–2023 were analyzed by Innovative Trend Analysis (ITA) and Innovative Polygon Trend Analysis (IPTA). The present paper is comprised of four chapters. Section 1 comprises a comprehensive literature review and the purpose of the paper. Section 2 delineates the study area and the methodologies that was employed. Section 3, the findings obtained as a result of the analyses are evaluated. Finally, Section 4 presents the conclusions of the study.

2. Materials and methods

2.1. Study area

The Black Sea Region is a region where the wind effect is felt intensely due to its environmental characteristics and geographical location. The region has the large water mass of the Black Sea in the north and the Eastern Black Sea Mountains in the south. This location causes the winds resulting from the pressure differences between the sea and the land to become stronger. Especially northerly winds blowing from the north and land winds from the northwest are dominant in the region. While the breeze blowing from the sea to the land provides coolness in the summer months, strong winds and storms are generally observed in the winter months. In addition, the fact that the Eastern Black Sea Mountains lie parallel to the coast creates an orographic effect on the speed and direction of the winds, which can lead to sudden wind changes and turbulence in the region. This is a decisive and critical factor for both local life and aviation operations.

Samsun-Çarşamba Airport is an airport located in the Black Sea Region and one of the important transportation points of the region. The airport, which was opened in 1998, serves domestic and international flights. The runway layout is designed parallel to the Black Sea and offers landing and takeoff opportunities for wide-body aircraft with its 3,000-meter-long runway. Since it is geographically close to the seashore, the effect of wind is carefully evaluated in operational activities. Especially northerly winds and northwesterly winds can be decisive on runway operations. In addition to commercial flights, the airport also serves training flights and cargo transportation (*DHMI*, 2023).

Zonguldak Airport is an airport located on the Black Sea coast and opened to civil aviation service in 2007. It is the only airport serving the Western Black Sea Region of Türkiye. The airport's runway is 1,881 meters long and is generally suitable for the landing and takeoff of small and medium-sized aircraft (*DHMI*,

2023). Due to its geographical location, intense winds and sudden changes coming from the Black Sea may occasionally put flight operations at risk. In addition to this information, the airport, located in the congested area between the sea and the mountains, can create difficult conditions during landing and takeoff.

Trabzon Airport is one of the busiest airports in the Eastern Black Sea Region and was put into service in 1957 (*DHMI*; 2023). The airport, which serves both domestic and international flights, is an important transportation gateway as it is the tourism and trade center of the region. The runway layout is designed parallel to the Black Sea and has a length of 2,640 meters. Due to its geographical location, the tight space between the sea and the mountains can cause wind turbulence. Crosswinds and sudden wind changes can pose difficulties for pilots, especially during landing (*Scherllin-Pirscher et al*., 2025; *Yan* and *Song*, 2024). Trabzon Airport is the main entry point for many international flights to the Black Sea Region and plays a critical role in the economic development of the region. The location of these three airports can be seen in *Fig. 3*.

Fig.3. The location of airports.

2.2. Innovative Trend Analysis (ITA)

ITA was proposed by *Şen* (2012) with the objective of graphically examining the trends of hydrometeorological parameters. The method involves dividing the time series into two equal parts, sorting these parts from smallest to largest, and placing the first part on the horizontal axis and the second part on the vertical axis, with these parts positioned opposite each other in the distribution graph. The points situated in the upper part of the 1:1 (45°) line demonstrate an increasing trend, whilst the points positioned in the lower part exhibit a decreasing trend. ITA, as

developed by *Şen* (2012), was further refined by *Şen* (2017a, 2017b) through the incorporation of a statistical significance test (Eqs.(1–6)).

$$E(s) = \frac{2}{n}[E(\overline{y_2}) - E(\overline{y_1})] \tag{1}$$

$$\sigma_s{}^2 = \frac{4}{n^2}[E(\overline{y_2})^2 - 2E(\overline{y_2 y_1}) - E(\overline{y_1})^2] \tag{2}$$

$$\rho_{\overline{y_2 y_1}} = \frac{E(\overline{y_2 y_1}) - E(\overline{y_2}) - E(\overline{y_1})}{\sigma_{\overline{y_2}} \sigma_{\overline{y_1}}} \tag{3}$$

$$\sigma_s{}^2 = \frac{8}{n^2}\frac{\sigma^2}{n}\left(1 - \rho_{\overline{y_2 y_1}}\right) \tag{4}$$

$$\sigma_s = \frac{2\sqrt{2}}{n\sqrt{n}}\sigma_s\left(1 - \rho_{\overline{y_2 y_1}}\right) \tag{5}$$

$$CL_{(1-\propto)} = 0 \pm s_{critical}\sigma_s \tag{6}$$

In Eqs.(1–6), $E(s)$ represents the first-order moment of the slope, n represents the data length, ρ represents the cross-correlation coefficient between the two halves, σ represents the standard deviation of the entire data series, $\sigma_s{}^2$ represents the variance of the trend slope and σ_s represents the standard deviation of the slope. $s_{critical}$ represents the Z value obtained from the standard normal distribution at a certain confidence level. Should the gradient of the trend exceed the upper confidence limit, it is considered to be an increasing trend; conversely, if it exceeds the lower limit, it is considered to be a decreasing trend. If these conditions are not met, it is considered that there is no statistically significant trend at a certain confidence level. In this study, the ITA significance test was performed at a 95% confidence level (*Şen*, 2017a,2017b*; Gümüş et al*, 2021, 2022*; Nacar et al*., 2022).

2.3. Innovative Polygon Trend Analysis (IPTA)

In the IPTA method developed by *Şen et al*. (2019), which can be applied to different time scales, parameters such as the mean, minimum, maximum, standard deviation and skewness of time series of hydrometeorological climate parameters can also be used as input. Average values of parameters were used in this study. In this method, as in ITA, time series are divided into two halves for all segments. The mean of the two half-series for each segment is calculated and plotted in the Cartesian coordinate system to create a polygon. In the graphical evaluation, the process steps in ITA are followed (*Şen et al*., 2019; *Çeribaşı et al*., 2021; *Gümüş et al*., 2022; *Hussain et al*., 2023; *Günes et al*., 2024).

3. Results

Knowing the prevailing wind direction is of critical importance for airport designers, pilots and air traffic controllers to ensure the safety of flight operations. First of all, the prevailing wind direction is a fundamental factor in runway design and orientation. Runways are usually built against a headwind, because the headwind allows aircraft to move safely over shorter distances during takeoff and landing (*ICAO*, 2020). Knowing the prevailing wind direction also enables safer approach and landing plans. By minimizing side and cross wind effects, pilots can make a safer landing.

Moreover, information of prevailing wind direction provides effective guidance in creating emergency strategies. It supports pilots in making the right decisions by influencing the selection of alternative runways or airports in case of a potential emergency landing situation. In addition, wind direction should be taken into account when designing the land around the airport. As a result, it can be said, that accurate analysis of the prevailing wind direction not only increases flight safety, but also offers strategic advantages in terms of operational efficiency and environmental sustainability.

In this study, monthly prevailing wind directions for the 16 years between 2008 and 2023 were examined for Samsun, Zonguldak, and Trabzon airports. In this context, the prevailing wind directions are given in *Table 1*.

Table 1. Prevailing wind direction table

Airports	**1**	**2 3 4 5**	**6**	**7**	**8**	**9**	**10**	**11**	**12**	**GENERAL**
Samsun	S	E E E E	NNW	NNW	NNW	SSE,E	SE,E	E	E	**E**
Trabzon	SSW	E E E E	E	SSW	SSW	SSW	SSW	SSW	SSW	**SSW**
Zonguldak	S	E E N N	N	NNW	NNW	E	E	E,S	E,S	**E**

In this context, according to the results obtained from the data, the prevailing wind direction for Samsun Çarşamba Airport was determined as east (E), for Trabzon Airport as south-southwest (SSW) and for Zonguldak Airport as east (E). Airports were selected as Zonguldak in the west of the Black Sea Region, Samsun in the middle, and Trabzon in the east in order to examine the behavior of the data more effectively.

The temporal changes of the monthly mean wind speed values of Samsun, Trabzon, and Zonguldak airports in the Black Sea region were investigated using ITA and IPTA. The ITA results of the airports are presented in *Table 2* and *Figs. 4, 5*, and *6,* while the IPTA results are presented in *Table 2* and *Fig. 7*.

Table 2. ITA and IPTA results

	Samsun				Trabzon				Zonguldak			
	ITA			IPTA	ITA			IPTA	ITA			IPTA
	$CL_{0.95}$	S	Trend	Trend	$CL_{0.95}$	S	Trend	Trend	$CL_{0.95}$	S	Trend	Trend
Jan.	0.16	0.02	↑	↑	0.28	0.11	↑	↑	0.14	0.03	↑	↑
Feb.	0.17	0.03	↑	↑	0.33	0.09	↑	↑	0.18	0.06	↑	↑
Mar.	0.18	-0.02	↓	↓	0.26	0.06	↑	↑	0.19	0.06	↑	↑
Apr.	0.15	0.00	↔	↔	0.39	0.14	↑	↑	0.18	0.05	↑	↑
May.	0.15	0.03	↑	↑	0.39	0.13	↑	↑	0.18	0.05	↑	↑
Jun.	0.16	-0.03	↓	↓	0.27	0.08	↑	↑	0.17	0.04	↑	↑
Jul.	0.16	0.01	↑	↑	0.31	0.10	↑	↑	0.18	0.04	↑	↑
Aug.	0.16	0.02	↑	↑	0.36	0.07	↑	↑	0.19	0.03	↑	↑
Sep.	0.14	0.01	↑	↑	0.30	0.11	↑	↑	0.16	0.03	↑	↑
Oct.	0.15	-0.02	↓	↓	0.29	0.12	↑	↑	0.15	0.03	↑	↑
Nov.	0.15	-0.02	↓	↓	0.32	0.14	↑	↑	0.17	0.06	↑	↑
Dec.	0.16	0.02	↑	↓	0.29	0.13	↑	↑	0.16	0.02	↑	↑

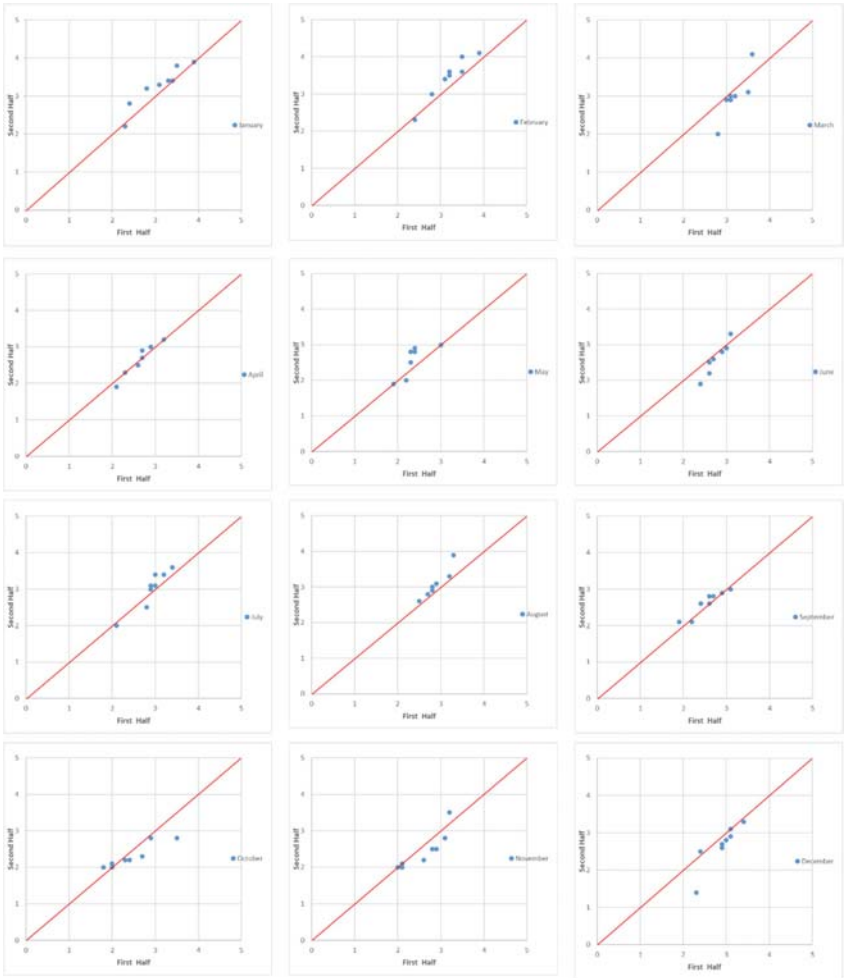

Fig. 4. ITA graphical results for Samsun.

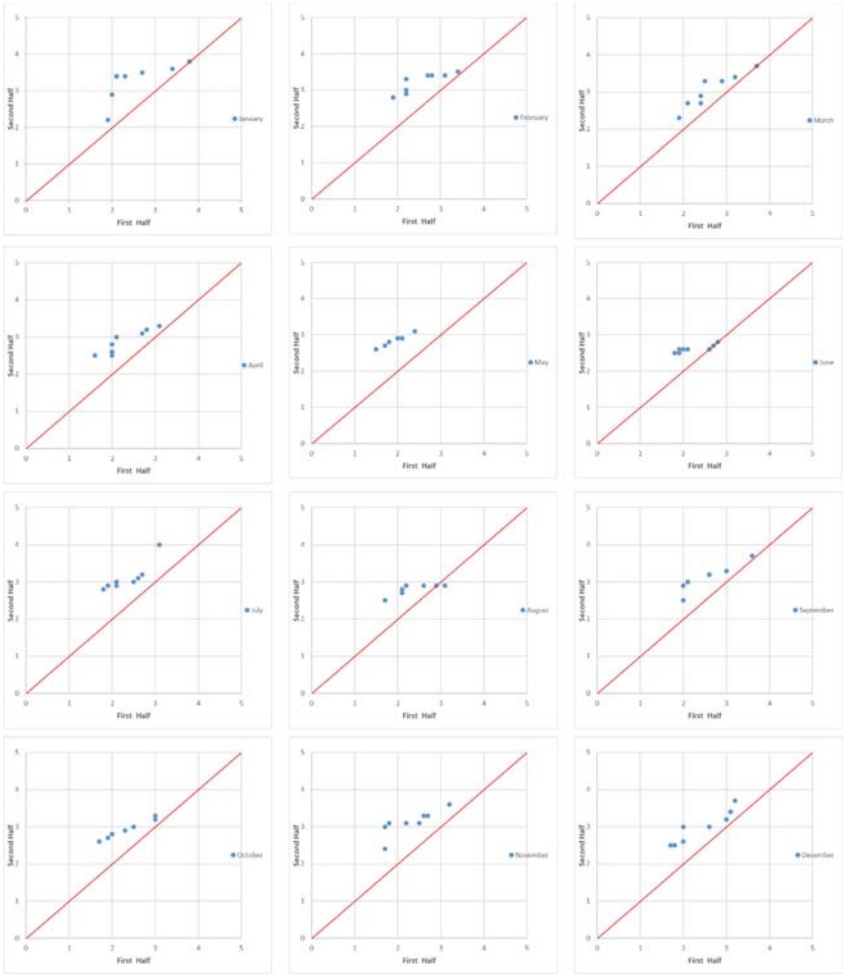

Fig. 5. ITA graphical results for Trabzon.

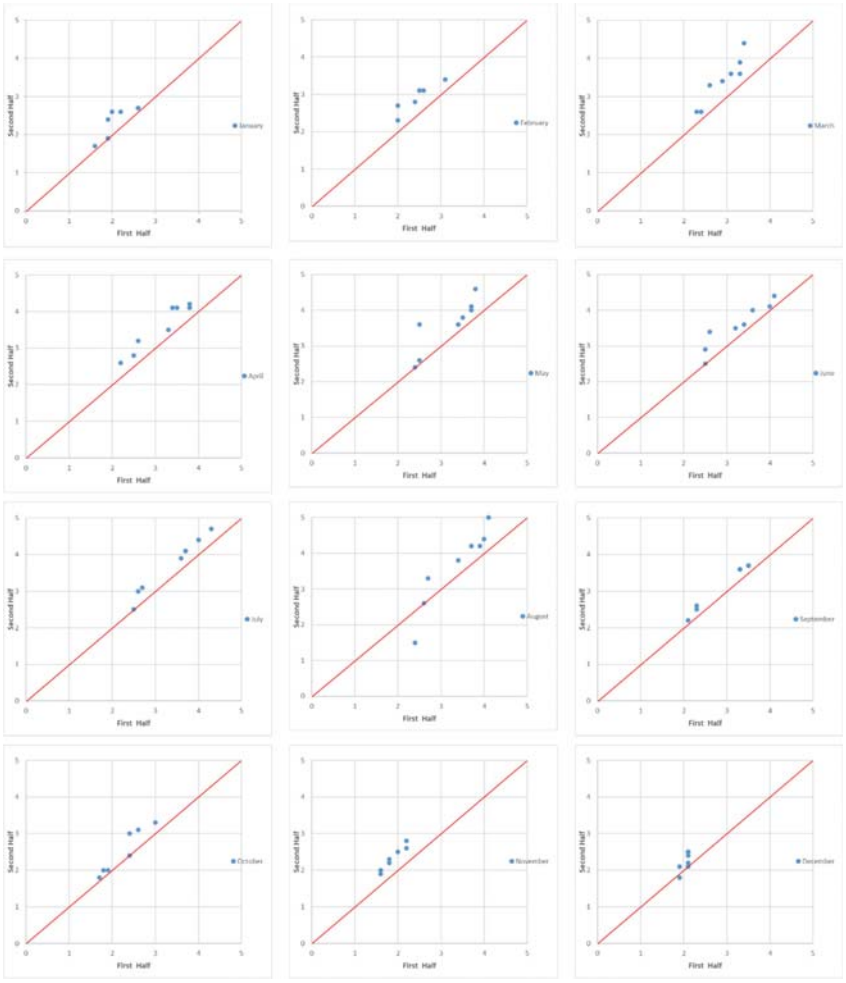

Fig. 6. ITA graphical results for Zonguldak.

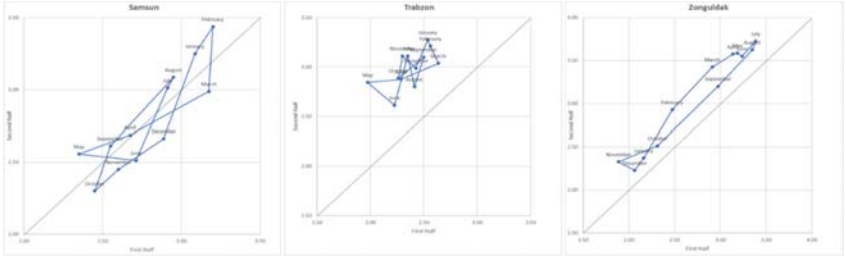

Fig. 7. IPTA graphical results for Samsun, Trabzon, and Zonguldak.

As demonstrated in *Table 2* and *Fig. 4*, which incorporate the ITA results for Samsun Airport situated within the Black Sea Region, it has been ascertained that wind speed trends exhibit variation by month. An increasing trend was identified in wind speed values in January, February, May, July, August, September, and December. Conversely, a decreasing trend was identified in March, June, October, and November. It is noteworthy that these increasing/decreasing trends are not statistically significant, as they are below the limit values at the 95% confidence level. In April, a value of "0" was calculated, indicating that wind speed did not exhibit a trend in that month. According to the IPTA results presented in *Table 2* and *Fig. 7*, they are parallel to ITA, with the exception of December. In December, IPTA determined a decreasing trend. As demonstrated in *Table 2, Figs. 5* and *6*, which incorporate the ITA and IPTA results of Trabzon airport in the east of the Black Sea Region and Zonguldak airport in the west, an increasing trend has been determined in all months at these two airports. These trends are not statistically significant when they remain below the limit values at the 95% confidence level.

The trend analysis of wind speed values at airports located in the center, western and eastern of the Black Sea Region has revealed an increasing trend in wind speeds in all months. According to the analysis results of Samsun, which is located in the center of the region, has shown variations in the determined trends according to the months of the year. The trend analysis results of the methods employed across the region indicate a generally supportive relationship between ITA and IPTA.

The influence of wind on air transportation holds significant importance in terms of operational efficiency and flight safety. Research and practical applications demonstrate that wind conditions play a pivotal role in shaping pilot decision-making processes and influencing the performance of aircraft, particularly during critical phases such as takeoff and landing. In this context, such studies are useful and important.

The study makes a unique and important contribution to the literature on reducing accident risks in airline transportation with the methods used and the analysis of meteorological factors. In particular, the effects of wind factor on flight safety are analyzed in detail and applicable recommendations are developed in many areas from runway arrangements to pilot training programs. The study provides a strategic basis for safer flight operations by determining the prevailing wind directions at Samsun, Zonguldak, and Trabzon airports. In addition, by predicting seasonal changes, the planability of flight operations is improved. The integration of simulation technologies to mitigate wind-related risks in pilots' decision-making processes has been proposed, and the sectoral benefits of these applications have been emphasized. The effects of wind factor on fuel consumption and flight times are also discussed in the context of environmental sustainability, and it is stated that these findings can shed light on sectoral innovations. In long-term planning, the potential impacts of climate change on

wind patterns should be considered. This study makes an important contribution to the future of the aviation industry, both theoretically and practically.

4. Conclusion

The effects of wind on air transport play a critical role in terms of operational efficiency and flight safety. In this study, 16 years of wind data for Samsun, Zonguldak, and Trabzon airports are analyzed, and the wind dynamics of the region are presented in detail. The findings of the study once again emphasized the importance of the wind factor not only in terms of flight safety but also in terms of airport infrastructure planning, development of pilot training programmes, and sectoral efficiency.

1. Regional wind characteristics and environmental factors

Geographical and climatic features in the Black Sea Region are the main factors determining the wind behavior in the region. Especially the locations of Samsun, Zonguldak, and Trabzon airports between the sea and the mountains cause difficulties such as orographic effects and sudden wind changes. In this study, it was determined that south-southwesterly winds prevail in Trabzon and easterly winds prevail in Samsun and Zonguldak. This information can be used to make flight operations in the region safer.

2. Contribution of methods: ITA and IPTA analyses

Innovative Trend Analysis (ITA) and Innovative Polygon Trend Analysis (IPTA) methods are the main analysis tools of this study. Thanks to these methods, changes in wind speeds and directions were analyzed in detail. Especially understanding the seasonal changes will increase the predictability in flight operations. The usability of these methods in airport design, risk management, and long-term planning provides a significant advantage.

3. Airport design and safety improvements

Wind factor plays a critical role in runway routing and airport layout. The findings of the study show that runway arrangements considering the prevailing wind directions will increase takeoff and landing safety. It can be emphasized that alternative runway designs should be evaluated, especially in areas where the side wind effect is intense.

4. Updating pilot training programmes

The effects of wind on flight are of great importance in the decision-making processes of pilots. In this context, the development and integration of simulation technologies into pilot training programmes will play a key role in the management of wind-related risks. Pilots who experience especially hazardous weather conditions in simulation environment will be more prepared for real operations.

5. Operational efficiency and environmental sustainability
The impact of the wind factor on fuel consumption and flight times is also important in terms of environmental sustainability. More effective utilization of natural advantages such as jet streams can reduce environmental impacts by saving fuel. The study reveals the potential for such impacts to improve operational efficiency.

6. Climate change and future strategies
Climate change may lead to changes in wind patterns, posing new operational challenges. Therefore, the effects of climate change need to be taken into account in long-term planning. The ITA and IPTA methods used in this study provide a suitable basis for long-term monitoring of such changes.

7. Importance of local microclimatic analyses
Microclimatic analyses specific to each airport will provide a better understanding of wind factors. Especially at airports with different geographical characteristics such as Trabzon, Zonguldak, and Samsun, local analyses can provide critical data to improve flight safety.

8. Land use and landscaping
Planning the land arrangements around the airports by considering the wind directions will be effective in reducing operational risks. The prevailing wind directions determined in the study can provide guidance for environmental regulations and construction around the airport.

9. Standardisation of data use and technology integration
Standardization of long-term wind data and integration with new technologies can increase operational efficiency. In particular, the integration of artificial intelligence-supported decision support systems will enable real-time analysis of wind data, offering both security and economic advantages.

10. Multidisciplinary cooperation and future investments
Effective management of the wind factor requires the cooperation of different disciplines such as meteorology, engineering, air traffic control, and pilotage. Strengthening this co-operation will contribute to the sector both technically and economically. Furthermore, increasing investments in technological developments should be a strategic priority for the future of the aviation sector.

As a result, wind factor management is of great importance not only for flight safety but also for operational efficiency, environmental sustainability, and infrastructure planning. This study has made significant contributions to the understanding and management of wind effects and has shed light on future studies. With long-term strategic plans, technological innovations, and

interdisciplinary cooperation, the aviation industry can achieve a safer, more efficient, and sustainable structure.

Authorship contribution statement: Ömer Faruk Uzun: Writing – review and editing, Writing – original draft, Validation, Supervision, Project administration, Methodology, Investigation, Conceptualization. Ramazan Gürsel Hoşbaş: Writing – review and editing, Writing – original draft, Visualization, Validation, Resources, Methodology, Investigation, Formal analysis.

Declaration of Competing Interest:The authors declare that they have no known competing financial interests or personal relationships that could have appeared to influence the work reported in this paper.

***Data availability*:**Data will be made available on request.

Acknowledgements:The authors thank the Turkish State Meteorological Service for providing the meteorological data. The authors also thank the reviewers for their constructive criticisms which have considerably improved this manuscript.

References

Airbus. 2020: Aircraft performance in tailwind conditions. Retrieved from https://www.airbus.com

Aviation NZ. 2023: Take-off and landing performance. Retrieved from https://www.aviation.govt.nz

Boeing. 2019: Operational challenges of crosswind landings. Retrieved from https://www.boeing.com

Castilho, D. S., et al. 2018: "STPA for continuous controls: A flight testing study of aircraft crosswind takeoffs." *Safety Science*, 108, 129–139. https://doi.org/10.1016/j.ssci.2018.04.012

Ceribasi, G., Ceyhunlu, A.I. and *Ahmed, N*. 2021: Analysis of temperature data by using innovative polygon trend analysis and trend polygon star concept methods: a case study for Susurluk Basin, Turkey. *Acta Geophys. 69*, 1949–1961. https://doi.org/10.1007/s11600-021-00632-3

Chen, F., Li, C., Peng, H., Chan, P. W., and *Chen, J*., 2025: Low-level Wind Shear Induced by Airport Buildings: A Numerical Simulation Study. *KSCE J. Civil Engin. 29*(6), 100103. https://doi.org/10.1016/j.kscej.2024.100103

DHMI . 2023: Türkiye'deki havalimanları. Retrieved from https://www.dhmi.gov.tr

Dolzhenko, N., Assilbekova, I., Abzhapbarova, A., Mussayeva, G., and *Sarzhanov, T*., 2024: Unification of Training Programs for Aviation Professionals as a Flight Safety Criterion. *J. Aerospace Technol. Manage. 16(2)*, https://doi.org/10.1590/jatm.v16.1320

Ebbatson, M., Harris, D., and *Jarvis, S*., 2007: Crosswind landings in general aviation: a modified method of reporting wing information to the pilot. *Int. J. Aviation Psychol 17*(4), 353–370.

FAA., 2020: Airport Design Advisory Circular 150/5300-13B: Airport Design. Retrieved from https://www.faa.gov/airports/engineering/design

FAA., 2021: Wind shear and turbulence: Mitigation strategies in aviation. Washington, DC: FAA Technical Center.

Fahlgren, G. 2007: Tail Wind Traps. *AeroSafety world*, *2*(3), 46–47.

FSF., 1999: Killer in aviation: FSF task force presents facts about approach and landing and controlled flight into terrain accidents (II ed.). Alexandria, USA: Flight Safety Foundation.

FSF., 2022: Airline accidents 2022. Retrieved from https://aviation-safety.net/database/2022-analysis (Access date: 23.09.2024)

Ghozali, A. L., Kuresih, K., Cahyanto, K. A., Iryanto, I., and *Gernowo, R*., 2024: Web Based Dashboard of Airplane Turbulence Mitigation. *Jurnal Ekonomi Teknologi dan Bisnis (JETBIS)*, *3*(11), 1821–1826. https://doi.org/10.57185/jetbis.v3i11.158

Gümüş, V., Dinsever, L. D., Şimşek, O., 2021: Trend Analysis of Historical Drought During 1929-2016 in Diyarbakır Station with Innovative Şen Method. *J. Nat. Haz. Environ. 7*(2), 362–373. https://doi.org/10.21324/dacd.884682

Gümüş, V., Şimşek, O., Açar, M. K. 2022: Assessing the Monthly Total Rainfall Trends at Artvin and Rize Stations using Different Methods. *Harran University Journal of Engineering 7*(3), 204–216. https://doi.org/10.46578/humder.1207593

Güneş, B., Demirtaş, B., Tuncer, G., Sönmez, O. 2024: Analysis of Temperature and Precipitation Data Using Innovative Trend Analysis Methods: Kucuk Menderes Basin, Türkiye. *Uludağ University Journal of The Faculty of Engineering*, *29*(2), 443–462. https://doi.org/10.17482/uumfd.1473532

Grace, H., Henry, J.K.M., Skempton, A.W., Lloyd Jones, R.F., Jones, R.F.L., Golder, H. Q., ... and *Alston, J*., 1957: Dıscussıon On Aırport Paper No. 35: The Plannıng And Desıgn Of The New Hong Kong Aırport. *Proceedings of the Institution of Civil Engineers*, *7*(2), 305–325.

Hahn, K. U. 1989: Effect of wind shear on flight safety. *Progress in Aerospace Sciences*, *26*(3), 225–259. https://doi.org/10.1016/0376-0421(89)90004-3

Huang, X., Zheng, J., Shao, A., Xu, D., Tian, W., and *Li, J*. 2024: Study of low-level wind shear at a Qinghai-Tibetan Plateau airport. *Atmos. Res. 311*, 107680 https://doi.org/10.1016/j.atmosres.2024.107680

Hussain, F., Wu, RS., Nabi, G. et al., 2023: Analysis of Temperature Data Using the Innovative Trend Pivot Analysis Method and Trend Polygon Star Concept: A Case Study of Soan River Basin, Potohar, Pakistan. *Pure Appl. Geophys*. 180, 475–507. https://doi.org/10.1007/s00024-022-03203-9

ICAO. 2020: Aerodrome design manual: Part 1 – Runways (4th ed.). ICAO. Retrieved from https://www.icao.int

Jiang, W., Chang, R. C., Yang, N., and *Xu, Y*. 2023: Severity assessment of sudden plunging motion for jet transport aircraft in response to severe atmospheric turbulence. *Aircraft engineer. aerospace technol 95*(10), 1633–1641.

Khattak, A., Zhang, J., Chan, P. -w., Chen, F., and *H. Almaliki, A*. 2024: A New Frontier in Wind Shear Intensity Forecasting: Stacked Temporal Convolutional Networks and Tree-Based Models Framework. *Atmosphere 15*(11), 1369. https://doi.org/10.3390/atmos15111369

Korecki, Z., Hoika, T., Bauer, M., and *Smrž, V*. 2024: New approach to military pilot education and training in the new security environment. *Transport Problems 19,* 137–150. https://doi.org/10.20858/tp.2023.19.2.11

Kurdyukov, A. P., Pavlov, B. V., Timin, V. N., and *Vladimirov, I. G*. 2004: Longitudinal anisotropy-based flight control in a wind shear. *IFAC Proceedings Volumes*, *37*(6), 423–426. https://doi.org/10.1016/S1474-6670(17)32211-5

Li, F., Xu, X., Li, J., Hu, H., Zhao, M., and *Sun, H*. 2024: Wind Shear Operation-Based Competency Assessment Model for Civil Aviation Pilots. *Aerospace 11*(5), 363. https://doi.org/10.3390/aerospace11050363

Liu, J., Qian, W., Bai, Y., and *Xu, X*. 2022: Numerical and Experimental Research on Flight Control of a V-Tail Configuration for the Wind Tunnel Model of Aircraft. *Aerospace*, *9*(12), 792. https://doi.org/10.3390/aerospace9120792

Lu, C., Le, N., Ding, Z. 2024: Flight Safety Assessment Method of Civil Aircraft During Approach Based on Cluster Analysis. In: Proceedings of the 6th China Aeronautical Science and Technology Conference. *CASTC 2023.* Lecture Notes in Mechanical Engineering. Springer, Singapore. https://doi.org/10.1007/978-981-99-8864-8_39

Maslovara, A., and *Mirković, B*. 2021: Impact of Tailwind on Airport Capacity and Delay at Zurich Airport. *Transportation Research Procedia 59*, 117–126. https://doi.org/10.1016/j.trpro.2021.11.103

Nacar, S., Şan, M., Kankal, M., Okkan, U. 2022: Trend Analysis of Meteorological Droughts for Different Climate Change Scenarios in Eastern Black Sea Region. *J. Inst. Sci. Technol. 12*(2), 843–856. https://doi.org/10.21597/jist.998196

Nae, G. 2021: Wınd shear assocıated wıth medıterranean cyclones actıvıty and the ımpact on flıght safety durıng wınter operatıons at henrı coanda otopenı and aurel vlaıcu baneasa aırports. *Review of the Air Force Academy 43*(1), 5–16. https://doi.org/10.19062/1842-9238.2021.19.1.1

NOAA. 2020: Climate Prediction Center: Understanding ENSO. Retrieved from https://www.cpc.ncep.noaa.gov/

Nechaj, P., Gaál, L., Bartok, J., Vorobyeva, O., Gera, M., Kelemen, M., and *Polishchuk, V*. 2019: Monitoring of Low-Level Wind Shear by Ground-based 3D Lidar for Increased Flight Safety, Protection of Human Lives and Health. *Int. J. Environ. Res. Public Health*, *16*(22), 4584. https://doi.org/10.3390/ijerph16224584

NTSB. 2019: Aviation accident database and synopses. Retrieved from https://www.ntsb.gov/_layouts/ntsb.aviation/index.aspx (Access date: 20.09.2024).

Onwuadiochi, I. C., Ijioma, M. A., Ezenwaji, E. E., and *Obikwelu, M. C*. 2019: Effects of wind shear on flight operations in Sam Mbakwe Airport, Imo State, Nigeria. *Tropical Built Environ. Journal*, *7*(1), 39–49.

Robins, R.E. and *Delisi, D.P*. 1993: Potential hazard of aircraft wake vortices in ground effect with crosswind. *Journal of Aircraft*, *30*(2), 201–206. https://doi.org/10.2514/3.48266

Salahudden, S. 2024: Impact of Wind and Wind Shear on Sliding Mode Controller Assisted Aircraft Spin Recovery. *Control Engin. Practice*, *145*,105872. https://doi.org/10.1016/j.conengprac.2024.105872

Scherllin-Pirscher, B., Nickovic, S., Votsis, A., Cvetkovic, B., Amiridis, V., Bolic, T., Brenot, H., Brock, G., Clarkson, R. J., Durant, A., Hirtl, M., Lekas, T. I., Mona, L., Nasser, H., Ryder, C. L., Ryuzaki, J., Suárez-Molina, D., Vimic, A. V., and *Basart, S*. 2025: Airborne soil-derived dust hazards in aviation. *Bull. Amer. Meteorol. Soc. 106*(1) E125–E145. https://doi.org/10.1175/BAMS-D-23-0311.1

Slihta, M., Lazareva, I., and *Šestakovs, V*. 2015: Evaluation of the dynamic characteristics of aircraft during landing in crosswinds. *Transport Aerospace Engin. 2*, 27–35. https://doi.org/10.1515/tae-2015-0004

Stival, L.J.L., Guetter, A.K., and *de Andrade, F.O*. 2017: The impact of wind shear and turbulence intensity on wind turbine power performance. *Espaço Energia*, *27*, 11–20.

Sumaja, K., Syahdian, A. S., and *Satriyabawa, I. K. M*. 2019: Analysing Crosswind, Headwind, And Tailwind At I Gusti Ngurah Rai Airport For Aircraft Risks Assessment During Take-Off And Landing Process.

Şen Z, 2012: Innovative Trend Analysis Methodology. *J. Hydrol Engin 17*, 1042–1046.

Şen Z, 2017a: Innovative trend significance test and applications. *Theor. Appl. Climatol. 127*, 939–947. https://doi.org/10.1007/s00704-015-1681-x

Şen, Z., 2017b: Innovative Trend Methodologies in Science and Engineering. Springer.

Şen, Z., Şişman, E., and *Dabanli, I*. 2019: Innovative polygon trend analysis (IPTA) and applications. *J. Hydrol. 575*, 202–210. https://doi.org/10.1016/j.jhydrol.2019.05.028

Van Es, G. W., van der Geest, P. J., and *Nieuwpoort, A. M. H*. 2001: Safety aspects of aircraft operations in crosswind, NLR-TP-2001-217.

Van Zante, J., and *Bond, T*. 2003: Overview of NASA's In-Flight Icing Education and Training for Pilots. In 41st Aerospace Sciences Meeting and Exhibit (p. 18) https://doi.org/10.2514/6.2003-18

Yan, Y., and *Song, L*. 2024: Wind Shear Response of Aircraft with C* and C*U Controller during Approach. *Aerospace*, *11*(6), 476. https://doi.org/10.3390/aerospace11060476

Yang, S., Yu, K., Lammers, T., and *Chen, F*. 2021: Artificial intelligence in pilot training and education–towards a machine learning aided instructor assistant for flight simulators. In *International* Conference on Human-Computer Interaction, 581–587. Cham: Springer International Publishing https://doi.org10.1007/978-3-030-78642-7_78

Zhang, H., Wu, S., Wang, Q., Liu, B., Yin, B., and *Zhai, X*. 2019: Airport low-level wind shear lidar observation at Beijing Capital International Airport. *Infrared Phys. Technol. 96*, 113–122. https://doi.org/10.1016/j.infrared.2018.07.033

Wu, Y., and *Liu, Y*. 2021: Research on Flight Technique and Hazard Control for Civil Airplane Crosswind Flight Test. In *2021* International Symposium on Electrical, Electronics and Information Engineering, 19–22. https://doi.org/10.1145/3459104.3459109

DOI:10.28974/idojaras.2026.1.5

IDŐJÁRÁS

Quarterly Journal of the HungaroMet Hungarian Meteorological Service
Vol. 130, No. 1, January – March, 2026, pp. 87–100

Spatiotemporal trends in wood decay risk across European Russia (1961–2020): A Scheffer Climate Index analysis

Elena Vyshkvarkova[1,*] and **Olga Sukhonos**[2]

[1]*A.O. Kovalevsky Institute of Biology of the Southern Seas of RAS,*
299011, Nakhimov Avenue 2, Sevastopol, Russia

[2]*Institute of natural and technical systems,*
299011, Lenina St., 28, Sevastopol, Russia

**Corresponding author E-mail: aveiro_7@mail.ru*

(Manuscript received in final form June 10, 2025)

Abstract—This study evaluates the risk of wood decay in cultural heritage sites across the European part of Russia by analyzing climatic influences on timber deterioration. Timber, a critical component of many heritage structures, is particularly vulnerable to fluctuations in air temperature and moisture, which accelerate biological decay processes. Using the Scheffer Climate Index (*SCI*) – a metric based on average monthly temperature and the number of precipitation days –, the research assesses decay risk over the period 1961–2020 with daily data from the ERA5 reanalysis. The *SCI* was decomposed into temperature and precipitation components, and trends were quantified using the nonparametric Mann–Kendall test, with analyses performed for both the 1961–1990 and 1991–2020 periods. Results reveal a southwestward increase in *SCI* values, with the highest risks (*SCI* > 100) along the Black Sea coast and Caucasus. Notably, northern regions, home to key heritage sites like Kizhi Pogost, exhibited statistically significant upward *SCI* trends (up to 0.6/year), driven primarily by rising temperatures. Between 1961–1990 and 1991–2020, low-risk areas decreased by 9%, transitioning to moderate risk, while high-risk zones remained stable (~13%). Temperature contributions to *SCI* increased by 5–20%, whereas precipitation impacts declined, except in northern regions. Sequential analysis highlighted trend onset in the 2000s, particularly in the northwest and Caucasus. These findings underscore a rising climatic threat to wooden architectural heritage and emphasize the need for enhanced conservation strategies to mitigate future decay risks.

Key-words: cultural heritage sites, wood decay, Scheffer Climate Index, climate change

1. Introduction

Wooden architectural heritage constitutes a significant portion of cultural heritage sites worldwide, with many structures and their components crafted from this traditional building material. As an organic material, timber is particularly susceptible to environmental degradation, with its physical and mechanical properties deteriorating under various atmospheric influences (*Brimblecombe* and *Richards*, 2024). Among environmental factors, moisture and temperature fluctuations play the most critical role in the degradation processes of historical wooden structures (*Sabbioni et al.,* 2009, 2010; *Brimblecombe et al.,* 2011).

The hygroscopic nature of wood makes it vulnerable to damage caused by variations in atmospheric humidity, whether through excessive or insufficient moisture levels (*Blavier et al*., 2023; *Soboń* and *Bratasz,* 2022). Precipitation further exacerbates wood deterioration when water penetrates surface cracks and pores (*Blavier et al.,* 2023). Biological agents, including fungi, bacteria (*Koziróg et al*., 2016), and insects, pose additional threats, with decay fungi representing the most significant cause of economic losses in wooden heritage (*Brimblecombe* and *Lankester,* 2013; *Sesana et al*., 2021; *Prieto et al.,* 2020). Fungal activity depends critically on specific temperature and moisture conditions (*Curling* and *Ormondroyd*, 2020), while higher temperatures generally accelerate both biological degradation and insect infestation (*Flyen et al.,* 2020).

Photochemical degradation from ultraviolet and visible light leads to surface discoloration, increased moisture absorption, and enhanced biodegradation (*Andrady et al*., 2019). Additionally, atmospheric salts contribute to structural damage through crystallization processes and pore formation (*Mi et al*., 2020; *Wang et al.,* 2024).

Recent climatic changes have significantly impacted global hydrological cycles, with substantial precipitation variations observed since the mid-20th century (*IPCC,* 2021; *WMO,* 2021). These systemic climate changes present new challenges for cultural heritage preservation (*Sesana et al*., 2021; *Hall et al*., 2016). Numerous studies indicate that increasing atmospheric humidity, coupled with rising temperatures, creates favorable conditions for enhanced biological activity, accelerating the decomposition of wooden structures by fungi, mold, algae, and insects (*Sesana et al*., 2021; *Prieto et al*., 2020; *Camuffo*, 2019).

The Scheffer Climate Index (*Scheffer,* 1971) remains one of the earliest and most widely used tools for assessing climate-related risks to wood. Originally developed for the contiguous United States, this index estimates regional decay potential based on temperature and precipitation parameters. Subsequent applications have extended to Canada (*Wang* and *Morris,* 2008; *Morris* and *Wang*, 2011), Europe (*Fernandez-Golfin et al*., 2016; *Brimblecombe* and *Richards*, 2023a,b), Korea (*Oh et al*., 2022), and Africa (*Richards et al*., 2023).

The European part of Russia boasts numerous masterpieces of wooden architecture, including UNESCO World Heritage sites like the Kizhi Pogost (18th

century) in Karelia, the Malye Korely open-air museum in Arkhangelsk Oblast (featuring 400-year-old structures), and the Vitoslavlitsy museum in Novgorod Oblast. Other significant examples include the Kostroma Sloboda Museum reserve, historical buildings in Suzdal and Vologda, and architectural monuments throughout Leningrad, Nizhny Novgorod, Smolensk, and Tver regions.

This region exhibits substantial climatic diversity and has experienced significant warming trends (+0.55°C per decade) with variable precipitation patterns (*The Third Assessment Report*, 2022). These changing conditions differentially affect wooden structures across the region, necessitating detailed assessment. This study, therefore, aims to evaluate the potential risks of climate-induced degradation to wooden architectural heritage throughout European Russia, providing crucial data for conservation planning in the context of ongoing climate change.

2. Materials and methods

The daily data on air temperature and precipitation from the ERA5 reanalysis (spatial resolution 0.5°*0.5°) (*Hersbach et al*. 2020) for the period 1961–2020 for the European part of Russia were used. Data are freely available from the Copernicus Climate Data Store (*Copernicus Climate Change Service*). The study region is limited by coordinates 40°–65° N, 25°–50° E.

The analysis of the influence of climatic conditions on wooden heritage sites was carried out using the Scheffer index (*Scheffer,* 1971). The index selects two parameters (air temperature and precipitation) and helps to assess the risk of wood decay.

The Scheffer Climate Index (*SCI*) is calculated using the formula:

$$SCI = \frac{\sum_{Jan}^{Dec}[(T-2)(D-3)]}{16.7}, \quad (1)$$

where T is the average monthly temperature (°C) and D is the average number of days per month with precipitation greater than 0.3 mm per day (*Scheffer*, 1971; *Lisø et al*., 2006).

Months with average air temperatures below 2 °C and/or very little precipitation add nothing to the climate decay potential, as these conditions are not conducive to decay development. Moreover, the reduction that negative values of (T – 2) or (D – 3) introduce into the sum of Eq.(1) is irrelevant to the conceptual basis for developing the Scheffer index. Therefore, in the present study, the product (T − 2) × (D− 3) is always equal to or greater than zero (i.e., if (T − 2) or (D − 3) is negative for the i-th month of the year, then it is set equal to zero for that month) (*Nikolitsa* and *Giarma*, 2019; *Kim* and *Ra*, 2013; *Brischke* and *Selter*, 2020).

Additionally, the contribution of the temperature component (T_{SCI}) and the precipitation component (D_{SCI}) were calculated while maintaining the conversion factor of 16.7:

$$T_{SCI} = \sum_{Jan}^{Dec} [(T - 2)] / 16.7 \quad (2)$$

$$D_{SCI} = \sum_{Jan}^{Dec} [(D - 3)] / 16.7 \quad (3)$$

The overall risk is assessed based on the *SCI* values as follows: a value less than 35 indicates low risk, values from 35 to 65 indicate moderate risk, values from 65 to 100 indicate high risk, and values above 100 indicate very high risk (*Scheffer,* 1971).

The calculation results are presented as spatial maps for the reanalysis grid points to avoid distortions associated with data interpolation. Trends were calculated using the least squares method, and statistical significance was assessed using the nonparametric Mann-Kendall test with a statistical significance level of 0.05. For each period, the median value of the index was calculated for each grid point. The median was chosen because the values of the *SCI* are not characterized by a normal distribution (*Richards et al.,* 2023).

The sequential form of the non-parametric Mann-Kendall test was used as a method for analyzing progressive trends of the time series, which allows one to detect the approximate beginning of a developing trend (*Sneyers,* 1990). The sequential Mann-Kendall (*Moraes et al*., 1998) was used to test the start of a trend within the series *x1*, …, *xn*. The magnitudes of annual or seasonal mean time series *xj* (*j* = 1, …, *n*) were compared by *xk*(*k* = *1*, …, *j* − 1). For each comparison, the number of *xk* > *xj* was counted and denoted by *nj* (*Zhao et al.,* 2015). The test statistic was given as follows:

$$t_j = \sum_1^j n_j (j = 2,3, \dots, n) \quad (4)$$

$$E(t) = \frac{n(n-1)}{4} \quad (5)$$

$$Var(t_j) = \frac{j(j-1)(2j+5)}{72} \quad (6)$$

The sequential value of statistic *U(t)* which is the forward sequence was calculated as

$$U(t) = \frac{t_j - E(t)}{\sqrt{Var(t_j)}}, \quad (7)$$

where *u(t)* is a standardized variable with a zero mean and standard deviation equal to one, which fluctuates around zero as the time series progresses.

U'(t), which is the backward sequence, was calculated with the same formula with the reverse data time series.

The intersection of the curves *U(t)* and *U'(t)* indicates the year of the beginning of the trend, and the intersection point should be between the critical values of the confidence interval, i.e., between -1.96 and +1.96 (*Barbieri et al*., 2017; *Temeliyeh et al.,* 2022; *Chatterjee et al*., 2014). If *U(t)* exceeded the upper or lower 95 % confidence limits (+1.96 and −1.96 for an α=5 % significance level), there was a significant upward or downward trend in the time series (*Liu et al.,* 2008). The intersection of forward and backward curves of the test statistic detected the approximate time of occurrence of the trend (*Barbieri et al*. 2017). If the curves *U(t)* and *U'(t)* intersect in the critical range several times or U(t) crosses the confidence line several times, then there are no significant trends in the time series (*Dufek* and *Ambrizzi*, 2007; *Alijani et al.* 2011, *Temeliyeh et al*. 2022).

The results are obtained for the entire period (1961–2020), as well as for two sub-periods (1961–1990 and 1991–2020) which are defined by WMO as climate norms.

3. Results

3.1. Spatial distribution of the SCI values, temperature and precipitation components

The median values of the *SCI* in the study area in the period 1961–2020 vary within the range from 0 to 160 (*Fig. 1a*). The highest values (above 80) were found on the Black Sea coast of the Caucasus. Throughout the analyzed period, there was an increase in the index values from the northeast to the southwest. In the second climatic period (1991–2020), relative to the first period, there was an increase in the *SCI* across almost the entire analyzed area, especially pronounced in the northeast of the region (an increase of up to 100%) (*Fig. 1b*). The southern regions of the European part of Russia are characterized by a slight decrease in the *SCI* index to 20%, with the exception of the Caucasus ridge, where there is an increase in *SCI* by 80–90% in the highland part (*Fig. 1b*). The risk of wood decay under the influence of climatic factors increases in the southwest direction (*Fig. 1c*). Very high risk (*SCI* values above 100) was found for the Black Sea coast of the Caucasus, Ciscaucasia, and Transcaucasia.

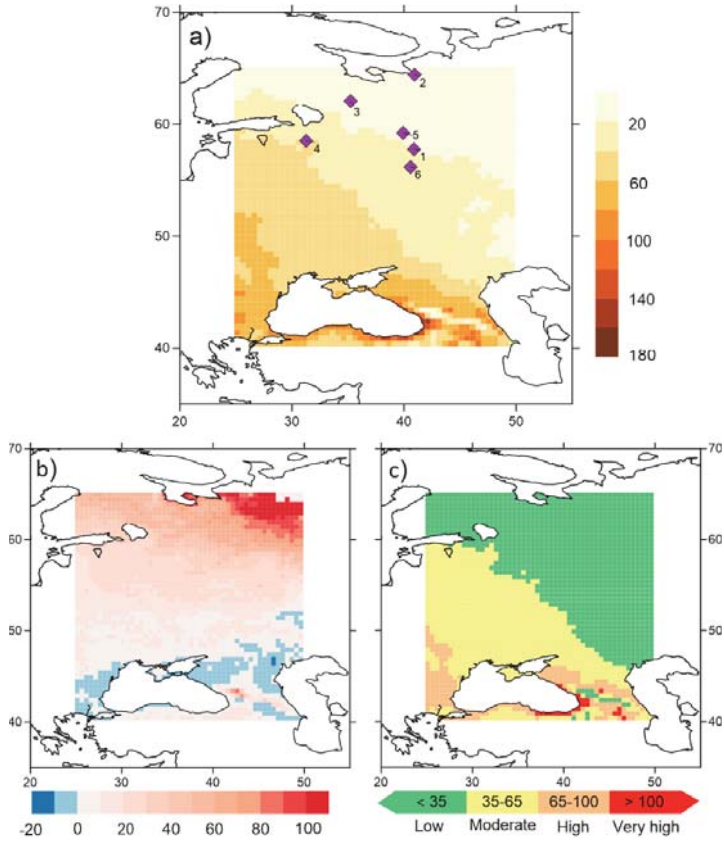

Fig. 1. Spatial distribution of (a) median values of the *SCI* for the entire period (1961–2020); (b) the difference (in %) of the index between the two sub-periods (1961–1990 and 1991–2020); (c) wood decay risk for the period 1961–2020. The diamonds in (a) correspond to the main sites of wooden architecture: *1* –Kostroma Sloboda Museum reserve, *2* –Malye Korely open-air museum in Arkhangelsk Oblast, *3* – Kizhi Pogost, *4* –Vitoslavlitsy museum in Novgorod Oblast, *5* and *6* – historical buildings in Suzdal and Vologda.

The presentation of the results in gradations of the *SCI* values shows that in the second climatic period (1991–2020), compared to the first period, there was a decrease (by 9%) in the area of the territory with a low risk of wood decay, due to an increase in the area with a moderate risk (from 34% to 43%). In the period 1991–2020, the areas of the territory with low and moderate risks become almost equal. The area with a high risk did not change between the two climatic norms and is about 13%.

The *SCI* includes two components: temperature and precipitation. Spatial maps of these components are shown in *Fig. 2*. The entire study area is characterized by an increase in the contribution of the temperature component to

the *SCI*. The change (growth) of the temperature component between the two subperiods in most of the study region is 5–15%. The maximum increase in the contribution of the temperature component to the *SCI* in the second climatic period was found for the territory of Lake Onega (location of the UNESCO cultural heritage site Kizhi Pogost) up to 20%. The opposite picture is observed for the precipitation component. Almost the entire territory shows a decrease in the contribution of precipitation to 15% in the second climatic period compared to the first. A slight increase in the contribution of precipitation (up to 5%) to the *SCI* is observed in the northern regions.

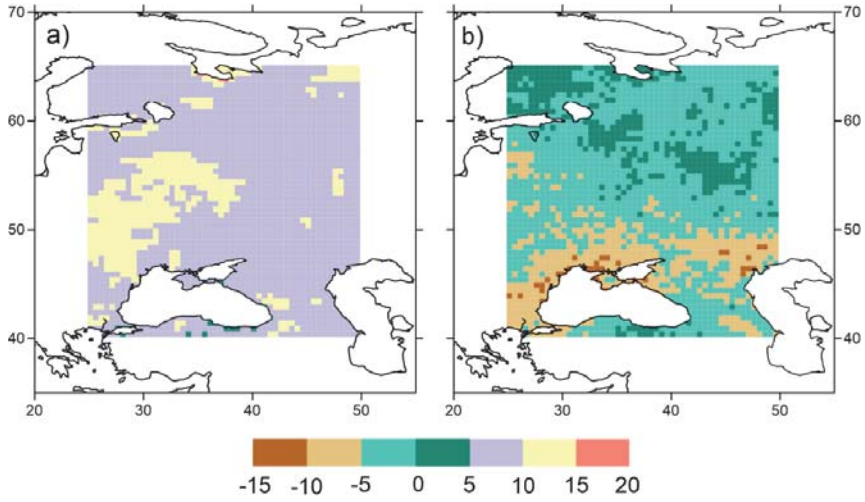

Fig. 2. Change (in %) in the contribution of the temperature (a) and precipitation (b) components of the *SCI* between two periods 1991–2020 and 1961–1990

3.2. Trends of SCI, temperature, and precipitation components

The *SCI* trends for the period 1961–2020 are predominantly positive in the study area. North of 50 degrees latitude, the trend values are statistically significant. The maximum trend values reach 0.6/year in the northwest of the region (*Fig. 3*). The Ciscaucasia is characterized by negative, but statistically insignificant trends, while the Caucasus Mountains itself has a positive *SCI* trend with values from 0.2 to 0.4/year for the period 1961–2020. The trends in the temperature component of the *SCI* are positive and statistically significant throughout the region, with the highest trend values on the northwest coast of the Black Sea and in the White Sea

area. Negative statistically significant trends in the precipitation component of the *SCI* are typical for the northern Black Sea region, the Caucasus Mountains, and the western coast of the Black Sea (*Sukhonos et al*., 2024).

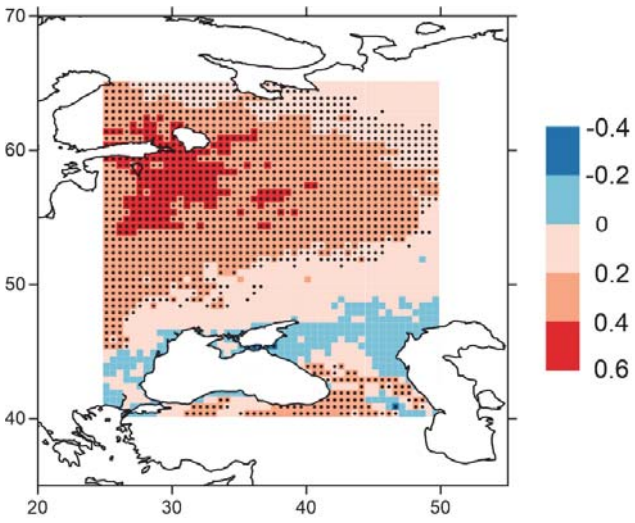

Fig. 3. Trends of the *SCI* for the period 1961–2020. Black dots are statistically significant trends ($p<0.05$)

Using the Mann-Kendall sequential test, estimates of the approximate date of the onset of a significant trend in the *SCI* are obtained. The *Fig. 4* shows spatial maps of statistically significant ($p<0.05$) intersection of the *U(t)* and *U'(t)* curves for the entire period 1961–2020. As it can be seen, the *SCI* index is characterized by upward trends in the northwestern areas of the study region and in the Caucasus Mountains. Single downward trends are found in the Ciscaucasia on the Caspian Sea coast. The temperature component of the *SCI* has upward trends throughout almost the entire territory of the study region for the period 1961–2020, with the exception of the Caucasus Mountains. The precipitation component is characterized by a small number of reanalysis grid points with statistically significant downward trends in the central regions and the Ciscaucasia.

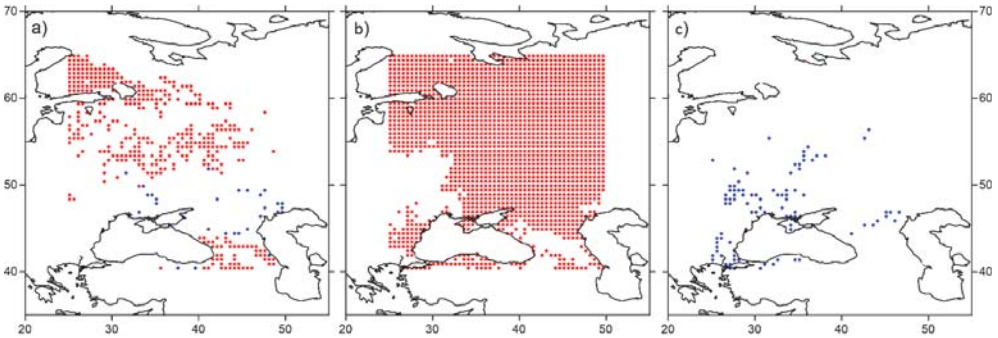

Fig. 4. Spatial distribution of grid points with statistically significant intersection of the *U(t)* and *U'(t)* curves ($p<0.05$) for the period 1961–2020 for *SCI* (a), temperature component (b), and precipitation component (c).

The percentage of grid points with trends of opposite signs is presented in *Table 1*. The maps presented in *Fig. 4* show the total number of statistically significant intersections of the *U(t)* and *U'(t)* curves for the entire period. The distribution by years of the number of grid points with the total number of intersections of the *U(t)* and *U'(t)* curves and the statistically significant ones for the period 1961–2020 are presented in *Fig. 5a*. In some years, the percentage of grid points with intersections reaches 5.3% (1980), while the percentage of significant intersections reaches approximately 2.5% in the same 1980 and in 2003. When comparing the two subperiods, it is clear that the number of intersections of the *U(t)* and *U'(t)* curves in the first period 1961–1990 is higher compared to the second period, but the percentage of statistically significant transitions increases in the second period. The largest number of statistically significant intersections of the curves *U(t)* and *U'(t)* occurs in the 2000s. The spatial distribution of grid points with statistically significant intersections of the *U(t)* and *U'(t)* curves related to the two sub-periods (*Fig. 5b*) shows that in the first period (1961–1990), grid points are concentrated in the central region of the study region, while in the second period (1991–2020), statistically significant intersections are localized in the Caucasus Mountains and in the northwest of the region (*Fig. 5b*).

Table 1. Percentage of grid points with significant intersections ($p<0.05$) of the *U(t)* and *U'(t)* curves

Indicator	Number of grid points (%)		
	total quantity	upward	downward
SCI	16.84	15.48	1.36
T_{SCI}	72.80	72.80	0.00
D_{SCI}	3.64	0.00	3.64

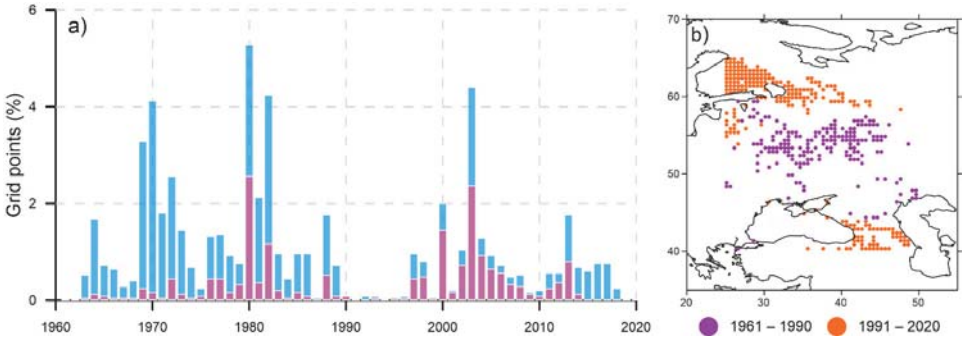

Fig. 5. (a) Percentage of grid points (blue bars) that intersect in each year and are statistically significant at the 95% level intersection (brown bars) of the *SCI*; (b) distribution of significant intersections of the curves *U(t)* and *U'(t)* for the *SCI* index, related to two periods without taking into account the sign of the trend.

4. Discussion and conclusions

Using the Scheffer Climate Index and the data from ERA5 re-analysis, the risk of wood decay of cultural heritage sites in the European part of Russia was assessed for the period 1961–2020. The risk of wood decay increases in the southern direction, the maximum values of the *SCI* were found for the Black Sea coast of the Caucasus, the Ciscaucasia, and Transcaucasia. Masterpieces of wooden architecture in the European part of Russia are located mainly in its northern regions, where the largest values of statistically significant trends of *SCI* were found. Previously, statistically significant trends in the number of freeze-thaw cycles and the number of days with relative air humidity over 80% for the same time period were obtained for the northern regions of the European part of Russia (*Vyshkvarkova* and *Sukhonos,* 2023).

A positive trend in the *SCI* values, and the resulting increase in the risk of wood decay, is found elsewhere in other studies. An increase in the *SCI* values, temperature and precipitation components, from 1900 to 2020 with varying intensity was found for three stations in Russia (St. Petersburg, Arkhangelsk, and Shenkursk in the Arkhangelsk region) (B*rimblecombe* and *Richards*, 2023a). There has been a significant increase in *SCI* for locations across the UK between 1990 and 2019. The highest values are found in the northern and western parts of the UK, but increases have been seen across the country (*Curling* and *Ormondroyd*, 2020).

Positive trends in the *SCI* values are expected to continue in the future, according to regional and global climate models in different regions of the globe. For example, the results of the global HadGEM3 model predict an increase in the

SCI values from 50 (1850–1879) to 75 (2070–2099) across Europe (*Richards* and *Brimblecombe*, 2022). In the coming years, an increase in the risk of wood decay can be expected in the Trentino-South Tyrol region, according to the CORDEX model ensemble for RCP4.5 and RCP8.5 scenarios (*Blavier et al*., 2024). For Africa, 13 CMIP6 models and the SPS585 scenario found that projections of future changes in the *SCI* are driven primarily by changes in temperature rather than precipitation. Despite significant disagreement in the simulated magnitude of the *SCI*, there was good agreement between models on the direction of change in Equatorial Africa, where the *SCI* is highest (*Richards et al*., 2023). Results from the HadGEM3-RA model under the RCP4.5 and 8.5 scenarios for Korea show that climate change will significantly increase the potential decay risk and, as a result, the vulnerability of wooden cultural heritage to fungal decay by the end of the century, even under the RCP 4.5 scenario (*Oh et al.,* 2022). Based on meteorological station data, the risk of wood decay for Iran is assessed as low in most areas and moderate in the northern part of the country along the Caspian Sea coast (*Helali et al*., 2021). Using long-term observational data (since the late 19th century), the authors (*Brimblecombe* and *Richards*, 2023b) assessed the past and future change in the *SCI* for Europe and concluded that the threat to wood heritage is increasing in temperate and continental regions of Europe, and decreasing along the northern Mediterranean coast. *Vandemeulebroucke et al*. (2021) showed the increase in mould and wood decay under RCPs 4.5 and 8.5 scenarios by the end of the 21st century using a solid masonry case study in Brussels, Belgium.

The use of sequential Mann-Kendall test allowed to establish some patterns of change in the sign of the *SCI* index trend. The two identified sub-periods have differences in the spatial distribution of upward and downward trends. The first period is characterized by a statistically significant change in the sign of the trend in the central regions, while in the second period, the areas of statistically significant intersections of the curves are in the northwest of the region and in the Caucasus Mountains.

Our results are consistent with those of other studies and show an increase in the risk of decay of wood of cultural heritage sites in many regions of the globe against the background of observed climate change. The northern regions of the European part of Russia, despite moderate values of the *SCI*, have the greatest positive trend, which indicates an increasing threat to wooden structures. Intensification of measures to support and protect cultural heritage sites consisting of wood or having wood components is required.

Funding. This work was supported by the state assignment of Institute of Natural and Technical Systems (Project Reg. No. 124013000609-2).

References

Alijani, B., Mahmoudi, P., Salighe, M., and *Rigi, A*., 2011: Study of annual maximum and minimum temperatures Changes in Iran. *Geograp. Res. 26,* 101–122.

Andrady, A.L., Pandey, K.K., and *Heikkilä, A.M.*, 2019: Interactive effects of solar UV radiation and climate change on material damage. *Photochem. Photobiol. Sci. 18,* 804–825. https://doi.org/10.1039/c8pp90065e

Barbieri, L.F.P., Correia, M. de F., Aragão, M.R. da S., Vilar, R.A.A,. and *de Moura, M.S.B.*, 2017: Impact of climate variations and land use change: A Mann-Kendall Application. *Rev Geama Recife 3(3),* 127–135.

Blavier, C.L.S., Huerto-Cardenas, H.E., Aste, N., Del Pero, C., Leonforte, F., Della, and *Torre, S.*, 2023: Adaptive measures for preserving heritage buildings in the face of climate change: A review. *Building and Environment 245*, e110832. https://doi.org/10.1016/j.buildenv.2023.110832

Blavier, C.L.S., Maines, E., Campalani, P., Huerto-Cardenas, H.E., Del Pero, C., and *Leonforte, F*., 2024: Assessing Climate Impact on Heritage Buildings in Trentino-South Tyrol: High-Resolution Projections and Adaptive Strategies. Preprint. https://doi.org/10.2139/ssrn.4985301

Brimblecombe, P., Grossi, C.M., Harris, I., 2011: *Climate change critical to cultural heritage*. In: Gökçekus H, Türker U, LaMoreaux JW (eds) Survival and sustainability: environmental concerns in the 21st century, Springer, 195–205

Brimblecombe, P., Lankester, P., 2013: Long-term changes in climate and insect damage in historic houses. *Studies in Conservation 58*, 13–22. https://doi.org/10.1179/2047058412Y.0000000051

Brimblecombe, P. and *Richards, J.,* 2023a: Köppen climates and Scheffer index as indicators of timber risk in Europe (1901–2020). *Heritage Science 11*, 148. https://doi.org/10.1186/s40494-023-00992-7

Brimblecombe, P. and *Richards, J.,* 2023b: Temporal resolution of climate pressures on façades in Oxford 1815–2021. *Theor. Appl. Climatol. 153*, 561–572. https://doi.org/10.1007/s00704-023-04498-x

Brimblecombe, P., Richards, J., 2024: Applied climatology for heritage. *Theor. Appl. Climatol. 155*, 7325–7333. https://doi.org/10.1007/s00704-024-05059-6

Brischke, C. and *Selter, V.,* 2020: Mapping the decay hazard of wooden structures in topographically divergent regions. *Forests 11(5)*, e510. https://doi.org/10.3390/f11050510

Camuffo, D., 2019: Climate change, human factor, and risk assessment. In: *D. Camuffo*, ed., Microclimate for cultural heritage, Elsevier, 303–340.

Chatterjee, S., Bisai, D., and *Khan, A*., 2014: Detection of approximate potential trend turning points in temperature time series (1941–2010) for Asansol Weather Observation Station, West Bengal, India. India. *Atmosp. Climate Sci. 4*, 64–69.

Copernicus Climate Change Service. Access to ERA5 Reanalysis Data. Available at: https://climate.copernicus.eu/climate-reanalysis [Accessed on 24 December 2024].

Curling, S.F. and *Ormondroyd, G.A*., 2020: Observed and projected changes in the climate based decay hazard of timber in the United Kingdom. *Scientific Reports 10*, e16287. https://doi.org/10.1038/s41598-020-73239-1

Dufek, A.S. and *Ambrizzi, T*., 2008: Precipitation variability in São Paulo State, Brazil. *Theor. Appl. Climatol. 93*, 67–178. https://doi.org/10.1007/s00704-007-0348-7

Fernandez-Golfin, J., Larrumbide, E., Ruano, A., Galvan, J., and *Conde, M*., 2016: Wood decay hazard in Spain using the Scheffer index: proposal for an improvement. *Eur J Wood Wood Prod 74*, 591–599.

Flyen, A.-C., Flyen, C., and *Mattsson, J*., 2020: Climate change impacts and fungal decay in vulnerable historic structures at Svalbard. *E3S Web Conf 172*, e20006. https://doi.org/10.1051/e3sconf/202017220006

Hall, C.M., Baird, T., James, M., Ram, Y., 2016: Climate change and cultural heritage: conservation and heritage tourism in the Anthropocene. *J. Heritage Tourism 11*, 10–24. https://doi.org/10.1080/1743873X.2015.1082573

Helali, J., Momenzadeh, H., Saeidi, V., Brischke, C., Ebrahimi, G., and *Lotfi, M.,* 2021: Decadal Variations of Wood Decay Hazard and El Niño Southern Oscillation Phases in Iran. *Front For Glob Change 4*, 693833. https://doi.org/10.3389/ffgc.2021.693833

Hersbach, H., Bell, B., Berrisford, P., Hirahara, S., Horanyi, A., Muñoz-Sabater, J., Nicolas, J., Peubey, C., Radu, R., Schepers, D., Simmons, A., Soci, C., Abdalla, S., Abellan, X., Balsamo, G., Bechtold, P., Biavati, G., Bidlot, J., Bonavita, M., De Chiara, G., Dahlgren, P., Dee, D., Diamantakis, M., Dragani, R., Flemming, J., Forbes, R., Fuentes, M., Geer, A., Haimberger, L., Healy, S., Hogan, R.J., Hólm, E., Janisková, M., Keeley, S., Laloyaux, P., Lopez, P., Lupu, C., Radnoti, G., de Rosnay, P., Rozum, I., Vamborg, F., Villaume, S., and *Thépaut, J.-N.*, 2020: The ERA5 global reanalysis. *Q. J. R. Meteorol. Soc. 146*, 1999–2049. https://doi.org/10.1002/qj.3803

IPCC 2021: Climate Change 2021: The Physical Science Basis. Contribution of Working Group I to the Sixth Assessment Report of the Intergovernmental Panel on Climate Change. In: *Masson-Delmotte, V., Zhai, P., Pirani, A., Connors, S.L., Péan, C., Berger, S., Caud, N., Chen, Y., Goldfarb, L., Gomis, M.I., Huang, M., Leitzell, K., Lonnoy, E., Matthews, J.B.R., Maycock, T.K., Waterfield, T., Yelekçi, O., Yu, R., Zhou, B.* (eds) Cambridge University Press, 3949 p. https://www.ipcc.ch/report/ar6/wg1/downloads/report/IPCC_AR6_WGI_Full_Report.pdf

Kim, T. and *Ra, J.B.,* 2013: Decay hazard (Scheffer) index values in Korea for exterior aboveground wood. *Forest Products Journal 63 (3-4)*, 91–94.

Koziróg, A., Rajkowska, K., Otlewska, A., Piotrowska, M., Kunicka-Styczynska, A., Brycki, B., Nowicka-Krawczyk, P., Koscielniak, M., and *Gutarowska, B.*, 2016: Protection of Historical Wood against Microbial Degradation – Selection and Application of Microbiocides. *Int. J. Mol. Sci. 17*, e1364. https://doi.org/10.3390/ijms17081364

Lisø, K.R., Hygen, H.O., Kvande, T., and *Thue, J.V.*, 2006: Decay potential in wood structures using climate data. *Build Res Inf 34*, 546–551.

Liu, Q., Yang, Z., and *Cui, B.,* 2008: Spatial and temporal variability of annual precipitation during 1961–2006 in Yellow River Basin, China. *J. Hydrol.361*, 330–338.

Mi, X., Li, T., Wang, J., and *Hu, Y.,* 2020: Evaluation of salt-induced damage to aged wood of historical wooden buildings. *Int. J. Anal. Chem*. e8873713. https://doi.org/10.1155/2020/8873713

Moraes, J.M., Pellegrino, H.Q., Ballester, M.V., Martinelli, L.A., Victoria, R.L., and *Krusche, A.V.,* 1998: Trends in hydrological parameters of southern Brazilian watershed and its relation to human induced changes. *Water Resour. Manage. 12*, 295–311.

Morris, P.I. and *Wang, J.*, 2011: Scheffer index as preferred method to define decay risk zones for above ground wood in building codes*. International Wood Products J. 2*, 67–70. https://doi.org/10.1179/2042645311Y.0000000012

Nikolitsa, G. and *Giarma, C.*, 2019: Estimation of decay potential of wooden elements above ground in Greece. *Build. Environ. 154*, 155–166

Oh, J.-J., Choi, Y.-S. sun Kim, G., and *Kim, G.-H.*, 2022: Assessment of the effects of projected climate change on the potential risk of wood decay in Korea. *J. Cultural Heritage 55*, 43–47. https://doi.org/10.1016/j.culher.2022.02.004

Prieto, B., Vazquez-Nion, D., Fuentes, E., and *Duran-Roman, A.G.*, 2020: Response of subaerial biofilms growing on stone-built cultural heritage to changing water regime and CO2 conditions. *Int. Biodeteriorat. Biodegradat. 148*, e104882. https://doi.org/10.1016/j.ibiod.2019.104882

Richards, J. and *Brimblecombe, P.*, 2022: Moisture as a driver of long-term threats to timber heritage—Part I: changing heritage climatology. *Heritage 5*, 1929–1946. https://doi.org/10.3390/heritage5030100

Richards, J., Brimblecombe, P., and *Engelstaedter, S.*, 2023: Modelling temperature-precipitation pressures on African timber heritage. *Int. J. Climatol. 43(16)*, 7447–7462. https://doi.org/10.1002/joc.8273

Sabbioni, C., Brimblecombe, P., and *Cassar, M.*, 2010: The atlas of climate change impact on European cultural heritage. Scientific analysis and management strategies. London: Anthem Press.

Sabbioni, C., Cassar, M., Brimblecombe, P., 2009: Vulnerability of cultural heritage to climate change. *Pollution Atmospherique 203*, 285–298

Scheffer, T.C., 1971: A climate index for estimating potential for decay in wood structures above ground. *Forest Products Journal 21*, 25–31.

Sesana, E., Gagnon, A.S., Ciantelli, C., Cassar, J.A., and *Hughes, J.J*., 2021: Climate change impacts on cultural heritage: A literature review. *WIREs Clim Change 12*, e710. https://doi.org/10.1002/wcc.710

Sneyres, R., 1990: Technical note no. 143 on the statistical analysis of time series of observation World Meteorological Organization, Geneva, Switzerland.

Soboń, M. and *Bratasz, Ł*., 2022: A method for risk of fracture analysis in massive wooden cultural heritage objects due to dynamic environmental variations. *Eur J Wood Prod 80*, 1201–1213. https://doi.org/10.1007/s00107-022-01841-3

Sukhonos, O.Yu., Vyshkvarkova, E.V., and *Voskresenskaya, E.N*., 2024: Trends in the Sheffer index as an indicator of the risk of destruction of wooden structures of cultural heritage sites in the European part of Russia. *Environ. Control Syst. 4,* 115–122. (in Russian). https://doi.org/10.33075/2220-5861-2024-4-115-122

Temeliyeh, Z.K., Temeliyeh, S.K., Temeliyeh, H.K., and *Mirabbasi, R*., 2022: Investigating the Trend of Temperature Changes in Isfahan Station, Iran Using the Sequential Mann-Kendall Method. *Water Harvesting Research 5(2*), 217–228. https://doi.org/10.22077/jwhr.2023.6429.1086

The Third Assessment Report on Climate Change and its Consequences in the Russian Federation, 2022: Kattsov, V.M. (ed) Roshydromet, St. Petersburg: Science-Intensive Technologies, 676 p

Vandemeulebroucke, I., Caluwaerts, S., and *Van Den Bossche, N.,* 2021: Factorial Study on the Impact of Climate Change on Freeze-Thaw Damage, Mould Growth and Wood Decay in Solid Masonry Walls in Brussels. *Buildings 11*, e134. https://doi.org/10.3390/buildings11030134

Vyshkvarkova, E., Sukhonos, O., 2023: Climate Change Impact on the Cultural Heritage Sites in the European Part of Russia over the Past 60 Years. *Climate 11*, e50. https://doi.org/10.3390/cli11030050

Wang, F., Huang, J., and *Zhou, Q*., 2024: Water-salt transport modeling and sulfate erosion mechanisms in cultural heritage under microclimate. *J. Build Engin 98*, e111393. https://doi.org/10.1016/j.jobe.2024.111393

Wang, J. and *Morris, P*., 2008: Effect of Climate change on above ground decay hazard for wood products according to the Scheffer index. Proceedings of the 29th Canadian Wood Preservers Association Annual Meeting Vancouver 2008, 92–103. https ://www.cwpa.ca/publi catio ns/#tab-2008-tab

WMO, 2021: State of the Global Climate 2020 – WMO, 1264, 56 p. https://library.wmo.int/doc_num.php?explnum_id=10618

Zhao, J., Huang, Q., Chang, J., Liu, D., Huang, S., and *Shi, X*., 2015: Analysis of temporal and spatial trends of hydro-climatic variables in the Wei River Basin. *Environ. Res. 139*, 55–64. https://doi.org/10.1016/j.envres.2014.12.028

INSTRUCTIONS TO AUTHORS OF *IDŐJÁRÁS*

The purpose of the journal is to publish papers in any field of meteorology and atmosphere related scientific areas. These may be

- research papers on new results of scientific investigations,
- critical review articles summarizing the current state of art of a certain topic,
- short contributions dealing with a particular question.

Some issues contain "News" and "Book review", therefore, such contributions are also welcome. The papers must be in American English and should be checked by a native speaker if necessary.

Authors are requested to send their manuscripts to

Editor-in Chief of IDŐJÁRÁS
P.O. Box 38, H-1525 Budapest, Hungary
E-mail: journal.idojaras@met.hu

including all illustrations. MS Word format is preferred in electronic submission. Papers will then be reviewed normally by two independent referees, who remain unidentified for the author(s). The Editor-in-Chief will inform the author(s) whether or not the paper is acceptable for publication, and what modifications, if any, are necessary.

Please, follow the order given below when typing manuscripts.

Title page should consist of the title, the name(s) of the author(s), their affiliation(s) including full postal and e-mail address(es). In case of more than one author, the corresponding author must be identified.

Abstract: should contain the purpose, the applied data and methods as well as the basic conclusion(s) of the paper.

Key-words: must be included (from 5 to 10) to help to classify the topic.

Text: has to be typed in single spacing on an A4 size paper using 14 pt Times New Roman font if possible. Use of S.I. units are expected, and the use of negative exponent is preferred to fractional sign. Mathematical formulae are expected to be as simple as possible and numbered in parentheses at the right margin.

All publications cited in the text should be presented in the *list of references*, arranged in alphabetical order. For an article: name(s) of author(s) in Italics, year, title of article, name of journal, volume, number (the latter two in Italics) and pages. E.g., *Nathan, K.K.,* 1986: A note on the relationship between photo-synthetically active radiation and cloud amount. *Időjárás 90,* 10–13. For a book: name(s) of author(s), year, title of the book (all in Italics except the year), publisher and place of publication. E.g., *Junge, C.E.,* 1963: *Air Chemistry and Radioactivity*. Academic Press, New York and London. Reference in the text should contain the name(s) of the author(s) in Italics and year of publication. E.g., in the case of one author: *Miller* (1989); in the case of two authors: *Gamov* and *Cleveland* (1973); and if there are more than two authors: *Smith et al.* (1990). If the name of the author cannot be fitted into the text: *(Miller,* 1989); etc. When referring papers published in the same year by the same author, letters a, b, c, etc. should follow the year of publication. DOI numbers of references should be provided if applicable.

Tables should be marked by Arabic numbers and printed in separate sheets with their numbers and legends given below them. Avoid too lengthy or complicated tables, or tables duplicating results given in other form in the manuscript (e.g., graphs). *Figures* should also be marked with Arabic numbers and printed in black and white or color (under special arrangement) in separate sheets with their numbers and captions given below them. JPG, TIF, GIF, BMP or PNG formats should be used for electronic artwork submission.

More information for authors is available: journal.idojaras@met.hu

Published by the HungaroMet Hungarian Meteorological Service

Budapest, Hungary

ISSN 0324-6329 (Print)

ISSN 2677-187X (Online)